Modeling and Simulation of Ion Channels

Christopher Maffeo, **Swati Bhattacharya**, **Jejoong Yoo**, **David Wells**, and **Aleksei Aksimentiev**
Department of Physics, University of Illinois, 1110 W. Green St., Urbana, IL

Aleksei Aksimentiev: aksiment@illinois.edu

1 Introduction

Transport of ions through pores in membranes is a process of fundamental importance to cell biology. In living organisms, such transport is facilitated by ion channels that utilize the ionic flux to perform diverse biological functions, such as cell-cell communication and signaling, osmotic stress response, muscle contraction, *etc*. The action of ion channels is responsible for most of what we (humans) perceive as reality in the form of sound, smell, sight, taste and touch, and forms the physiological basis for thought. Biomimetic ion channels are ubiquitous in engineering, with application ranging from water desalination to fuel cells.

Since the discovery of excitable ionic membranes, modeling and simulation have been an integral part of the development of the field. From the early studies of Hodgkin and Huxley to the most recent fully atomistic simulations of ion conductance, the key challenge in this area remains the prediction of electrical response of a membrane incorporating ion channels to external stimuli such as transmembrane voltage, chemical ligands, tension, *etc*. The ever increasing complexity of the computational models of ion channels reflects the dramatic advances of our experimental knowledge about these systems, most importantly, fully atomistic structures of several ion channels[1–3] and direct experimental observations of a single channel's action,[4–7] with more discoveries yet to come.

Here, we review efforts to model and simulate ion channels that occurred within the past ten years. First, we briefly describe early phenomenological models of excitable membranes and briefly review recent developments in this area. Next, we describe several membrane channel systems that have been studied extensively by various computational approaches. Our selection of systems is based solely on their popularity among modelers and is neither intended to provide a representative overview of the evolutionary development of ion channels nor presented in any particular historical order. Next, we describe the most common computational methods used to study ion channels. Table 1 links the systems and methods by providing explicit references to the studies of specific systems performed using specific methods. The second half of the review is organized according to the most typical questions of interest: ion binding and permeation pathways, ion conductance, selectivity and gating. The last section summarizes recent development in the field of stochastic sensors— biomimetic ion channels with promising applications in biomedical diagnostics. At the end of this review, we briefly describe our perspective on the development of the field within the next ten years.

Correspondence to: Aleksei Aksimentiev, aksiment@illinois.edu.

2 Early phenomenological models

Early work on phenomenological modeling of ion channels actually occurred well before the existence of ion channels had been established, or even surmised.[395] Rather, researchers were attempting to understand the mechanism of signal propagation in nerve cells. Nerve cells at rest maintain an *action potential*, defined as the electrical potential of the nerve interior relative to the exterior. Rest action potentials are negative and generally in the range of −40 to −95 mV.[395] Interestingly, the axons of nerve cells support the transmission of a pulse of slightly positive action potential, which carries the signals used for communication in a neural network. The technique used by Hodgkin and Huxley, called a *voltage clamp*, is illustrated schematically in Figure 1a. In a voltage clamp experiment, the transmembrane voltage is held constant, and the resulting current is measured. Such experiments determine the membrane permeability as a function of voltage and time.

Early models described the axon as a "cable", with a conductive core surrounded by a less conductive, capacitive sheath, later identified as a membrane. This model corresponds to the circuit diagram shown in Figure 1b. Further experiments showed that during excitation the membrane permeability increases dramatically. Additionally, it was found that assigning a variable *electromotive force*, or emf, to the membrane provided a better fit to the experimental data, yielding the circuit diagram shown in Figure 1c. Finally, the brilliant experiments and insight of Hodgkin and Huxley[396] established that the currents associated with action potential changes were in fact carried by *multiple* ion species, primarily K^+ and Na^+. This conceptual leap removed the need for a variable emf in the equivalent circuit diagram, instead assigning separate emfs and resistances for transport of K^+ and Na^+ species. They also found a small, so-called "leakage" current associated with a constant resistance. The final circuit model is shown in Figure 1d.

The realization that changes in the action potential were manifested through multiple ion species was a major advance. Experiments isolating the K^+ and Na^+ permeability of the membrane revealed a fascinating twist: under an externally applied potential, K^+ resistance drops and stays low, while Na^+ resistance drops initially but then returns to its previous level. Figure 2 shows the conductance of squid axon to sodium and potassium.

The *Hodgkin-Huxley*, or HH, model describes the behavior of the two independent ionic resistances introduced in Figure 1d. For convenience, we restate these quantities as their inverses, the ionic conductances g_K and g_{Na}. In the model, g_K and g_{Na} vary between zero and maximum values $\bar{g}_K$ and $\bar{g}_{Na}$, respectively. In other words,

$$g_K = x_K \overline{g}_K$$
$$g_{Na} = x_{Na} \overline{g}_{Na}$$

The goal of the HH model is to describe the behavior of the coefficients x_K and x_{Na}. In the model, x_K and x_{Na} are only dependent on time and voltage.

We first describe how the potassium coefficient x_K is represented in the HH model. To best fit the experimental data, the HH model supposes that four independent particles control the potassium conductance. Although Hodgkin and Huxley did not know of the existence of ion channels, here we will assume that the particles control a potassium channel. Figure 3a schematically shows a potassium channel and the controlling particles. Each particle may be in one of two states: active or inactive. In order for the channel to conduct, *all four particles must be active*. Following Hodgkin and Huxley, let us say that the probability of a particle

being active is n. The probability of the channel being conductive is then n^4. The average current is then

$$I_K = n^4 \overline{g}_K (V - \varepsilon_K) \quad (1)$$

where V is the applied voltage and ε_K is the emf of the potassium channel. The emf originates in the ion concentration gradient across the membrane, which is driven by ion pumps such as Na^+-K^+ ATPase.[398]

In the HH model, the switching of a particle between active and inactive states is described by *first-order kinetics*. Because of this, we may describe the behavior of n in terms of two values: the *steady-state* value n_∞, which is the value that n approaches given enough time; and a time constant τ_n, which describes how quickly n approaches n_∞. Mathematically, the value of n obeys the following differential equation

$$\frac{dn}{dt} = \frac{n_\infty - n}{\tau_n}. \quad (2)$$

Importantly, n_∞ and τ_n are functions of the applied voltage. The behavior of n_∞ and τ_n under a change of voltage is schematically shown in Figure 3c. Notice that the probability of the channel being in a conducting state (n^4) rises with increasing transmembrane bias.

Activation of sodium channels in the HH model is similar to that of potassium channels, with one essential difference: instead of four identical controlling particles, sodium channels are controlled by three identical particles, and a fourth particle of different type. Let's say the probability of each of the three particles being active is m, while this probability for the fourth particle is h. It is the action of this fourth particle that controls deactivation of the channel under an external voltage. Figure 3b shows a schematic representation of a sodium channel. The average current through a sodium channel is then

$$I_{Na} = h^3 m \overline{g}_{Na} (V - \varepsilon_{Na}) \quad (3)$$

where ε_{Na} is the emf of the sodium channel. Analogously to n for the potassium channel, the behavior of h and m are described by steady-state values h_∞ and m_∞ and time constants τ_h and τ_m, obeying the differential equations

$$\frac{dh}{dt} = \frac{h_\infty - h}{\tau_h}, \quad (4)$$

$$\frac{dm}{dt} = \frac{m_\infty - m}{\tau_m}. \quad (5)$$

The behavior of h_∞, τ_h, m_∞, and τ_m under a change of voltage is shown in Figure 3d. The time constant τ_h is much higher than τ_m, meaning that the deactivating particle reacts much more slowly to a change of external potential than the activating particles. Thus, we see how the conductance traces shown in Figure 2a are explained: upon switching from the normal polarized potential value (low V in Figure 3c–d) to higher values, the activating particles quickly switch on, due to their low time constant τ_m; because of the relatively high value of τ_h, the inactivating particle is slow to react, and continues to allow conduction; but

eventually, the inactivating particle does indeed switch the channel back off, and the conductance drops.

Finally, we would be remiss if we did not mention a related theory, the *Goldman–Hodgkin–Katz theory*. The GHK theory relates voltage, current, and ionic permeabilities.[395] One form of the theory is the *GHK voltage equation*:

$$V_0 = \frac{RT}{F} \ln \frac{P_K[K]_o + P_{Na}[Na]_o + P_{Cl}[Cl]_i}{P_K[K]_i + P_{Na}[Na]_i + P_{Cl}[Cl]_o} \quad (6)$$

Here, V_0 is the zero-current voltage, R is the gas constant, F is the Faraday constant, P_X is the permeability of ion species X, and $[X]_o$ and $[X]_i$ are the concentrations of ion species X on the outside and inside of the axon, respectively. The permeability P_X describes how easily ions cross the membrane:

$$P_X \equiv -M_X/\Delta c_X \quad (7)$$

where M_X is the flux of X across the membrane, and c_X is the concentration difference. Among other things, the GHK voltage equation may be used to find the action potential given concentrations and permeability ratios of potassium, sodium, and chloride ions. Interested readers are directed to Hille[395] for a more thorough treatment.

The HH model was a great leap forward in our understanding of nerve cells, and excitable membranes in general, and continues to influence research work in the field. Recent studies on expanding the HH model include incorporation of the HH model into finite element frameworks,[399,400] adding noise to the HH model,[401–403] and the modeling of coupled neurons.[404] Wong *et al.*[400] proposed a model of cardiomyocytes that described concerted action of various types of ion channels. Rowat[401] examined the mechanisms behind the interspike frequency of a stochastic HH model with applications to irregular neural spiking. Tuckwell and Jost[402] performed a detailed analysis of the first- and second-order moments of voltage and *n*, *m*, and *h* in a stochastic HH model. Linaro *et al.*[403] developed a technique for mapping HH-derived Markov models of explicit channel activation-deactivation events to a computationally more tractable form for more efficient simulation. Finally, Che *et al.*[404] described the behavior of neurons exposed to a low-frequency electric field. The power and simplicity of the HH model will no doubt continue to influence research for another 50 years.

3 Most common targets of computer modeling

Sustained, unidirectional transport of ions across a biological membrane requires energy input. According to the type of energy sources, ion transport can be assigned to one of the following broad categories. Passive transport is driven by the ion-motive force, or emf, which combines the gradient of the electrostatic potential with the concentration difference across a membrane. In a typical biological setting, the difference between *cis* and *trans* ion concentrations creates the transmembrane gradient of the electrostatic potential. In a laboratory setting, the electrostatic gradient is most commonly imposed by applying an external voltage source. The concentration gradient across the membrane can act along or against the electrostatic gradient. Despite being passive, the transport can still be selective and gated by voltage, tension and chemical stimuli. The focus of this review is primarily on membrane channels that facilitate passive transport of ions.

Over the course of evolution, nature has developed numerous ways to transport ions against the ion-motive force. The most prominent examples are ion pumps that utilize the energy of

ATP hydrolysis to transport ions across the membrane against the concentration gradient. Some of these pumps can work in reverse, synthesizing ATP by transporting ions along the concentration gradient. In so-called antiporters and cotransporters, transport of one ion species is coupled to transport of the other. Some membrane channels can couple transport of ions to transport of larger uncharged solutes and/or protons. In turn, proton transport can be coupled to electron transport, for example, in respiratory chain proteins. Thus, the inner and outer membranes of a living cell are full of various ion-transporting entities whose concerted action and synchronized response to external stimuli keep the cell alive. Interested readers are directed to Alberts *et al.*[398] for a complete overview of the field, to Khalili-Araghi *et al.*[333] for a recent review of modeling efforts in the field of active transport, and to a study by Beard[405] for an example of modeling a system of ion channels in an organelle.

At present, modeling and simulations of ion channels are generally limited by the experimental knowledge about them. Although the HH theory is a beautiful example to the contrary, more often than not a theoretical study of an ion channel requires some knowledge of the channel's structure, ideally, at atomic resolution. Whereas the "no structure—no study" rule is adopted by the majority of researchers working in the field of computer modeling of ions channels, there are notable exceptions[418,419] that deduce the structural architecture of the channel from its ion conductance properties.

Predicting the structure of a membrane channel from its sequence is a formidable task. Hence, development of computational models of ion channels was, in a way, led by crystallographers and their ability to solve atomic structures of ion channels. Membrane channels are notoriously difficult to crystallize and are often too large for the NMR method to work. Therefore, atomic resolution-structures have been obtained for only a very limited number of ion channels, and, hence, many studies have focused on the same systems. Below we briefly review the ion channels of known structures that are the most common targets of computational studies.

3.1 Gramicidin A

Gramicidins are small bacteria-produced antibiotics that, when dimerized in a head-to-head fashion (Figure 4a), are able to transport a monovalent cation across a membrane once about every 100 ns.[39] Gramicidin works by eliminating the ion gradient across the membrane of Gram-positive bacteria. Gramicidin was the first clinical antibiotic in use and is still used today in conjunction with other antibiotics.

All-atom molecular dynamics simulations (MD) have been instrumental in the interpretation and refinement of NMR results.[28] Gramicidin A was the subject of the first MD simulation of an ion channel almost 30 years ago.[420] Advances in the availability of computational resources have permitted far more realistic models including lipid bilayers and full solvent to be simulated for significant durations. Gramicidin A now serves as a model system and test-bed for new techniques.[21]

3.2 Potassium channels

Potassium ion channels are key constituents of electrical signaling networks in the nervous system. When open, potassium channels conduct K^+ ions at rates remarkably close to the diffusion limit (about 10^8 ions per second)[421] and display incredible sensitivity to the size and valency of ions. Thus, K^+ channels can quickly release ions from within the cell in response to appropriate stimulus, affecting the action potential. Since some K^+ channels are voltage sensitive, this can result in a cascade of channel activations that propagates through an axon. K^+ channels have been the target of prospective treatments for an array of disorders, including multiple sclerosis.[422,423]

Taken from Gram-positive bacterium *Streptomyces lividans*, the K$^+$ channel KcsA is similar in sequence to vertebrate voltage-dependent K$^+$ channels, but is easily expressed in *Escherichia coli*, making it the prototypical K$^+$ channel for laboratory studies. Like all K$^+$ channels, the sequence of KcsA contains a completely conserved motif that is crucial for its K$^+$ specificity. Depicted in Figure 5, the first atomic-resolution structure of a K$^+$ channel revealed a tetrameric transmembrane pore with an intracellular passage leading to a large (10 Å diameter) cavity with a hydrophobic lining followed by an atomically-narrow ~4 Å long selectivity filter that leads to the extracellular side of the membrane.[1] A more complete structure of this channel was recently resolved,[410] featuring long cytoplasmic helices that appear to stabilize the closed conformation of KcsA at high pH. In contrast to the pore region, the arrangement of cytoplasmic helices in KcsA is not a universal structural element of K$^+$ channels.

In the selectivity filter, four rings, each featuring four negatively-charged carbonyl-oxygen atoms, hold two K$^+$ ions that are separated by a single water molecule. The ions present in the selectivity filter are mostly desolvated, which carries an enormous free energy penalty that is offset by interactions with the negatively charged surface of the filter. Thus, the large forces experienced by translocating ions balance delicately to allow a smooth free energy landscape that permits rapid permeation through the pore. The balance of these forces must be carefully tuned to select K$^+$ over other monovalent ions such as Na$^+$. Though the latter carries the same charge as K$^+$ and is only 0.4 Å smaller, experiments suggest that K$^+$ channels bind K$^+$ with as much as 1,000 times greater affinity than Na^{+}.[1]

The selectivity filter can become occupied by divalent ions, which generally block the current through the channel. The Kir, or inward rectifying, family of potassium channels uses this mechanism to impede K$^+$ ions moving out of the cell. More generally, potassium channels are regulated through a variety of other means that include modification through ligand binding and voltage- and pH-dependent gating. Many biologically produced toxins target K$^+$ channels to interfere with a victim's nervous system.

Due to the biological importance of K$^+$ channels and the fact that the pore domain of bacterial KcsA is homologous to that of eukaryotic K$^+$ channels, the seminal structure of KcsA[1] motivated many computational and theoretical studies.[148] The formal analogy between electric current in man-made circuits and ion conductance through the channels[424] led researchers to develop and apply continuum electrostatics theories of ion channels.[103–109] The availability of high-resolution crystal structures stimulated development of new atomistic simulation techniques for studying selectivity, conductance, and gating behaviors of K$^+$ channels, using either implicit[110–117] or explicit[29,88,111–113,116–197] solvent models. Ligand docking coupled with free energy calculations was recently used to study methods to enhance the specificity of naturally occurring neurotoxins for Kv1.3, which can suppress chronically activated memory T cells implicated in autoimmune disorders including multiple sclerosis.[422,425] To overcome the time and length scale limitations of the all-atom approaches, several multiscale methods have also been developed,[107,198–202] using K$^+$ channels as target application systems.

3.3 Mechanosensitive channels

All living creatures have mechanosensors.[426,427] For example, we can hear sound because our auditory sensory cells can detect ciliary vibrations caused by acoustic vibrations. We can also feel the pressure on our skin and blood vessels, and feel full when we eat food because of tension sensors in cell membranes. Plants, which are immobile and less responsive, also have mechanosensors; a representative example is the gravity sensor, which allow roots and shoots to grow in opposite directions. Interested readers are referred to a recent review by Kung and coworkers[426,427] for more detailed information.

A breakthrough in the biophysical study of mechanosensation was the cloning[428,429] and structural characterization of simple prokaryotic mechanosensitive channels (MSCs).[407,408,430,431] When the concentration of osmolytes in a bacterial cell is significantly higher than the concentration of osmolytes in the environment, the gradient of osmolyte concentration across the cell membrane can cause huge turgor pressure inside the bacterial cell. If left to develop fully, such osmotic stress can easily rupture the cell wall, killing the bacterium. To prevent this from happening, bacteria have evolved "safety valves" —the MSCs—that open when the surface tension in the membrane exceeds a threshold value, making the membrane permeable to most small solutes and water molecules.[432] Most importantly, the channels return to a closed state when tension drops. Thus, MSCs are essential for the survival of bacteria.

In 1998, Chang *et al.* reported the first high resolution structure of MSC of large conductance (MscL) from *Mycobacterium tuberculosis* in a closed conformation.[407] MscL is a homopentamer, with each subunit having two transmembrane (TM) helices, TM1 and TM2, see Figure 4b. In the closed conformation, five TM1 helices form a pore and TM2 helices surround the inner TM1 helices. Recently, Liu *et al.* reported a crystal structure of tetrameric MscL from *Staphylococcus aureus* in an expanded intermediate state.[431] So far, two crystal structures of the *Escherichia coli* MSC of small conductance (MscS) have been reported, one in a nonconductive conformation[408] and the other in an open conformation.[430] Those high-resolution structures show that the MscS is a homoheptamer with three TM helices per subunit, see Figure 4c. Seven TM3 helices form a channel with a diameter of 5 and 13 Å in a closed and open conformations, respectively, see Figure 6.[430]

Despite the fact that mechanosensation is universal and essential for all living creatures,[427] its mechanism is significantly less understood if compared to the mechanisms of other senses such as vision, smell, and taste.[427] Since the first MSC was discovered in 1987[432] and the first crystal structures of MscL and MscS were revealed in 1998 and 2002,[407,408] both MscL and MscS have served as model systems for the computational studies of mechanical gating. Because of its very nature, this problem has attracted the attention of investigators from various disciplines, including traditional MD simulations, homology modeling, continuum mechanics, and coarse-grained MD simulations, see Sections 5.2.2 and 5.4.1 for more details. The computational methods developed for studies of MscL and MscS will surely be of great value in future studies of more complex mechanisms of mechanosensation.

3.4 Porins

Outer-membrane porins (OMPs) of Gram-negative bacteria are transmembrane proteins that allow the bacterial cells to interact with their environment through passive diffusion of water, ions and small hydrophilic molecules (<600 Da) across their outer membranes. Wide channels such as OMPs and toxins are designed by nature for the permeation of metabolites rather than merely small ions. However, often they exhibit interesting behavior such as selectivity towards certain ions and serve as model systems to test computational models of ion transport and are therefore of interested to this review.

OMPs are beta-barrel structures usually forming homotrimeric water-filled pores. The porin channel is partially blocked by a loop (L3) that is folded inside the beta barrel forming a constriction region that determines the size of the solutes that can traverse the channel. Several crystal structures of porins have been determined at high resolution.[415,433–437] Some porins exhibit moderate ion selectivity, *e.g.*, *Escherichia coli* OmpF (shown in Figure 4i) and OmpC are two cation selective porins while the *Pseudomonas aeruginosa* OprP [438] is a phosphate-selective porin. The cation selectivity is known to depend on the salt concentration and the valence of the ions. Gram-negative bacteria that lack porins have other

substrate specific channels that allow the passage of small molecules. For instance, the OccK1, an archetype of the outer membrane carboxylate channel family from *Pseudomonas aeruginosa* (previously named OpdK) is a monomeric β-barrel with a kidney-shaped central pore as revealed by the X-ray structure.[439] The members of the OccK subfamily of channels are believed to facilitate the uptake of basic amino acids.[440] A detailed examination of the conductance characteristics of several members of the OccK subfamily of channels by Liu and coworkers[441] revealed diverse single channel electrical signatures, non-ohmic voltage dependent conductance, and transient gating behavior. Single molecule electrophysiology analysis along with rational protein design have revealed discrete gating dynamics involving both enthalpy and entropy driven current transitions.[442,443] Studies of porins are relevant to the development of antibiotics. To affect bacteria, antibiotics must first pass through their outer wall, which is a process facilitated by porins. Porin alteration has been implicated in antibiotic resistance.[444] In addition, engineered porins such as the OmpG have potential for use as stochastic sensors.[77]

Functionally related to porins, α-hemolysin— a toxin produced by *Staphylococcus aureus*— is secreted as a monomer, but assembles on target cell membranes to form a homo-heptameric channel, which leads to an uncontrolled permeation of ions and small molecules and causes cell lysis. The X-ray structure of α-hemolysin[445] revealed a mushroom-like shape with a beta-barrel stem protruding from its cap domain, see Figure 4k. Its ability to self-assemble in biological or synthetic membranes and its structural stability over a wide range of ion concentrations, temperatures and pH make α-hemolysin an excellent platform for stochastic sensing applications,[446] including detection of DNA sequence by measuring the ionic current.[447] An interesting feature is the rectification behavior of the channel, which has been explored by both implicit solvent[88] as well as all-atom MD simulations.[90,93]

Another large water-filled biological nanopore is MspA—the major outer membrane porin of *Mycobacterium smegmatis* that allows the uptake of hydrophilic nutrients from the environment. The crystal structure, resolved by Faller and coworkers in 2004,[448] reveals a homo-octameric goblet-like structure with a central channel. The porin has a constriction that is lined by two belts of aspartate residues (Asp[90] and Asp[91]) that diminish the permeability of nonpolar solutes. Genetically modified variants of the MspA channel may enable practical nanopore DNA sequencing,[449,450] providing a higher signal-to-noise ratio for nucleic acid detection than α-hemolysin.[451]

3.5 Other channels

The voltage dependent anion channel (VDAC) residing in the mitochondrial outer membrane serves as a conduit for metabolites and electrolytes. VDACs mediate the passage of ions such as K^+, Cl^-, Ca^{2+} and small hydrophilic molecules such as ATP between the cytosol and the mitochondria and regulate the release of apoptotic proteins. The pore has a voltage dependent conductance with an anion-selective high-conductance state at low transmembrane potential and a slightly cation-selective low-conductance state at high potential.[452] Several NMR and X-ray structures of human as well as mouse VDACs[453–455] have become available. Initially, the significance of these structures was questioned on account of an apparent conflict with biochemical and functional data.[456] However, additional NMR[457,458] and theoretical studies[259,262,268] have shed light on the structure-function relation, reaffirming the biological relevance of the structures.

The ClC chloride channels found in both prokaryotic and eukaryotic cells regulate the selective flow of Cl⁻ions and are believed to play an important role in regulation of blood pressure, pH and membrane excitability. These channels conduct not just Cl⁻, but also other anions such as HCO_3^-, SCN⁻ and NO⁻. Unlike cation channels, they do not discriminate strongly between different species of anions. Defects in these channels are implicated in

several diseases such as myotonia congenita, Bartter's syndrome and epilepsy.[459] In the last decade, structures of ClC orthologues from two bacterial species, *Salmonella serovar typhimurium* and *Escherichia coli* have become available.[460] The X-ray structures reveal the ClC channels to be homodimers with two identical but independent pores, see Figure 4j. Some prokaryotic members of the ClC family of channels are now believed to be ion transporters, although the line between ion-channels and transporters is getting blurred.[461] There have been a few simulation studies of the permeation pathways[260,261] of the ClC channels.

The nicotinic acetylcholine receptor (nAChR) belongs to a superfamily of Cys-loop ligand-gated ion channels. It couples a cationic transmembrane ion channel with binding sites for the neurotransmitter acetylcholine (ACh) so that the gating of the channel is linked to the binding of ACh. The nAChR owes its name to the ability of nicotine to mimic the effects of ACh in opening up the pore. The nAChR is composed of a ring of five protein subunits, with three domains: a large N-terminal extracellular ligand binding domain (LBD), a transmembrane domain (TM) and a small intracellular domain, see Figure 4h. There are two ACh binding sites in the ligand-binding domain and the pore opens when both are occupied.[414] Although the complete high resolution structure of the nAChR is absent at present, X-ray and electron microscopy structures of some of its components are available.[413,414] The nAChR plays a critical role in neuronal communication converting neurotransmitter binding into membrane electric depolarization. The channel is found in high concentrations at the nerve-muscle synapse. nAChR is implicated in a variety of diseases of the central nervous system including Alzheimer's disease, Parkinson's disease, schizophrenia and epilepsy.[462] It is also believed to play a critical role in mediating nicotine reward and addiction.[463] Although detailed study of the gating mechanism is precluded by the lack of a complete structure of the nAChR, as well as the time scales involved, there have been several studies on the TM domain[212,215] and the LBD.[218]

AmtB is a representative bacterial ammonium transporter, which belongs to Amt/MEP family.[464] Some bacteria and plants use ammonium as a nitrogen source, and they have various forms of ammonium transporters for the uptake of ammonium.[464,465] On the other hand, ammonium is a toxic metabolic waste, which should be quickly removed by transporters, usually for mammals.[466] There exist several high-resolution crystal structures of bacterial AmtB,[409,467–470] and the *Escherichia coli* crystal structure has become the paradigm for the study of the transport mechanism of ammonium,[409] see Figure 4d. Usually, AmtB proteins are crystallized as a homotrimer. Each monomer consists of eleven transmembrane helices that form a channel for ammonium. The channel is highly hydrophobic, raising the possibility that ammonium passes the channel in a de-protonated form (ammonia) at some point during transport.

4 Most common simulation methods

Among a large number of computational approaches proposed and employed for studies of ion channels, most fall within the following three categories: All-atom molecular dynamics (MD), which is a fully microscopic description with all atoms treated explicitly; Brownian dynamics (BD), in which only the ions are treated explicitly while the solvent and the protein and lipids are represented implicitly; and approaches based on Poisson-Nernst-Planck (PNP) theory, in which the ionic concentration is treated as a continuum. Each of the three approaches has limitations and advantages. The MD method is considered the most computationally expensive but also the most accurate. The PNP and BD approaches are, in general, less computationally expensive but also provide less detail. At the same time, the MD method has the smallest temporal and spatial range, followed by BD methods, followed

by PNP approaches. Figure 7 schematically illustrates typical setups for the three modeling approaches applied to the same system.

The above classification, however, is rather approximate and can be misleading. Thus, the level of computational complexity often depends on the desired level of detail, whereas the accuracy depends on the assumptions made in deriving the parameters of the model. Even the most sophisticated MD simulations rely on the MD force field, which is a classical model that may or may not be adequate for describing a certain phenomenon. In this respect, full quantum or combined quantum mechanics/classical mechanics approaches (QM/MM) can, in principle, provide the highest degree of accuracy. However the time scales accessible to these methods is severely limiting. Interested readers are directed to reviews of QM/MM approaches for simulations of biomolecules[471,472] and to a recent review of computational approaches to ion transport in nanopores.[473] On the other hand, it is possible to incorporate atomic level details in BD and even PNP approaches, see, for example, recent work by Comer and Carr.[371,373]

Other considerations often neglected when evaluating the "computational cost" of a certain approach are the qualifications and ambitions of the researcher performing the modeling tasks and the availability of well-documented and ready-to-use codes. For example, it is always possible to increase the computational complexity of the problem by including an exorbitant amount of water in an all-atom simulation or using very fine mesh size in continuum calculations. One could also easily spend several months writing, debugging or porting a computationally-efficient code, while the same time could have been used to run a more computationally-intensive but ready-touse and tested code. Thus, there are no simple rules in choosing an optimal simulation method and researchers new to the field are urged to seek expert advice for their particular problem.

4.1 Continuum models

Ion channels are complex systems with many degrees of freedom and, hence, are challenging to model in atomistic detail. Continuum theories based on Poisson-Boltzmann (PB) and Poisson- Nernst-Planck (PNP) equations are powerful tools that make simulation of such systems tractable. The main idea is to employ a continuum description for all components of the system, *i.e.* the solvent, ions, and the ion channel. The water, membrane and the channel are represented as fixed, structureless dielectrics while the ions are described by specifying the local density throughout the system. Figure 7a schematically illustrates a PNP model of α-hemolysin.

4.1.1 Electrostatics of ion channels—The PB equation is the most popular theoretical model for describing the electrostatics around a charged biomolecule in ionic solution. In a system of interacting mobile charged particles, the electrostatic potential arises due to the combined effect of the charged biomolecules, ions, and dielectric properties of the environment. The PB model assumes that the distribution of charges in the system is related to the electrostatic potential according to Boltzmann statistics. For the purpose of describing electrostatics of a single biomolecule, the PB equation, which was first introduced independently by Gouy (1910) and Chapman (1913) and later generalized by Debye and Hückel (1923), is most frequently written as

$$\nabla \cdot (\varepsilon(\mathbf{r})\nabla\psi(\mathbf{r})) = -4\pi\rho^f(\mathbf{r}) - 4\pi\sum_i c_i^\infty z_i q \exp\left(\frac{-z_i q\psi(\mathbf{r})}{k_B T}\right)\lambda(\mathbf{r}) \quad (8)$$

where $\varepsilon(\mathbf{r})$ is the position-dependent dielectric constant, $\psi(\mathbf{r})$ is the electrostatic potential, ρ^f ($\mathbf{r}$) is the fixed charge density of the biomolecule, c_i^{∞} represents the concentration of ion species i at infinite distance from the biomolecule, z_i is the valency of ion species i, q is the proton charge, k_B is the Boltzmann constant, T is the temperature and $\lambda(\mathbf{r})$ describes the accessibility of position $\mathbf{r}$ to ions (for example, it is often assumed to be zero inside the biomolecule). A solution to the PB equation gives the electrostatic potential and equilibrium density of ions throughout the space. The PB equation invokes a mean-field approximation that neglects non-electrostatic ion-ion interactions (e.g. vdW or water-mediated), the dielectric response of the system to each ion, and effects due to correlations in the instantaneous distribution of ions. Because of these, the PB equation fails to describe the electrostatics of highly charged objects such as DNA in high-concentration ion solutions with quantitative accuracy.[474] In the context of ion channels, which rarely carry such a high charge density, the PB theory has been widely used to calculate the free energy cost of transferring a charge from bulk solution to the interior of the channel[105,287] (see Table 1), to characterize ion-channel interactions[88,294] and to compute the distribution of the transmembrane electrostatic potential.[103,104,294,299] Such continuum electrostatic calculations have also been used to estimate the relative stability of protonated and unprotonated states of ionizable residues in an ion channel (discussed in 61,475). DelPhi[476] and APBS[477] are two popular computer codes for numerically solving the PB equation.

4.1.2 Ion transport—While the PB model provides insights into the equilibrium energetics of an ion channel, modeling of the ion flux requires a non-equilibrium approach. In most ion channels, the time scale of ion permeation ranges from tens of nanoseconds (porins) to microseconds and even milliseconds (in active transport). Thus, observing a statistically significant number of ion permeation events requires long trajectories that are still rather expensive to obtain using an all-atom approach. The Poisson-Nernst-Planck model gives access to long time scales albeit at a lower temporal and spatial resolutions. As in the PB model, the lipid, protein and water molecules are approximated as dielectric continua, while ions are described as continuous density distributions. The current density is obtained from the Nernst-Planck (NP) theory, which is widely used in studies of electrolyte transport. In the NP theory, ion fluxes arise from two sources: the gradient of ion concentration and the gradient of the electrostatic potential. Traditional Nernst-Planck equations do not describe ion-channel interactions. However, the classical Nernst-Planck equations may be modified to include the ion-channel interactions via an effective potential. Thus, the flux of ion species i, J_i, is written as

$$\mathbf{J}_i(\mathbf{r},t) = -D_i(\mathbf{r}) \left(\nabla c_i(\mathbf{r},t) + \frac{c_i(\mathbf{r},t)}{k_B T} \nabla \mathscr{W}_i^{eff}(\mathbf{r}) \right), \quad (9)$$

where D_i and c_i are the diffusion constant and the number density of ion species i, respectively, and $\mathscr{W}_i^{eff}(\mathbf{r})$ is the effective potential that usually combines the electrostatic potential $\phi(\mathbf{r})$ and a core-repulsive potential $U_{Core}(\mathbf{r})$, the latter describing interactions between ions and the protein channel and not between the ions themselves.

The concentration and the flux of each ionic species obey the continuity equation

$$\frac{\partial c_i(\mathbf{r},t)}{\partial t} + \nabla \cdot \mathbf{J}_i(\mathbf{r},t) = 0. \quad (10)$$

Under steady state conditions, the concentration and the flux do not vary with time and $\nabla \cdot \mathbf{J}_i(\mathbf{r}) = 0$. The electrostatic potential is calculated from the Poisson equation

$$\nabla \cdot (\varepsilon(\mathbf{r})\nabla\varphi((r))) = -4\pi \left(\rho^f(\mathbf{r}) + \sum_i q_i c_i(\mathbf{r}) \right), \quad (11)$$

where $\varepsilon(\mathbf{r})$ is the dielectric constant, q_i is the ion charge and $\rho^f(\mathbf{r})$ is again the (fixed) charge density due the protein.

The above coupled partial differential equations constitute the PNP equations and may be solved by a variety of methods in one or three dimensions. Typically, the NP and the Poisson equations are solved self consistently to simultaneously obtain the electrostatic potential $\phi(\mathbf{r})$ and the ionic concentration $c_i(\mathbf{r})$ under appropriate boundary conditions.

Modeling ion channels within the PNP framework is computationally inexpensive compared to MD and BD simulations because the problem of many-body interactions is avoided through a mean-field approximation. An undesirable side-effect, some important physics is neglected by this approximation. Below, we discuss some of the shortcomings of the PNP equations in the context of ion channels, as well as extensions to the equations that address these shortcomings. Interested readers are directed to comprehensive reviews on this subject.[12,299,307,310,478]

Prior to the surge of popularity of the all-atom MD method, continuum electrodiffusion theories played a major role in development of our understanding of ion fluxes in nanochannels.[8,12,55] Early attempts to use the electrodiffusion theory to describe ion flux through nanochannels[279–281,286] led to the development of simplified models based on a self-consistent combination of the Poisson equation and Nernst-Planck equations that were subsequently applied to various channel systems.[282–284] Most of the early studies dealt with either one-dimensional models or simplified geometries that lacked a detailed description of the protein structure and static charge distribution. These studies connected qualitative features of the current-voltage-concentration relationship to structural and physical features of the models. For example, the PNP theory was used to demonstrate how charges at the channel openings can produce current rectification,[285,479] and how a channel with ion-specific binding sites can exhibit lower conductance in a mixture of two ion types than in a pure solution of either type.[480] A lattice relaxation algorithm able to solve the PNP equations for a 3D model was developed by Kurnikova and coworkers[8] in later years. This procedure allows the protein and membrane to be mapped onto a 3D cubic lattice with defined dielectric boundaries, fixed charge distribution and a flow region for the ions.

Like the PB equation, the system of PNP equations constitute a mean-field theory that neglects the finite size of the ions, the dielectric response of the system to an ion, and ion-ion correlations. In fact, the PNP equations reduce to the PB equation for systems with zero flux everywhere. The validity of a continuum dielectric description and mean-field approaches in the context of narrow pores has been the subject of much debate. For example, Chung and coworkers observed considerable differences between the conductance through idealized pores using the BD and PNP approaches.[287,294] The authors argued that the mean-field approximation breaks down in narrow ion channels due to an overestimation of the screening effect by counterions within the pore. For larger channels like porins at physiological or lower ion concentrations are described quite accurately by the PNP equations. However, the currents computed based on the PNP models can be considerably higher (by 50% for OmpF) than in equivalent BD simulations.[55]

When a charge in a high dielectric medium is brought near to a low dielectric medium, a repulsive surface charge is induced at the dielectric boundary. In continuum descriptions such as PB and PNP, the induced charge density includes (usually) cancelling components

from both positive and negative average charge densities. The interaction energy between a charge and its induced charge density is often called the dielectric self-energy. The dielectric self-energy due to the average charge density and the average induced charge density at the dielectric boundary is, in general, smaller than the interaction energy between point charges and corresponding induced charge averaged over all configurations. Put another way, a point charge approaching a low dielectric medium is strongly repelled by its induced image charge, and this repulsion is largely lost by the implicit averaging in mean-field descriptions.

The PB and PNP equations have been modified to include the interaction of an ion with the charge density it induces.[11,294,296] Although the corrections account for the interaction of an ion with its induced dielectric charge, they do not account for the interaction of the induced charge with a second, nearby ion. Similarly, the mean-field approximation inherently ignores effects involving correlations in the instantaneous ion distribution. For example, the narrowest portion of the potassium channels almost always contains two ions that move in a concerted fashion (see Section 5.1.1), which cannot be properly treated by continuum theories. Nevertheless, it was concluded that the dielectric self-energy accounts for most of the discrepancy between PNP and BD results in the case of narrow channels.[294]

Although early electrodiffusion studies of Levitt considered hard-sphere repulsion between ions by iteratively correcting the ion concentration,[279] many studies have since ignored such finite-size effects. Recently, the PNP equations have been adapted to incorporate finite-size effects using classical density functional theory to describe many-body hard sphere interactions between ions and solvent.[290,291,300,481] Unforntunately, these approaches often yield cumbersome integro-differential equations. Finite-size effects can be included in the PNP equations by introducing an entropic term that discourages solvent crowding by ions.[309] The latter approach yields a tractable set of corrected PNP equations. Both the PNP and BD methods usually ignore thermal fluctuations of the protein and lipid bilayer. However, these can be effectively captured by combining results from MD or Monte Carlo simulations with 3-D PNP calculations[92]

The PNP approach continues to play a major role in improving our understanding of the physics of ion channels. The computational efficiency of the PNP model is unparalleled for studies of ion conductance in a low ion concentration regime, where the PNP method is expected to be the most accurate. The method is highly efficient at predicting the effect of a channel's geometry on the current-voltage dependence at physiological voltages and can be used to screen for mutations that affect conductance of a channel. The calculation of currents can be quite accurate in the case of larger channels, such as porins. PNP is perhaps the only method that can presently simulate the interplay of ion conductances in an ensemble of ion channels (such as in a realistic biological membrane) explicitly taking the structural features of the channels into account. Finally, the PNP approach is rather flexible to include descriptions of additional physical effects, for example, hydrodynamic interactions[354,364,369,370] or the effect of a semiconductor membrane on the ionic current.[361,382,383]

4.2 Brownian dynamics

The BD method allows for simulations of explicit ion permeations on the microsecond-to-millisecond time scale by treating solvent molecules implicitly. In a way, the BD method offers a good compromise between all-atom MD and continuum electro-diffusion approaches. Computational efficiency is achieved by reducing the number of degrees of freedom. Typically, a moderate number of atoms of interest (usually the ions) are simulated explicitly, while the solvent is accounted for via friction and stochastic random forces that act in addition to the electrostatic and steric forces arising from other ions, the protein, and the lipid bilayer. For the calculation of electrostatic forces, the water, the membrane and the

protein channel are usually treated as continuous dielectric media. The channel is treated as a rigid structure and thermal fluctuations are typically ignored. Figure 7b schematically illustrates a BD model of α-hemolysin.

4.2.1 General formulation of the BD method—In the Brownian dynamics method, a stochastic equation is integrated forward in time to create trajectories of atoms. The 'uninteresting' degrees of motion, usually corresponding to fast moving solvent molecules, are projected out in order to develop a dynamic equation for the evolution of the 'relevant' degrees of freedom. The motion of the particles is described by a generalized Langevin equation

$$m_i \ddot{\mathbf{r}}_i(t) = \mathscr{F}_i - \int_0^t dt' M_i(t-t') \dot{\mathbf{r}}_i(t') + \mathbf{f}_i(t). \quad (12)$$

The force on the *i*th particle $\mathscr{F}_i$ is obtained from an effective potential $\mathscr{F}_i = -\nabla_i \mathscr{W}(\{\mathbf{r}_i\})$

The potential function is a many body potential of mean force (PMF) that corresponds to the reversible thermodynamic work function to assemble the relevant particles in a particular conformation while averaging out the remaining degrees of freedom, *i.e.* the effect of all other atoms is implicitly present in $\mathscr{W}(\{\mathbf{r}_i\})$. The second term on the r.h.s is the damping force representing the frictional effect of the environment and, finally, $\mathbf{f}_i(t)$ is a Gaussian fluctuating force arising from random collisions. The frictional force depends on previous velocities through the memory kernel $M_i(t-t')$. The first and second moments of the random force are given by $\langle \mathbf{f}_i(t) \rangle = 0$ and $\langle \mathbf{f}_i(t) \cdot \mathbf{f}_j(0) \rangle = 3k_B T M_i(t) \delta_{ij}$, where k_B is the Boltzmann constant and T is the temperature. Both the drag force and the stochastic force incorporate the effect of the solvent. In the Markovian limit, the memory kernel is a Dirac delta function that leads to the traditional Langevin equation

$$m_i \ddot{\mathbf{r}}_i(t) = \mathscr{F}_i - \gamma_i \dot{\mathbf{r}}_i(t) + \mathbf{f}_i(t). \quad (13)$$

The friction coefficient γ_i is related to underlying molecular processes via the fluctuation-dissipation theorem.

In the overdamped regime (which applies to the motion of an ion in water), the inertial term can be ignored so that the Langevin equation is reduced to

$$\dot{\mathbf{r}}_i(t) = \frac{D_i}{k_B T} \mathscr{F}_i + \zeta_i(t), \quad (14)$$

where $D_i = k_B T / \gamma_i$ is the diffusion coefficient of the *i*th particle and $\zeta_i(t)$ is a Gaussian random noise with a second moment given as $\langle \zeta_i(t) \cdot \zeta_i(0) \rangle = 6D_i \delta(t)$.

4.2.2 BD simulations of ion channels—A Brownian dynamics simulation requires two basic ingredients: a description of the forces applied to each ion and the diffusion coefficient for each ion. The diffusion coefficient for the ions should be, in general, position-dependent, and can be obtained from all-atom MD simulations[373,482,483] or estimated using analytical techniques.[88,484] However, in most cases, a single, position-independent diffusion constant is used for all ions of the same species.

Each ion experiences a force that depends on its position, as well as the positions of all the other ions in the system. The potential corresponding to the forces on the ions is the multi-ion PMF, which is the multi-dimensional free energy surface that is usually broken into an

ion-ion PMF and a PMF due to the pore, solution and other biomolecules.[373] The PMFs can be calculated from all-atom MD or even quantum chemistry simulations, but such calculations are computationally expensive.

A more typical approach was presented by Roux and coworkers, which we summarize here.[55,62,63,299] The multi-ion PMF can be written:

$$\mathscr{W}(\{\mathbf{r}_\alpha\})=\sum_\alpha\sum_{\gamma\neq\alpha}u_{\alpha,\gamma}(|\mathbf{r}_\alpha-\mathbf{r}_\gamma|)+\sum_\alpha U_{core}(\mathbf{r}_\alpha)+\sum_\alpha q_\alpha[\varphi_{sf}(\mathbf{r}_\alpha)+\varphi_{rf}(\mathbf{r}_\alpha)]. \quad (15)$$

where $u_{\alpha,\gamma}(r)$ is the ion-ion interaction, U_{core} is a repulsive potential preventing the ions from entering the ion-inaccessible regions, ϕ_{sf} is the electrostatic potential arising from the permanent protein charge distribution and ϕ_{rf} is the reaction field potential arising from the electrostatic polarization of the various dielectric boundaries. The static field may be computed from an atomic model of the pore using the PB equations.[55,62,63,485] Any externally imposed transmembrane bias may be included in the calculation of the electrostatic potential. Usually, the ion-ion interaction includes van der Waals and Coulomb terms:

$$u_{\alpha,\gamma}(r)=4\varepsilon_{\alpha,\gamma}\left[\left(\frac{\sigma_{\alpha,\gamma}}{r}\right)^{12}-\left(\frac{\sigma_{\alpha,\gamma}}{r}\right)^6\right]+\frac{q_\alpha q_\gamma}{\varepsilon_{bulk}r};$$

where $\varepsilon_{\alpha,\gamma}$ and $\sigma_{\alpha,\gamma}$ are the parameters for the 6–12 Lennard-Jones potential, q_α and q_γ are the charges of the ions, and ε_{bulk} is the dielectric constant of bulk water. The local dielectric constant of the water in the interior of the pore may be extracted from atomistic simulations, but it is usually assumed to have the bulk value of 80. Solvation effects can be approximately described by including a short-range solvation potential,[55,287,486] but that is rarely done in practice. A web-based interface for GCMC/BD simulations of ion channels has recently become available.[268]

Early BD studies were performed using one-dimensional representations of channels.[487] Later, these were extended to more realistic three-dimensional geometries, though these often lacked atomic detail.[63,486] However, the X-ray structure of an ion channel can be used to create a more realistic model of the channel by computing electrostatic and core repulsion potential maps from the all-atom structure. Brownian dynamics simulations have been applied to several biological channels including OmpF,[55,62–64] K+ channels,[110–115,117] α-hemolysin,[88,95] VDAC,[268] and gramicidin.[16,17] Roux and coworkers have developed a grand canonical Monte Carlo/Brownian dynamics (GCMC/BD) method[62,63,103] to allow for fluctuations in the total number of ions in the system and asymmetric ion concentration conditions. For detailed treatment of the subject, interested readers are directed to a review of the computational methods.[299,473]

Recently, Comer and Aksimentiev[373] used all-atom MD to determine full three-dimensional PMF maps at atomic resolution for ion-ion and ion-biomolecule interactions, thereby fully accounting for short-range effects association with solvation of ions and biomolecules. Using such full 3D-PMFs in BD simulations of ion flow through a model nanopore containing DNA basepair triplets yielded ionic currents in close agreement with the results of all-atom MD but at a fraction of the computational cost. The authors indicate that such atomic-resolution BD method can be developed further to incorporate the conformational flexibility of the pore and DNA by altering the PMF maps on-the-fly.

4.3 All-atom molecular dynamics

The all-atom MD method can provide unparalleled insight into the physical mechanisms underlying biological function of biomacromolecules. By explicitly describing all the atoms of the system of interest and the majority of interatomic interactions, this method has the potential to compete with experiment in completeness and accuracy of description of microscopic phenomena. In the case of an ion channel, one can, in principle, directly observe ion conductance and gating at the spatial resolution of a hydrogen atom and the temporal resolution of single femtoseconds. Critical to the above statement is the assumption that the all-atom MD method is equipped with a correct description of interatomic interactions and enough computational power is available. Despite ever-increasing availability of massive parallel computing platforms, making quantitative predictions using MD remains challenging, in part due to imperfections of the inter-atom interaction models. Below we briefly review the formulations of the all-atom MD method and describe recent advances in the field.

4.3.1 General formulation of the all-atom MD method—In MD simulations of biomacromolecules, atoms are represented as point particles, and the connectivity (or covalent bonds) among those atom are given *a priori*. Covalently bonded atoms interact with each other through bonded potentials, while the other atom pairs interact through nonbonded potentials:

$$U(\mathbf{r}^N) = U_{\text{bonded}}(\mathbf{r}^N) + U_{\text{nonbonded}}(\mathbf{r}^N), \quad (16)$$

where $\mathbf{r}^N$ denotes the coordinates of N atoms in a system. Bonded interactions model quantum mechanical behavior of covalently connected atoms by means of harmonic bond, angle and improper dihedral angle restraints, and periodic dihedral angle potentials:

$$U_{\text{bonded}} = \sum_{\text{bonds}} K_b(b-b_0)^2 + \sum_{\text{angles}} K_\theta(\theta-\theta_0)^2 + \sum_{\text{torsions}} K_\chi\{1+\cos(n\chi-\delta)\} + \sum_{\text{impropers}} K_\varphi(\varphi-\varphi_0)^2, \quad (17)$$

where K_b and b_0 are the bond force constant and equilibrium distance, respectively; K_θ and θ_0, the angle force constant and equilibrium angle, respectively; K_χ, n, and δ, the dihedral force constant, multiplicity and phase angle, respectively; K_ϕ and ϕ_0, the improper force constant and equilibrium improper angle.[488] The nonbonded potential usually consists of Lennard-Jones (LJ) potential for van der Waals interactions and Coulomb potential for electrostatic interactions:

$$U_{\text{nonbonded}} = \sum_{\text{nonbond}} \left\{ 4\varepsilon_{ij}\left[\left(\frac{\sigma_{ij}}{r_{ij}}\right)^{12} - \left(\frac{\sigma_{ij}}{r_{ij}}\right)^6\right] + \frac{q_i q_j}{\varepsilon r_{ij}} \right\}, \quad (18)$$

where ε_{ij} is the well depth; σ_{ij}, the finite distance at which the LJ potential is zero; r_{ij}, the interatomic distance; $q_{i,j}$, atomic charges. The bonded parameters are empirically calibrated based on the quantum mechanical calculations of small molecules, whereas the nonbonded parameters are mainly derived from quantum chemistry calculations (*e.g.*, partial charges) and empirical matching of thermodynamic data (*e.g.*, hydration free energy).

A biomolecular force field is a set of bonded and nonbonded parameters defined in Eq. (17) and Eq. (18). Presently, several biomolecular force fields exist. The force fields can be categorized into types based on whether all the atoms are explicitly treated or not. All-atom force fields, which include CHARMM,[489] AMBER,[490,491] and OPLS-AA,[492,493] treat all atoms explicitly. In the united-atom force fields (*e.g.*, GROMOS[494,495]), some nonpolar hydrogen atoms are neglected.

For the simulations of channel proteins, a lipid force field is as important as a protein force field because the channels are embedded in lipid bilayers. Among the all-atom force fields, the CHARMM force field includes parameters for lipids; the latest update at the time of writing this review is CHARMM36.[496] Together with the AMBER force field for the protein, the general all-atom AMBER force field (GAFF) can be used to describe the lipid bilayer.[497,498] Officially, OPLS does not include lipid parameters. Among the united-atom force fields, GROMOS comes with lipid parameters.[499] Berger *et al.* reported an improved GROMOS-based lipid parameters based on the condensed phase properties of pentadecane.[500] This lipid force field has been widely used in combination with other protein force fields such as AMBER, OPLS, and GROMOS.[501] For the in-depth review of various force fields, we refer interested readers to a comprehensive review by Mackerell.[488]

4.3.2 Ion channels in native environment—Unlike soluble proteins that are surrounded only by water, ion channel proteins are embedded in a lipid bilayer and therefore are in contact with both water and lipids. Due to drastically different chemical and electrostatic properties of lipid and water, proper descriptions of protein-lipid and protein-water interactions are key for the successful simulation of a membrane channel. To model ion conduction through a relatively rigid channel (*e.g.*, gA or KcsA channel), it is possible to use an implicit solvent model of the channel's environment, in which the volume occupied by lipid and water is treated as continuum media of dielectric constants 2 and 78, respectively.[299] However, when interactions between a channel and a lipid membrane are significant (*e.g.*, in mechanosensitive channels), explicit modeling of lipid molecules is essential.

The tails of lipids are long and equilibrate slowly, making it significantly more difficult to assemble a model of a channel embedded in an explicit lipid bilayer than a model of a fully soluble protein. Usually, the system setup involves the following steps. Starting from a pre-equilibrated and solvated lipid bilayer membrane, one makes a pore in the bilayer by deleting a minimal number of lipid molecules so that the protein can fit. Next, an all-atom model of the protein is placed in the pore, which is followed by energy minimization and equilibration of the system using the MD method having the channel's coordinates restrained to their crystallographic values. Finally, when the protein-lipid interface is well equilibrated, one can perform a production run without applying restraints on the channel. For detailed step-by-step instructions for building atomic-scale models of ion channels in lipid bilayer environment, interested readers are directed to a tutorial about MD simulations of membrane proteins.[502] Even though a fully automated procedure is not yet available, several programs can assist a beginner in building a new system. VMD[503] contains the Membrane Builder plugin. Jo *et al.* has a web-based service, CHARMM GUI Membrane Builder (http://www.charmm-gui.org/input/membrane).[504,505]

An alternative method for creating an all-atom model of an ion channel in its native environment is to first carry out self-assembly simulations using a coarse-grained (CG) MD method.[74,165,379] The main difference between the CG and all-atom MD methods is the level of detail used to describe the components of the system. Typically, one CG bead represents about 5–10 atoms. Being much more computationally efficient (and lower resolution), the CG model allows millisecond-time scale simulations on commodity computers. Interested readers are directed towards recent reviews on this subject.[506–508]

In the CG simulations of self-assembly, CG models of lipids, solvent and a membrane protein are placed with random positions in desired proportions. During the course of a CGMD simulations, the lipid molecules spontaneously form a lipid bilayer around a protein. After obtaining a stable model, the CG model can be reverse-coarse grained into a fully atomistic model (see, for example, a study by Maffeo and Aksimentiev[330]). A great

advantage of this approach is that it requires no a priori knowledge of the position of the membrane channels relative to the membrane. An obvious disadvantage is that one has to have a reasonable CG model to carry out the self-assembly simulations and a reliable procedure to recover the all-atom details from the final CG model. Currently, it is not possible to use a CG approach to model ion conductance through large membrane channels due to inaccurate treatments of the membrane and water electrostatics in most CG models. However, work to improve CG methods is ongoing,[509,510] and such simulations should become possible in the near future.

4.3.3 Homology modeling—Usually, an all-atom MD simulation of a channel protein can be performed only when an atomic-resolution structure of the channel is available. This requirement severely limits application of the MD method. Fortunately, membrane channels of different organisms often have similar aminoacid sequences. The sequence similarity can be used to build an all-atom model of the channel that does not have an experimentally determined structure through a procedure called homology modeling.[511] Briefly, homology modeling proceeds as follows. First, a sequence alignment between a target sequence and a homologous sequence—for which a structure is known—is performed. Second, the secondary structures (*e.g.*, *α*-helices and *β*-sheets) of the target sequence from the homologous sequence are built. Finally, loops connecting the secondary structures are modeled and the overall structure is refined. There exist many tools for the homology modeling (*e.g.*, Modeller by Sali *et al.*[511]).

The homology modeling method has been successfully used for building initial structures of several ion channels for subsequent all-atom MD simulations. Capener *et al.*[512] built an inward rectifier potassium channel (Kir) based on a high-resolution structure of KcsA.[1] Sukharev *et al.* used the crystal structure of *Mycobacterium tuberculosis* MscL[407] to model closed, intermediate, and open structures of *Escherichia coli* MscL.[231,232] Law *et al.* combined the crystal structure of the *Lymnea stagnalis* acetylcholine binding protein and the EM structure of the transmembrane domain of the *torpedo electric ray* nicotinic channel to build an entire human nicotinic acetylcholine receptor.[213]

4.3.4 Free energy methods—Perhaps the greatest disadvantage of the MD method is that simulations are costly and are currently limited to the microsecond time scale—a duration insufficient to observe statistically significant numbers of most biologically relevant processes, such as gating or ion permeation events for most channels. Very often, a researcher is interested in the free energy difference between two conformational states of the system as well as the free energy landscape that the system must traverse to transition between the states. For this landscape to be well defined, an order parameter x that describes when the system is in one of these states must be identified. Then, the free energy along this order parameter is just the potential of the mean force (PMF) $W(x)$ experienced by the system at any given value of x. By definition,

$$W(x) = W(x^{\star}) - k_B T \log \left[\frac{\langle \rho(x) \rangle}{\langle \rho(x^{\star}) \rangle} \right].$$

$\langle \rho(x) \rangle$ is the average distribution function and $x^{\star}$ and $W(x^{\star})$ are arbitrary constants, usually representing the bulk with $W(x^{\star}) = 0$.[513] The PMF can be calculated from brute-force all-atom simulations simply by observing the fraction of time x dwells at a particular value, and building a histogram to estimate $\langle \rho(x) \rangle$. In practice, such simulations do not efficiently sample x and are, therefore, too computationally demanding to enjoy regular use.

Fortunately a host of techniques have been developed for the purpose of calculating the PMF. Interested readers are directed to recent comprehensive reviews on this subject.[514,515]

One of the most important and widely used methods for obtaining the PMF is the umbrella sampling method, which is employed to enforce uniform sampling along one or more order parameters. Typically, external potentials are used to restrain the system about the specified values of the order parameters in an ensemble of equilibrium simulations.[516] The effect of the restraining potentials can be removed and data from multiple simulations combined to construct the potential of mean force (PMF) along the order parameter by using the Weighted Histogram Analysis Method (WHAM).[517] This method is widely considered a gold standard against which other PMF-producing methods are compared, though the simulations are generally recognized as being rather costly to perform.

A similar method, free energy perturbation (FEP), allows one to estimate the free energy difference between two similar systems. In practice, one creates a path from one system to the other that can be taken in small discrete steps that connect a series of intermediate states. The small differences in the system's total energy between two adjacent states is averaged to obtain the free energy change for the step connecting the states. These small free energy changes are summed to find the total free energy difference between the systems.[518,519] The FEP method is, in principle, very flexible and can be used to find the free energy of enforcing a restraint upon the system, allowing one to estimate the PMF. In practice, the umbrella sampling method is easier for finding the PMF, but FEP can be applied to problems beyond the scope of umbrella sampling. For example, using FEP one can model the effect of rather abstract changes to the system, including the free energy required to create or destroy atoms, or to mutate atoms from one type to another. Such procedures must carefully consider the complete thermodynamic cycle for the results to remain physically meaningful.

Other equilibrium methods for finding the PMF exist, but it is also possible to estimate the PMF from non-equilibrium simulations.[520–526] For example, during a steered MD (SMD) simulation, one end of a spring is tethered to an atom and the other end of the spring is pulled at a constant velocity. The force applied on the atom is recorded, allowing one to estimate the PMF using the Jarzynski equality,[527] which averages the work over a large ensemble of simulations.

4.3.5 Ionization states of titratable groups—There are numerous examples demonstrating that channel gating and ion conductance depend on the ionization states of several key residues (typically, Asp, Glu, and His) of the channel.[70,71,84,118,124,127,528,529] Therefore, assigning correct ionization states to titratable amino acid groups is critical to successful MD simulations of ion channels. For the titration process shown in Figure 8 (R^- + H^+ ⇌ RH), the equilibrium constant, K_a and pK_a are defined by

$$K_a = \frac{[R^-][H^+]}{[RH]} \quad (19)$$

and

$$pK_a = -\log\frac{[R^-]}{[RH]} + pH \quad (20)$$

where Eq. (20) is the *Henderson–Hasselbalch equation*. Eq. (20) indicates that the relative populations of ionization states depend on both pK_a of the group and *pH* of the environment. For example, a titrating group with $pK_a = 7$ in water has a 50% chance of being in a protonated state at $pH = 7$. Because the pK_a of all amino acids in water is known, determining ionization states of amino acids in water at a given pH is trivial. However, determining the ionization states of amino acids buried in a protein or a membrane is nontrivial because the pK_a significantly depends on the local environment.[475,530]

Figure 8 illustrates a thermodynamic cycle that is used for the calculation of a pK_a shift.[475,530] Here, ΔG and ΔG_{ref} indicate the free energy difference between two ionization forms of a titratable group in water and in protein or membrane environment, respectively, whereas ΔG_1 and ΔG_2 indicate the transfer free energy of RH and R$^-$ from water to the protein or membrane environment, respectively. In a given environment, one can estimate the probability of observing two ionization states RH and R$^-$ if ΔG is known:

$$\frac{[R^-]}{[RH]} = e^{-\Delta G / k_B T}. \quad (21)$$

However, accurate calculation of ΔG is nontrivial even in pure water because the protonation process involves various free energy components such as transfer of a hydrogen ion from water to the vicinity of a protein, formation of a bond between the hydrogen and a protein, and charge redistribution after the bond is formed.[475,530] Instead, one calculates the difference between ΔG and ΔG_{ref}, $\Delta\Delta G = \Delta G - \Delta G_{ref}$. Then, the pK_a of an ionizable residue buried in a protein or a membrane is obtained as

$$pK_a = pK_{a,ref} + \frac{1}{2.303 k_B T} \Delta\Delta G, \quad (22)$$

where $pK_{a,\,ref}$ is the experimentally determined pK_a in water. Calculating $\Delta\Delta G$ instead of ΔG is convenient because one can usually assume that non-electrostatic components cancel out and $\Delta\Delta G$ can be approximated by a simple charging free energy using either an all-atom force field or continuum electrostatic model.[475]

Usually, $\Delta\Delta G$ is computed by performing free energy calculations (*e.g.* FEP, see Section 4.3.4) in water (ΔG_{ref}) and in protein or membrane environment (ΔG) and taking the difference between them. An alternative method of computing $\Delta\Delta G$ (and hence the pK_a shift) is to perform PMF calculations to obtain transfer free energies, ΔG_1 and ΔG_2 (see Figure 8), utilizing the following equality: $\Delta\Delta G = \Delta G - \Delta G_{ref} = \Delta G_2 - \Delta G_1$. Therefore, one can calculate $\Delta\Delta G$ by performing two PMF calculations for RH and R$^-$ and taking the difference between them. A series of pK_a shift calculations of model amino acids in the membrane environment demonstrated how those two different methods can be used consistently to determine the ionization states of amino acids.[531–536]

While free energy calculations using atomistic MD simulations are the most rigorous way to estimate the pK_a shift, this approach is computationally expensive. Alternatively, pK_a shifts can be more efficiently calculated using continuum electrostatic models such as the PB theory,[91,537–547] see Section 4.1.1 for details. In the continuum electrostatic framework, membrane and water can be represented as continuum media with dielectric constants of ~80 and <10, respectively,[548,549] and the pK_a shifts can be computed using popular computer codes for numerically solving the PB equation such as DelPhi[476] and APBS.[477]

Several web applications automate such pK_a shift calculations, including H++,[550] PROPKA[551] and PBEQ-Solver.[552]

4.3.6 Accelerated molecular dynamics simulations using a special-purpose machine—Presently, the practical time scale of a continuous all-atom MD simulation is, at most, several microseconds, much shorter than the duration of typical biologically important processes, even when using state-of-the-art supercomputers and MD codes. Recently, D. E. Shaw and coworkers demonstrated that millisecond all-atom MD simulations can be performed by using Anton, a special-purpose hardware designed only for MD simulations.[553–556] Such a groundbreaking advance in MD simulation technique equipped with an accurate model for biomolecules might indeed lead to a "computational microscope", with which one can observe biochemical processes at spatial and temporal resolutions unreachable by any experimental method.[553,556] Indeed, Anton is named after Anton van Leeuwenhoek, an early microscopist who made great advances in the field.

Every modern computer, including Anton, utilizes a parallel architecture—a simulation is performed using multiple computational nodes that communicate with one another. Thus, overall performance depends on not only the computation speed of each node but also communication speed. The Anton developers accelerated the computation speed by designing an application-specific integrated circuit (ASIC) that is optimized to almost all common routines used in MD simulations, including computation of nonbonded and bonded forces, computation of long-range electrostatic interactions, constraints of chemical bonds, and integration of Newton equation. To enhance the communication speed, they optimized the network within an ASIC as well as between ASICs to the common communication patterns of MD simulations. Detailed information on the design of Anton can be found in a recent publication.[553]

Since Anton went into production, D.E. Shaw and coworkers have demonstrated the potential of special-purpose machine to revolutionize computational studies of ion channels. Anton's unique ability to probe biologically relevant time scales has led to a number of discoveries. For example, they have shown explicitly how a voltage-gated potassium channel (KV) switches between activated and deactivated states;[183,196] successfully simulated drug-binding and allostery of G-protein-coupled receptors (GPCRs) in collaboration with several experimental groups;[557–559] identified Tyr residues that are responsible for the low permeability of Aquaporin 0 (AQP0) compared to the other aquaporins;[560] and revealed the transport mechanism of Na^+/H^+ antiporters (NhaA) showing that the protonation states of three Asp residues in the center of the channel are essential.[529] Anton has shown the tremendous advantages of special-purpose hardware for MD simulation, and there is little doubt that more such machines will be developed and lead to even more illuminating discoveries.

4.4 Polarizable models

All currently popular force fields represent non-polarizable models of biomolecules and use fixed atomic charges. However, there are several known issues that can possibly limit the application of such non-polarizable force fields to simulations of channel proteins. First, the electrostatic environment in a channel can be drastically different from that in the solvent environment. For example, the selectivity filter of KcsA consists of carbonyl oxygens, and the filter is occupied by only a few ions or water molecules.[1] Thus, the parameters describing ion-carbonyl interactions that were empirically calibrated in the solvent environment could cause artifacts when used in the selectivity filter, which was pointed out by Noskov *et al.*[141] Second, the dielectric constant of lipid hydrocarbons with non-polarizable force fields is 1, a factor of two less than in experiment.[561] The twofold

underestimation of the dielectric constant doubles the energy barrier for an ion crossing a membrane.[424] In the PMF studies of ion conductance through a gramicidin channel,[29,30] Allen *et al.* proposed to correct for this artifact *a posteriori*, however, a polarizable force field could be a much better solution. Third, multivalent cations such as Mg^{2+} and Ca^{2+} are difficult to describe using a non-polarizable model because their high charge density induces polarization of water in the first solvation shell.[562,563] Therefore, a polarizable model might be essential in MD simulations of channels permeated by divalent cations. Fourth, spatial separation of positively and negatively charged groups in lipids creates a dipole along the membrane normal that deviates considerably from experimental estimations when computed from all-atom simulations.[564] Harder *et al.* pointed out that this artifact arises from the lack of polarizability by showing that the agreement with the experiment is significantly better when employing a polarizable model.[565]

Motivated by the apparent limitations of the current non-polarizable models, many research groups proposed various polarizable models.[566] However, developments of those polarizable models are still at the initial stage, and the application of polarizable models to the channel proteins is still limited. The two most practical polarizable models of biomolecules are the Drude oscillator and AMOEBA force fields.[566] Ponder and co-workers developed the AMOEBA force field, in which molecular polarization can be achieved by using permanent atomic multipoles.[567–569] Equipped with an analytic solution that treats intramolecular polarization, the AMOEBA force field can deal with flexible molecules such as peptides and lipids.[567] Even though the AMOEBA force field is not ready for all biomolecules (*e.g.*, lipid), it shows promising results; for example, reproducing structural and thermodynamic data such as solvation structure and solvation free energy of small drug-like molecules [569] and ion solvation.[568]

In the classical Drude oscillator model (*e.g.*,[570]), polarization is achieved by a charge harmonically bound to an atomic center. In the presence of an electric field, the mobile charge oscillates around a position slightly displaced from the atomic center, inducing a dipole moment. By using the Drude model, several promising results have been reported. For example, the description of monovalent and divalent cations is improved,[563] and hydration free energies of small molecules can be calculated more accurately.[571] However, as for the AMOEBA force field, the application of the Drude oscillator model is currently limited to small molecules in an aqueous solution. Thus, the polarizable models must be further developed and tested before they can be applied to an ion channel system.

Although it will take some time for the polarizable models to replace the currently popular non-polarizable models, especially for the simulations of channels, there already have been meaningful attempts to test the polarizable models in the membrane environment. For example, Vorobyov *et al.* applied the Drude oscillator model to calculate the transfer free energy of an arginine analogue to the lipid bilayer and compared the results with those from the non-polarizable models.[572] More recently, Wang *et al.* used the Drude oscillator model in combination with a non-polarizable model to study the transfer of ammonium through an ammonium transporter.[277] In this study, ammonium, water, and side chains were treated using the polarizable model to better describe the less aqueous character of the channel while the other parts were treated using the non-polarizable model. The successful demonstration of such a hybrid approach is a very promising development that will likely grow in popularity until full polarizable simulations become feasible.

5 Typical questions of interest

Ideally, a simulation study of an ion channel would provide a comprehensive description of all aspects of the channel's function. In reality, computational studies are limited by the

accuracy of the methods chosen, the availability of computer resources, and experimental knowledge of the system. Among the many topics that could be probed about the function and biological role of an ion channel, we focus on the following four: ion binding sites and permeation pathways, ionic conductance, selectivity and gating. The fifth subsection of this section details the use of computational methods in biosensing applications of ion channels. Although all five can be integral parts of the same ion transport mechanism, such division is possible, in part, due to the separation of the time scale amenable to a particular modeling method and the corresponding physical time scale. Thus, for some channels, the time scale of 100 ns is sufficient to observe selective ionic transport, whereas for the other channels this time scale is barely sufficient to determine the most probable locations of ions. In general, the experimental conductance of an ion channel gives a good estimate of the time scale of ion permeation events and can be used to choose an adequate simulation method.

5.1 Ion binding sites and permeation pathways

To understand the microscopic details of ion selectivity and conductance, one must know where ions are likely to be in the channel. The density of ions in a channel can be obtained through all-atom simulation and is directly related to the potential of mean force (PMF). The PMF is enormously valuable because it plainly exposes the pits and barriers an ion must traverse during its journey across a membrane. The PMF may yield significant insights into the specificity of a channel for certain ionic species, and it can support conjectures regarding the impact of the protein structure on ionic conductance. Binding of multivalent ions can alter the structural features of a membrane channel[573] and influence the outcome of structure determination studies.[574,575]

5.1.1 Potassium selective channels—Potassium ion permeation across cell membranes has a long history of quantitative study. Hodgkin and Keynes found a relation between the ratio of K^+ ions flowing into and out of a cell and the voltage difference across the cell membrane which described the data across a wide range of intra and extracellular K^+ concentrations with only one free parameter, *n*.[576] Seeking a theoretical explanation for the excellent fit of their heuristic equation, they proposed the "knock-on" model in which K^+ ions move single file through a chain of $(n − 1)$ K^+ occupied sites, colliding with one another so they all move in a concerted fashion. Hodgkin and Keynes found that the channel is occupied by 2–3 K^+ ions. Their explanation is remarkably close to the mechanism revealed through X-ray crystallography and scores of simulation studies, which showed that the selectivity filter includes four binding sites usually occupied by two ions with a third ion sometimes present near one of the two openings (see Figure 9).

Simulation studies of the KcsA K^+ channel have employed a broad spectrum of methods to study occupancy of the selectivity filter by a set of ions. The most used is the umbrella sampling method, described in Section 4.3.4.

The three-ion PMF for the process of ion permeation through the KcsA filter was obtained in 2001.[126] The PMF allowed the authors to identify concerted transition pathways for the ions, demonstrating that the shallowest pathways for permeation involved concerted motions of pairs of ions. However, pathways involving all three ions were also observed with barriers that were ~1 kcal/mol larger than pathways involving only two ions. The simulations revealed which of the binding sites were most attractive to K^+. A subsequent SMD study confirmed the concerted motion of pairs of K^+ ions in the selectivity filter.[164]

In 2008, a study compared several methodologies for finding the PMF, namely SMD in conjunction with the Jarzynski equality (JE), umbrella sampling, and another free-energy calculation technique called metadynamics.[176] Metadynamics belongs to a class of newer enhanced sampling protocols in which the system is pushed away from regions of phase

space that have already been sampled.[577–579] All of these methods seek to map the free energy along one or more coordinates, though SMD is inherently one-dimensional. A typical choice for studies of single-file ion permeation is the position of one or more ions along the pore axis.

The PMFs of ion permeation through KcsA obtained from SMD and umbrella sampling simulations were qualitatively similar and revealed overlapping minima and maxima.[176] The results obtained using these two methods were found to be sensitive to the conformation of the residues in the filter and the position of the ion in the cavity just outside the filter, which could change on the time scale of the simulations. The PMFs obtained using the SMD method were created by combining data from multiple simulations, demonstrating the advantage of increased parallelization. However, for such an approach to be valid, individual simulations should be sufficiently long to average over conformational fluctuations. Unfortunately, the authors did not sample equivalent amounts using these two methods, and thus a direct comparison could not be obtained. In general, the SMD method results in a PMF that has barriers considerably larger than those determined from umbrella sampling simulations.

5.1.2 gramicidin A—For details of the history of gramicidin A in all-atom simulation, we refer interested readers to recent reviews.[21,39] Here, we highlight the methodologies used to study ion channels that have been validated using gramicidin A.

The first applications of quantitative MD methods to the study of ion channels were free energy perturbation calculations (FEP; see Section 4.3.4) on gramicidin A, which provided significant insight into the ion translocation process. The first such study was performed over twenty years ago and compared the solvation free energy of a Na^+ ion in gramicidin A at different positions in the pore to the solvation free energy in bulk solution.[18] The results of this study can be considered as a low-resolution PMF that indicated a series of rather large (~5 kcal/mol) pits and barriers within the channel. Another FEP study determined the relative solvation free energy for Na^+ in a singly-and doubly-occupied gramicidin A relative to bulk water.[19] The Na^+ ions were then mutated into the other four common monovalent cations. These calculations demonstrated that small ions are less likely to doubly occupy gramicidin A compared to large ions, agreeing with experiment and supporting the validity of the underlying model. The umbrella sampling method was recently used to determine a two-ion PMF, demonstrating that double occupancy in gramicidin A is not favorable.[46]

Single ion permeation through gramicidin A has since been studied numerous times using the umbrella sampling[35,41,50,51] and SMD[38,42,43,48] methodologies. Studies employing the umbrella sampling[50] and SMD[48] approaches have cautioned that extensive simulations are needed to obtain complete convergence using either method. Sampling on the order of hundreds of nanoseconds may be required to achieve the convergence irrespective of the chosen method, although unidirectional SMD simulations were found to exhibit severe hysteresis in relatively short simulation when compared to umbrella sampling.[41]

5.1.3 Others Channels

PLN: The uptake of Ca^{2+} by Ca^{2+}-ATPase is regulated by the membrane protein phospholamban (PLN), which acts as an inhibitor. Although more than 75% of PLN in a lipid bilayer membrane is pentameric, the only known function of PLN, i.e. Ca^{2+}-ATPase inhibition, involves a PLN monomer and not a pentamer, though there were a few experimental reports of ion conductance involving PLN.[580,581] Using the SMD[330] and the umbrella sampling[345] methods, it was recently shown that the channel-like NMR model of the PLN pentamer does not conduct ions, in agreement with more recent experimental studies.[582]

VDAC: The Im group carried out all-atom MD study of the human VDAC1 to characterize the ion permeation and selectivity of the pore.[262] The study revealed that negatively charged Asp and Glu residues serve as traps for K^+ ions as they pass through the channel. The one-dimensional multi-ion PMF computed for K^+ and Cl^- revealed the reason for the anion selectivity of the channel: a higher free energy barrier for K^+ ions to enter the channel.

OmpF: Im and Roux explored the ion density profiles, and the conductance of the *E. coli* porin, OmpF in a detailed study employing MD, BD and PNP approaches.[55,67] All three approaches revealed distinct ion pathways for K^+ and Cl^- ions through the pore determined by the distribution of charged residues in the porin. The phosphate selective porin, OprP, was recently studied using equilibrium, SMD, and umbrella sampling simulations.[80] The study revealed two negatively-charged phosphate binding sites in the interior of the pore in close proximity to one another, each with a free energy minimum of about 8 k_BT. Findings relating to the preference of OprP for phosphate over Cl^- will be discussed below.

AmtB: Luzhkov *et al.* performed FEP and pK_a calculations (see Sections 4.3.4 and 4.3.5) using all-atom MD simulations to study the interaction of ammonium with the external binding sites and determine the protonation states of ammonium.[278] They concluded that ammonium (NH_4^+) is dominant over ammonia (NH_3) near the external binding sites and that deprotonation can occur only inside the channel. Bostick *et al.* also performed free energy calculations using all-atom MD simulations.[275,276] By calculating the transfer free energy of both ammonium and ammonia, they showed a possible transport mechanism of ammonium through the channel. Moreover, they emphasized the importance of dehydration in the channel for the deprotonation of ammonium. Most recently, Wang *et al.* used hybrid polarizable mechanics/molecular mechanics (PM/MM) simulations and hybrid quantum mechanics/molecular mechanics (QM/MM) simulations to elucidate the permeation mechanism of both ammonium and protons.[277]

ClC: Cohen and Schulten[260] explored the mechanism of anion conduction across the ClC chloride channel by PMF calculations using atomistic simulations. The resulting PMF revealed that the energy barrier for conduction of a single Cl^- ion is prohibitively high. Interestingly, the energy barrier was reduced to 4 kcal/mol in the presence of two Cl^- ions in the pore, suggesting that the incoming Cl^- pushes the central Cl^-. Suenaga *et al.* performed all-atom MD simulations to test the hypothesis that ClC channels are H^+–Cl^- exchange transporters. Their results suggested that cations such as H^+ and Na^+ facilitate the channel opening and Cl^- conduction.[261] Chung and coworkers utilized BD and MD simulations to reveal the binding site of Cl^- in the channel, the electrostatic barrier of Cl^-, and the gating by an external Glu residue in atomistic detail.[265,266] Recently, the first eukaryotic ClC transporter was crystallized,[583] and Cheng *et al.* compared the Cl^- transport through the eukaryotic channel with that through the prokaryotic channel.[264] Their PMFs of Cl^- in the channel suggested that proper protonation of the external Glu gate is critical for conduction.

5.2 Ion conductance

The force driving the permeation of ions through an ion channel is the transmembrane potential arising from an unequal distribution of ions on the two sides of the membrane. A small charge imbalance in the vicinity of the pore gives rise to the potential difference.[173] Explicit modeling of such charge imbalance is difficult in all-atom MD simulations of a single bilayer system as such simulations usually employ periodic boundary conditions, so that the solution found at the two sides of the membrane is one continuous volume. One possibility is to use a single bilayer and two electrolyte compartments terminated by a vacuum/water interface.[329] An alternative approach is to use a twin bilayer system that includes two solution phases[584] of unequal ionic makeup that can generate a transmembrane

electric field solely based on ion dynamics. In early studies employing the twin bilayer setup, the two membranes were used to define the compartments of different ion concentration. A transmembrane potential was established due to a small charge imbalance between the two compartments, which was sufficient to generate short, unsustained ion flux through the membrane channels. To produce a continuous ion flux, the charge imbalance between the two compartments has to be maintained. Kutzner *et al.* recently demonstrated a method to exchange ion/water pairs between the compartments and thus sustain the charge imbalance.[339] This method was applied to bacterial porin PorB of *Neisseria meningitis* to determine the ion conductance and selectivity of the porin.

The double membrane approach, however, requires larger systems, which significantly increases the computational overhead. A simpler alternative is to apply an external electric field normal to the membrane to generate ionic flux through the pore. Despite the apparent artificiality of the method, Roux[173] provided a rigorous theoretical framework for this strategy. An early study by Crozier *et al.*,[289] in which the flow of sodium ions was simulated through a simplified channel-membrane system under an imposed electric field, demonstrated the feasibility of modeling an ionic current through a membrane. In 2005, Aksimentiev and Schulten[90] showed that the current–voltage relationship of *α*-hemolysin could be directly computed from all-atom MD simulations by applying an external electric field. The multi-nanosecond trajectories obtained in this 2005 study firmly established all-atom MD as the method of choice for exploring conductance properties of nanopores and using MD simulations to guide the development of nanopore sensors.[585] A similar approach was later applied in the studies of MscS by Sotomayor *et al.*[244] and E. *coli* porins OmpF and OmpC by Pezeshki *et al.*[79,81] A recent study provides a detailed description of the external electric field approach.[346]

5.2.1 Potassium channels—MD simulations of K^+ translocation through the selectivity filter of Kv1.2 allowed for direct observation of the "knock-on" mechanism during a small number of permeation events.[151] Subsequent brute-force simulations permitted estimation of the channel's conductance at several transmembrane biases.[151,183] The simulated conductance was found to be nearly three times larger than the experimentally measured one. The discrepancy could be partially attributed to a domain that was missing in the simulated structure and may obstruct ion access in experiment. The simulations determined a five-step map of the translocation cycle, which was in agreement with the cycles proposed from multi-ion free energy calculations.[126] The brute-force approach allowed for direct observation of the kinetics between these steps, identifying dehydration of the incoming K^+ ion as the rate-limiting step of ion transport through the selectivity filter.

5.2.2 Mechanosensitive channels—Among the two bacterial mechanosensitive channels with known high-resolution structure (MscL and MscS), MscS has been the subject of ion conductance studies for several reasons. The conductance of the open MscL channel was experimentally determined to be fairly large, suggesting the pore diameter of up to 30 Å.[231,232] Through such a wide channel, small solutes can pass almost freely, making the study of ion conductance less interesting. In contrast, the first MscS conformation reported by Bass *et al.*[408] had been initially thought to capture the channel in an open, ion conducting form. However, subsequent computational studies determined that the transmembrane channel in that MscS structure was not wide enough to furnish a fully hydrated transmembrane pore.[241,242]

Anishkin *et al.* and Sotomayor *et al.* performed pioneering MD simulations of MscS.[241,242,247] In their all-atom MD simulations, they characterized the structural stability of MscS based on the structure determined by Bass *et al.*[408] The simulations revealed partial collapse of the pore, suggesting that the MscS conformation was, at best, partially open. The

simulations examined the distribution of water and ions in the channel, revealing dehydration of the narrowest part of the transmembrane pore. Anishkin *et al.* also performed SMD simulations by pulling a chloride ion along the channel, concluding that the pore was not large enough for the conductance of chloride.[242] Vora *et al.* studied ion conductance through MscS using the BD method, also concluding that the pore in the crystal structure of MscS was not large enough for that structure to represent a fully open conformation.[229]

Unlike the previous studies, in the all-atom MD simulations of Spronk *et al.*,[243] an external electric field was applied, mimicking the physiological transmembrane potential. In the latter study, the authors observed an increase in hydration and ion conduction through the channel, suggesting that the crystal structure captured a conformation close to an open state. Subsequently, Sotomayer *et al.* also reported an increase of the MscS pore radius upon the application of large transmembrane potential (1.2 V) in an all-atom MD simulation.[244]

Recently, Vásquez *et al.* proposed fully closed and open conformations of MscS based on electron paramagnetic resonance spectroscopy and all-atom MD simulations.[256,257] In this open MscS conformation, the pore diameter was about 10 Å throughout the channel, which is large enough to yield a conductance consistent with the experimental measurements.

MscS has a large balloon-like cytoplasmic domain, which might play an important role in ion conductance, see Figure 4c. Recently, Gamini *et al.* probed ion conductance through the pores in the cytoplasmic domain using Glu^- and K^+ as model ions.[248] Their results suggested that the cytoplasmic domain is a molecular sieve that balances effluxes of Glu^- and K^+ through MscS.

The conductance of MscS has also been modeled using continuum electrostatics methods (see Section 4.1). For example, Sotomayor *et al.* used atomistic MD simulations to generate multiple conformations of the channels and the continuum transport theory to compute the ionic current for these conformations.[258,586] Recently, Song *et al.* calculated the ionic currents through MscS using a simplified Nernst-Planck (NP) theory and rather realistic BD simulations.[225] The study has shown the ability of the NP theory to reproduce the results of the corresponding BD simulations.

5.2.3 α-Hemolysin—Noskov and coworkers[88] explored the current-voltage relationship of the *α*-hemolysin channel using GCMC/BD and 3D-PNP approaches (described in sections 4.2.2 and 4.1.2, respectively). One of the inputs for the GCMC/BD study was the position dependent diffusion coefficient of each ion type. To incorporate the effect of the channel size, a reduction factor for the diffusivities was calculated as per Pain and Scherr.[587] The study showed the I-V characteristic to be asymmetric with a higher current at positive bias (with the *trans*-entrance at a higher potential than the *cis*), which was in qualitative agreement with experiments.[588,589] The study also revealed that by switching off the charges on the pore, the asymmetry in the conductance practically disappeared, indicating that it is the charge distribution of the pore that is responsible for the asymmetry rather than the shape.

The MD study by Aksimentiev and Schulten[90] was the first to demonstrate that atomistic simulations can be used to obtain channel conductances with quantitative accuracy. Specifically, the study found the transmembrane currents, driven by an external electric field applied normal to the membrane, to be in excellent agreement with experiment. The large pore diameter and the high salt concentration made direct comparison between simulation and experiment possible. A recent MD study by Bhattacharya *et al.*[93] probed the cation dependent rectification of the *α*-hemolysin nanopore. The rectification of the ionic current was found to dependent on the type of cations and increased from Li^+ to Cs^+, both in

simulations and experiments. The MD simulations showed that the cationic contribution to the ionic current was the dominant factor influencing current asymmetry. The cation type-dependent asymmetry of the ionic current was explained by differential affinity of the cations to the charged residues at the *trans*-entrance of the pore, which modulated the number of ions entering the narrowest part of the pore. Recent experimental studies using site-directed mutagenesis[590] and cysteine-scanning mutagenesis[347] of the *α*-hemolysin channel revealed that the ion-selectivity, gating and conductance properties are significantly affected by the location and the type of charges on the pore.

5.2.4 Outer membrane porins—Over the past ten years, there have been a number of studies addressing ion conductance properties of various OMPs (see Table 1). Im and coworkers carried out pioneering studies of OmpF using a combination of GCMC/BD,[62,63] MD[55,67] and continuum[55] methods. These first studies of OmpF revealed asymmetric character of ionic conductance and produced concentration-conductance relations that were in good agreement with experiment.[55] OmpF was a test-bed for development of the GCMC/BD method.

Using the all-atom MD method, Pezeshki and coworkers explored ion conductance of two structurally similar *E. coli* porins, OmpC and OmpF, over a range of temperatures, pH values and KCl concentrations.[79,81] The results of the MD simulations were in good agreement with experiment at low salt concentrations and room temperature. The authors observed considerable differences between the simulated temperature dependence of conductance and experiment, which was attributed to the MD force field because the latter was optimized for simulations at room temperature. The temperature dependence of the channel's conductance was found to differ from that of a corresponding bulk solution, indicating the importance of ion-pore interactions. Using all-atom MD, Modi and coworkers investigated the temperature-dependent transport of the ionic liquid 1-butyl-3-methyl-imidazolium chloride (BMIM-Cl) through OmpF.[86] The study indicated that aqueous solution of BMIM-Cl can reduce the rate of antibiotics transport through OmpF, which could lead to practical applications of BMIM-Cl in the field of nanopore sensors.

The transmembrane pore of OmpF contains several titratable residues. Hence, its conductance can depend on the solution pH. Varma *et al.* used all-atom MD simulations to determine pK_a (see Section 4.3.5) of several key residues of OmpF.[70,71] The study has shown that the pore size and conductance of OmpF become consistent with the X-ray structure and electrophysiology data, correspondingly, only when appropriate protonation states are assigned to the key Asp residues.[70,71] The study of Vrouenraets *et al.* has investigated the effect of point mutations in OmpF, finding ionization states of the residues to be the key factor affecting the ion conductance.[84]

5.3 Selective permeability

Concentration gradients of different types of ions support a variety of intra- and inter-cellular signals. It is, therefore, vital to have membrane channels that can distinguish and selectively conduct ions of different types. One can easily imagine an electrostatic mechanism for regulating the flux of different ion species based on the ion charge, but what about channels that select a particular ion from all ions of the same charge?

Experimental studies suggesting existence of Na^+ and K^+ selective channels began as early as 1960.[591] By 1971 it had been inferred that the K^+ channel has a wide inner opening leading to a narrow passage, which blocks the passage of large cations. However, the K^+ channel also prefers the conductance of K^+ over Na^+ and Li^+, even though the latter are smaller. The "snug-fit" explanation, offered in 1972,[592] suggested that it is not electrostatically favorable for a Na^+ ion to enter an oxygen-lined cage unless that cage is of

the same size as the Na$^+$ ion; otherwise the Na$^+$ will not form favorable electrostatic contacts compared to its solvation shell. However, the "snug-fit" mechanism requires a rather rigid pore, incompatible with most protein structures, which can only be described as soft and flexible. Given that sodium and potassium appear to differ only on a scale significantly smaller than the size of an atom, it is incredible that *flexible* atomic-scale structures can yield permeabilities for the ions that may differ by a factor of 1,000.[593] The importance of sub-angstrom scale structures and the requirement of distinguishing between various physical factors naturally lend the study of ion selectivity to the all-atom MD methodology.

5.3.1 Potassium channels—The structures of all K$^+$ channels feature a completely conserved constriction called the selectivity filter, which is lined with four rings of negative carbonyl-oxygen groups. The structure of KcsA revealed two K$^+$ ions separated by a single water molecule occupying this region. In K$^+$ channels, the selectivity filter presents a barrier to ion transport and, in general, the larger the barrier, the slower the expected rate of transport. Thus, early MD studies have focused on the free energy difference experienced by K$^+$ and Na$^+$ ions in the selectivity filter. Due to the great similarity of between these ions, the free energy perturbation (FEP) method has been the protocol of choice for such studies.

The FEP method, introduced in Section 4.3.4, can evaluate the free energy cost of transforming one atom into another through an unphysical pathway. Because the end points of this transformation are physically meaningful, the change in free energy is also physically meaningful when considered as a step in a thermodynamic cycle. For example, the difference in binding free energy between K$^+$ and Na$^+$ in an ion channel, $\Delta\Delta G$, can be found from the free energies of transforming the K$^+$ into Na$^+$ inside the channel, and transforming Na$^+$ to K$^+$ in a bulk solution.[123] Both of these terms can be obtained from FEP, however, care must be taken that the FEP simulations are long enough that the system relaxes completely and fluctuations are fully averaged.

Early FEP simulations demonstrated a preference for K$^+$ over Na$^+$ in the selectivity filter of KcsA.[120,123,141,594] However, limited by the computational resources available at the time, these simulations also suffered from problems: small system sizes that treated the lipid bilayer, protein, or water in unrealistic ways; sub-nanosecond durations of simulations at each FEP step; and/or external restraints that enforced crystal structure-like conformation on the selectivity filter. Despite these limitations, the range of values for $\Delta\Delta G$ (5–17 kcal/mol for a single ion) were in apparent agreement with experimental measurements of relief of Ba^{2+} blockades by Na$^+$ and K$^+$.

Recently, a combination of MD simulations and X-ray crystallography suggested that the smaller monovalent cations, Na$^+$ and Li$^+$, have their own binding site in the plane of a carbonyl-oxygen ring of the selectivity filter of KcsA as depicted in Figure 10, rather than between two rings as for K$^+$.[595] Subsequently, one-, two-, three- and four-ion umbrella sampling simulations provided PMFs for a Na$^+$ or K$^+$ ion permeating K$^+$-filled selectivity filters of KcsA and Kir-Bac1.1.[191,596] The authors of one study note that FEP simulations utilizing short trajectories may not provide the ion with enough opportunity to find its preferred binding site, and that such studies likely overestimate $\Delta\Delta G$, which the authors estimated to be 2–3 kcal/mol.[596] Additional umbrella sampling simulations of a Ba^{2+}-occupied filter demonstrated that the results can be quantitatively reconciled with Ba^{2+} blockade measurements because the Na$^+$ and K$^+$ ions are influenced differently by the bound Ba^{2+} ion. Although the latter study[596] has not yet garnered response, it demonstrates the utility of a thorough simulation for interpretation of experimental measurements. Thus, the story of potassium channel selectivity may still be incomplete.

5.3.2 Outer membrane porins—Porins often exhibit selectivity towards specific molecules. For instance, the outer membrane protein OprP of *Pseudomonas aeruginosa*, an analogue of PhoE porin of *Escherichia coli*, is a phosphate selective pore. What is particularly interesting is that it is not just anion selective, but can discriminate between anions. OprP is highly selective towards the permeation of inorganic phosphate (P_i) over other anions from the external environment to the interior of the cell.597 Atomistic simulations performed by Pongprayoon *et al.*[80] employing constant velocity SMD and umbrella sampling demonstrated that a lysine cluster near the periplasmic end of the pore selected ions by binding P_i with greater affinity than small anions such as Cl^-. The periplasmic mouth of the pore can accommodate a fully solvated Cl^- ion, which is therefore dielectrically screened from the positively charged lysine cluster. P_i, on the other hand, is partially dehydrated when it enters the pore at the periplasmic side and therefore interacts strongly with the lysine residues. The extracellular end of the porin, however, allows the passage of both Cl^- and P_i.

Another interesting porin that has been widely studied using computational methods is the moderately cation selective OmpF trimer. The I_{K^+}/I_{Cl^-} ratio obtained from atomistic simulations by Pezeshki *et al.*[79] was found to be approximately 1.2, which is similar to older estimations by Im and Roux obtained from GCMC/BD and PNP approaches.[55] The key to the conductance and selectivity of the porin lies in its structure. One of the loops on the extracellular side, the L3, is of special importance as it folds back into the beta-barrel constricting the channel. Positively charged arginine residues on the wall of the porin face the negatively charged residues on the loop, creating a transverse electric field in the constriction region of the OmpF. This field can orient molecules and cause a separation of ion fluxes.[55,65] Experimental as well as computational studies[83] have shown that it is possible to alter and even reverse the selectivity of the OmpF by mutating the charged residues in the constriction region (both on the L3 loop and the pore wall).

5.4 Ion channel gating and blockages

Proper cellular function requires that ions be released at certain times, but not at other times, and this variable ion conductance is called gating. For example, the mechanosensitive channels in bacteria open to prevent rupture of the cell when tension in the bilayer increases due to osmotic stress. Mechanosensitive channels also initiate the conversion of mechanical vibrations in the inner ear into electrical signals. Similarly, voltage, pH, and ligand induced-gating allow signals to be initiated or propagated depending on the cellular conditions.

Gating almost always involves changes in the conformation of the channel. Until very recently, brute force atomistic simulations of such changes were not possible because of the time scale limitations. Below, we discuss exemplary studies, including mechanical gating of the bacterial mechanosensitive channels of small and large conductance and voltage gating of a K^+ channel. Additionally, we discuss blockades of ion channels caused by neurotoxins, which may have pharmacological significance.

5.4.1 Mechanical gating—Even though several crystal structures of MSCs are available, their gating mechanisms remain elusive. Unlike ligand- or voltage gated ion channels, where gating is triggered by a relatively local structural change, gating of mechanosensitive channels involves a global structural transition.[231,232] Consequently, the time-scale of the gating is significantly greater than in other channels, as is the length scale that needs to be considered.[222] Although the large length scale and long time scale of the mechanosensitive gating pose practical problems in computational studies of the gating mechanism, the prokaryotic MscL and MscS channels are ideal systems to develop the computational

methodology because of the relative simplicity of these channels that are believed to be tension sensors only.

When only one MSC crystal structure was available (a closed conformation of MscL from *My-cobacterium tuberculosis*, Tb-MscL), Sukharev and coworkers proposed a gating model for *E. coli* MscL, in which the channel opens via an "iris-like" mechanism.[231–233] Starting from the closed conformation, they modeled the intermediate and final open conformations in atomistic detail by utilizing various experimental information and empirical energy functions of the CHARMM force field. In the open conformation, the pore size was predicted to be ~ 30 Å, while the pore size of the closed crystal structure was only a few angstroms, impermeable to small molecules. Physiological studies provided estimates of the open pore diameter that were close to the result of the Sukharev model (*e.g.*,[255,598,599]).

Using the gating model of *E. coli* MscL, several groups performed MD simulations to test the model and observe the gating transition in all-atom detail.[230,234,236–239] Kong *et al.* carried out targeted MD simulations to observe the transition from closed to open conformations of the *E. coli* MscL model.[230] Gullingsrud *et al.* used SMD to induce opening of the closed conformation of *E. coli* MscL.[234,238] In the SMD simulations, it was assumed that the forces on the protein by membrane stretching apply only to the residues at the water-lipid interface, which was based on observations of the pressure profile in pure lipid bilayers.[239] The same study used the pressure profile calculations to estimate the magnitude of the SMD force (35–70 pN).

Other than gating by tension, Elmore *et al.* considered the effects of point mutations and lipid compositions on the Tb-MscL structures using MD simulations.[235,240] Later, Meyer *et al.* studied the effect of a single-tailed lipid (which has high spontaneous curvature) on the structure of *E. coli* MscL.[249] The simulations began from a manually built dome-shaped structure containing an *E. coli* MscL channel embedded at the top of the dome. During a 9.5-ns simulation, the researchers observed spontaneous restructuring of the periplasmic loops of MscL, which was in agreement with experimental observations. Recently, Debret *et al.* simulated *E. coli* MscL embedded in a lipid bilayer whose hydrophobic thickness was significantly smaller than the height of *E. coli* MscL.[250] The researchers observed tilting of transmembrane helices, suggesting that hydrophobic mismatch can lower the activation energy of *E. coli* MscL opening. Another all-atom MD simulations of Tb-MscL emphasized the interplay between protein and lipid bilayer by showing that inclusion of the protein significantly increases the mechanical rigidity of a lipid annulus.[251]

Despite a number of ingenious efforts, gating by tension has not been observed in all-atom MD simulations without applying artificial driving forces. The main difficulty is the time scale of the mechanical gating, which is significantly longer than the time scale of an all-atom MD simulation. To overcome the time scale problem, several researchers applied more computationally efficient methods at the expense of accuracy. Phillips and coworkers used continuum elasticity theory to evaluate the energetics of membrane deformation by the inclusion of MscL, neglecting the internal energy of MscL for simplicity.[226–228] Their analytic calculations showed that gating of MscL proteins can be modulated by the mechanical properties of the membrane.[226,227] Moreover, they also demonstrated how the function of multiple MscL channels can be coupled. Later, Chen and coworkers applied computational continuum mechanics to study the gating of MscL.[221–223] In their novel approach, they explicitly considered the conformational change of MscL by modeling the MscL structure using a simple elastic rod-like representation of the transmembrane helices. By combining such a simple model of MscL with a continuum model of the membrane in a finite element framework and parameterizing the models using all-atom MD simulations, they were able to observe mechanical gating of MscL just by stretching the membrane.

Particle-based coarse graining offers another route toward a simpler model of mechanical gating. In this framework, groups of atoms are represented by single interaction beads, which dramatically increases the computational efficiency of the MD simulation. The interactions between such coarse-grained beads are calibrated to reproduce the thermodynamic properties of model systems obtained from all-atom MD simulations or experiments (*e.g.*, transfer free energy of small molecules from water to hydrocarbon). Marrink and coworkers applied their novel coarse-grained model, MARTINI,[252] to Tb-MscL.[253,254] Specifically, they were able to simulate gating of MscL just by stretching the membrane[253] or pressurizing a vesicle that contained embedded MscL channels.[254]

When the time scale accessible to an MD simulation is significantly shorter than the time scale of gating, one can accelerate the simulation by applying biasing forces (*e.g.*, SMD). However, the quality of such accelerated simulations depends critically on how realistic the biasing forces are. In this sense, combining single-molecule experiments with SMD simulations can be very successful. For example, Corry *et al.* recently demonstrated that the distance measurements from Förster resonance energy transfer (FRET) confocal microscopy can be used as a guide for the SMD simulation.[255] Starting from a closed conformation, the researchers induced a closed-to-open conformational transition by performing SMD simulations that utilized distance constraints derived from FRET measurements on an open MscL channel. Because of the distance constraints, the simulations produced a reasonable structural model of the MscL pore in an open state.

5.4.2 Potassium channels—Potassium channels, which all share a common sequence for the selectivity filter, demonstrate voltage-, pH-, and Ca^{2+}-dependent gating of an intracellular gate, which limits K^+ access to the selectivity filter and extracellular solution. However, the selectivity filter is itself a fragile structure that can be inactivated. Inactivation of the selectivity filter occurs more readily when the intracellular gate is open.[186]

It may be insightful to consider purely solution-dependent inactivation and inhibition of the selectivity filter. A potassium ion channel will nearly irreversibly inactivate if it is placed in electrolyte solution of very low ion concentration. All-atom MD simulations suggested a mechanism of such inactivation by demonstrating severe distortion of the selectivity filter when it is depleted of K^+ ions that partially neutralize the negative carbonyl-oxygens lining of this structure.[137,143,182] Similarly, conductance of K^+ channels can be blocked by other ions, such as Na^+ or Cs^+, which bind to the selectivity channel.

The Kv channels are all voltage gated. Crystallographic studies have provided structures for several open-pore Kv channels featuring a charged voltage-sensitive subunit surrounded by lipids for each monomer of the tetramer.[411,600,601] The voltage-sensitive subunits are expected to move and rearrange in response to a voltage change in such a way that a small but measurable transient capacitative current is observed across the membrane. The associated charge is known as the gating charge.

The gating charge times the change in the potential provides the free energy required to change conformations and gate the channel. Using all-atom simulations, the gating charge can be directly computed by measuring the difference in the center of charge of the system between open and closed conformations.[185] A more sophisticated approach allows the assessment of each residue's contribution to the gating charge through the calculation of the difference between the free energy cost of charging each residue in the closed and open states.[185]

There is currently no crystallographically obtained closed-pore structure of a voltage gated K^+ channel. However, in a study that utilized 1.3 μs of all-atom MD simulation, the open-

pore structure was refined and a possible closed-pore structure for Kv1.2 was obtained.[185] Using these structures, the gating charge was found to be somewhat smaller than the experimentally measured gating charge, suggesting that the computational model represented an intermediate conformation at the onset of activation.

Very recently, special-purpose hardware enabled all-atom simulations of a Kv1.2/Kv2.1 chimera on the gating-time scale as observed experimentally (> 300 μs).[196] The simulations demonstrated that the crystal structure accurately represents the functional open pore. In a series of simulations different only by the transmembrane voltage and initial conditions, the channel was brought from the open state to a fully closed state. Simulations were also performed to simulate different stages of channel activation. Gating of the channel occurred by structural rearrangements of the voltage-sensitive domains that affected the hydrophobic cavity leading to the selectivity filter. These rearrangements caused dewetting and collapse of the cavity. The time scales of various steps during the process agreed well with available experimental measurements.[196]

Although not based on such long simulations, a study of a pH-sensitive potassium channel suggested that gating for this protein may occur through a rather different mechanism. An arginine residue near the extracellular side of the membrane was identified through mutagenesis as providing pH-sensitivity.[602] The PMF of K^+ ions in the selectivity filter was obtained through all-atom MD when the protonation state of that arginine residue was varied. The authors of this study suggested that the observed 3–4 kcal/mol increase in the barriers for K^+ translocation accounted for gating and arose from additional flexibility that protonation of the arginine sensors granted to the selectivity filter.[602] However, it should be noted that since no X-ray structure is available, a homology model of the K_{2P} channel built from Kv1.2 was used for this study.

Thus, potassium channels share a great deal of structural and sequence similarity around the selectivity filter, but can be gated in a variety of ways. All-atom simulation techniques have provided a great deal of insight into the structural mechanisms of the gating processes. In one exemplary study,[196] brute-force all-atom MD simulations described the complete gating process of a voltage-sensitive potassium channel on a time scale of hundreds of microseconds. At this time, it remains to be seen whether other potassium channels use similar mechanisms to gate.

5.4.3 Blockades—Some toxins bind and inactivate particular target channels. The potential for specificity of channel-binding toxins makes them an attractive source for pharmaceutical innovation. The all-atom MD methodology has been used to find the standard binding free energies of many small ligands, but only recently have researchers attempted to find the binding free energies of large ligands. In particular, several studies demonstrated challenges and shortcuts when computing standard binding free energies of charbydotoxin binding to various voltage sensitive potassium channels.[116,603,604]

Of greater pharmacological interest, the Kv1.3 K^+channel has been identified as a target treatment of multiple sclerosis and other autoimmune disorders.[422] In a recent study, the toxin ShK, which blocks Kv1.3 but also Kv1.1, was docked to several K^+ channels and the binding free energy was calculated.[425] Surprisingly, the simulations revealed different binding geometries to Kv1.3 and Kv1.1, but similar binding free energies that agree well with experimentally determined values. The authors concluded with mutations to ShK that may enhance the selectivity of Kv1.3 over Kv1.1.

At present, free energy calculations require too much computing power and are not automated enough to be used as a predictive tool by the pharmaceutical industry. In

particular, reliably docking potential drug candidates remains a challenge. Nevertheless, the combination of special purpose hardware for performing MD simulations very quickly and improved automation of tools for calculating binding free energies may give rise to the use of all-atom simulations in advanced computation drug screening within the pharmaceutical industry.

5.5 Biosensing with channels

About twenty years ago, Bezrukov,[605] Kasianowicz[447] and co-workers demonstrated the possibility of using ionic channels as molecular Coulter counters to detect the presence and characterize the type of biomolecules. The basic principle of the approach is the following. A membrane containing a single ion channel separates electrolyte solution into two compartments connected only through the transmembrane pore of the channel. A transmembrane bias is imposed using an external voltage source, producing a steady ionic current through an open pore. The transmembrane bias facilitates unidirectional transport of charged biomolecules from one compartment to the other. Each passage is detected as transient reduction (a blockade) of the ionic current flowing through the pore. The duration and magnitude of the ionic current blockades can indicate the length and chemical composition of a nucleic acid polymer,[447,606–608] suggesting the possibility of recording the nucleotide sequence of a DNA strand directly by measuring the ionic current flowing through a nanopore.

Critical to the success of the above approach is the lack of spontaneous gating of the ion conductance, which, if present, can easily be confused with the signal resulting from interaction of the channel with a biomolecule. Due to it's superior structural stability, the α-hemolysin channel was the first nanopore to be considered for biosensing applications.[447,609] However, other channels such as the bacterial porin MspA,[449–451] and man-made silicon-based[610–612] and graphene[613–615] nanopores have been successfully used for detection of biomolecules. Apart from DNA sequencing, numerous other applications have been proposed for nanopores, including detection of small analytes,[589,616,617] drug design,[390,618] pathogen detection[619] and force spectroscopy.[620–622] Interested readers are directed to several reviews on this subject.[446,623–627]

Modeling and computer simulations have played a major role in development of nanopore applications.[585] There have also been numerous theoretical studies of various aspects of polymer capture and translocation through nanopores. Typically such studies involve the application of scaling concepts of polymer physics or transport equations[628–630] to elucidate the dynamics of charged polymer capture and translocation. All-atom simulations have been used as a kind of a computational force microscope to directly relate the microscopic events taking place in a nanopore to the ionic current blockades recorded in experiment.[377,585]

5.5.1 α-hemolysin—Amongst many β-barrel proteins, α-hemolysin has been the channel of choice for most experimental studies because of its exceptional structural stability under harsh experimental conditions. The known crystallographic structure and relatively straightforward site-directed mutagenesis procedures permit rational engineering of this channel to enhance sensitivity of ionic current blockades, for example, by introducing a molecular adapter[616] or other site-specific mutations.[631,632]

The 2005 publication by A. Aksimentiev and K. Schulten[90] pioneered the application of the all-atom MD method for prediction of the ionic conductance of membrane channels. The simulations demonstrated, for the first time, quantitative accuracy of the MD method in predicting the absolute value of the ionic current, reproducing the asymmetric current-voltage dependence of α-hemolysin, and characterizing the electro-osmotic effect. The simulations also suggested a microscopic mechanism explaining the pH-dependence of the

noise in the ionic current recordings.[633] The study has also demonstrated a method for computing the average distribution of the electrostatic potential in a membrane channel directly from an all-atom MD simulation.[90] Following the successful study of ionic conductance through α-hemolysin, the researchers were challenged by an experimentalist (A. Meller, Boston U) to predict the influence of the global orientation of a DNA strand in α-hemolysin on the velocity of DNA transport and the ionic current blockades. This was a blind test as no prior information about the outcome of experiments was given. To find out the molecular origin of the observed differences, MD simulations were performed on α-hemolysin systems having DNA threaded through in two different global orientations, from 3′ to 5′, and from 5′ to 3′. The outcome of the simulations revealed a propensity for DNA nucleotides to tilt toward their 5′-ends in confined environments, which was linked to observable differences in DNA translocation dynamics and ionic current blockades.[97] The results of the MD simulations were in qualitative agreement with experiment. Due to limited computational resources, direct quantitative comparison was not possible at that time.

The α-hemolysin channel has been a test-bed for developing advanced simulation techniques. The Roux group explored permeation of ions through the α-hemolysin channel using 3D-PNP as well as the Grand Canonical Monte Carlo Brownian Dynamics (GCMC/ BD) approaches[88] in the absence of any analytes. The study revealed that the asymmetric conductance of the pore arises from the permanent charge distribution in the pore. Another PNP study examined the influence of charged residues in α-hemolysin on the asymmetry of the current-voltage dependence.[89,100] Shilov and Kurnikova[96] employed MD simulations to investigate the energetics and dynamics of a β-cyclodextrin (βCD) molecule confined inside the α-hemolysin pore. The Roux group investigated the effect of βCD on the ion selectivity of α-hemolysin through MD simulations and PMF calculations.[94] The simulations have shown that electrically neutral βCD enhances the concentration of Cl⁻ in the nanopore by causing a partial desolvation of the ions which reduces the dielectric shielding by the solvent. The GCMC/BD method was used to account for multi-ion effects in a subsequent study.[94] Simakov and Kurnikova devised a modified PNP approach to incorporate a soft repulsion model of short-range interactions between mobile ions and protein.[92]

To overcome the time scale limitation of the MD method, the Aksimentiev group developed a method for accelerating simulations of DNA transport through nanopores that preserves all-atom features of the MD model.[98] The key idea of the method, dubbed Grid Steered MD (G-SMD), was the selective amplification of the electrostatic potential that drives DNA transport while maintaining all other interactions unchanged. Using G-SMD the Aksimentiev group performed multiple simulations of DNA transport through α-hemolysin and determined the dependence of the translocation velocity on the sequence and orientation of the DNA strands,[98] a task that was considered formidable at that time.[634] De Biase and coworkers recently developed a theoretical framework to model DNA translocation across a nanopore by combining the GCMC/BD algorithm with a coarse-grained polymer model for DNA,[102] which enabled multi-microsecond simulations at a fraction of the cost of all-atom MD. When applied to model translocation of poly(dA) and poly(dC) strands through α-hemolysin, the model yielded results in reasonable agreement with experiments. Reiner *et al.*[367] developed an elegant continuum theory to describe the results of nanopore mass spectroscopy experiments with quantitative accuracy.[635] Bond *et al.* employed all-atom MD simulations to explore the translocation of short strands of DNA through a simplified model of the α-hemolysin pore comprising the stem of the pore surrounded by a membrane mimetic slab.[99] The study examined the effect of cationic amino acids on the translocation dynamics of DNA. Compared to wild type α-hemolysin, arginine mutations were found to reduce the transport rate of DNA through the pore, as well as the ionic current.

5.5.2 MspA—The long stem of α-hemolysin can accommodate up to twelve DNA nucleotides, which makes the detection of single nucleotides by measuring ionic current difficult. The MspA porin has recently emerged as a viable alternative to α-hemolysin on account of its superior architecture. MspA has a goblet like structure with a constriction region that is about 1 nm, ideal for holding just one or two nucleotides, see Figure 11a. Butler and coworkers showed that by eliminating the negative charge in the constriction, a variant of MspA, called M1 MspA, was capable of detecting single DNA strand electrophoretically driven through the pore.[449] A series of subsequent experimental work in the Niederweis and Gundlach groups have since established that the current resolution of the MspA variant is superior to that of α-hemolysin[636] and that single nucleotide substitutions can be detected on a random heteropolymeric background using a tethered DNA.[451] However, the primary challenge is that the translocation rate of DNA through MspA is several orders of magnitude higher than the rate required to resolve the type of DNA nucleotides by measuring ionic current. The two main strategies to control DNA translocation are to engineer intrinsic brakes in the MspA structure or use an auxiliary enzyme, such a DNA polymerase.[637]

The first computational study of MspA was recently carried out by Bhattacharya and coworkers.[348] The study reports extensive all-atom MD simulations that explored the effect of positively charged arginine residues on the translocation rate of DNA and the ionic current. On account of the high computational overhead due to the large system size, the authors performed the majority of the simulations using a truncated version of the pore (see Figure 11b and c). Since the DNA was found to be quite mobile even when confined to the nanopore, the authors adopted an ensemble approach to sample the configurational dynamics of the DNA. The ensemble method was shown to be a viable alternative to following a single long time scale trajectory, which is currently possible only using special purpose supercomputers such as Anton. The ensemble approach allowed the use of traditional supercomputers to obtain combined trajectory length of tens of microseconds within reasonable physical time. The simulations have shown that by introducing several arginine residues near the constriction of MspA, the DNA permeation rate can be reduced by a factor of 10–30 due to the formation of multiple salt-bridges between the DNA backbone and the guanidinium groups of the arginine substitutions as well as due to base-stacking interactions. Furthermore, the simulations predicted that such mutations would not eliminate the nucleotide sensitivity of the ionic current blockades. The study explained why similar mutations introduced in α-hemolysin reduced the ionic current practically to zero,[638] making such mutants unsuitable for DNA sequencing applications.

5.5.3 Other nanopore systems—Other β-barrel nanopores have been explored for stochastic sensing applications. For instance, an MD study of the bacterial porin OmpG was carried out by Chen and coworkers to determine the origin of its spontaneous gating activity.[77] Based on the simulation study, a variant of the porin with stabilizing mutations was created and was used for detection of adenosine diphosphate after inserting a cyclodextrin molecular adapter.[77]

Using 3D-Poisson equations and linear transport theory,[360] Vidal and coworkers demonstrated that a nanopore in a heavily doped silicon membrane connected to a voltage source can be used as an electrically tunable ion filter. The PNP model was used to study ion transport through synthetic nanopores in several studies[359,363,366] exploring rectification and ion selectivity. A Langevin dynamics approach to study the transport of flexible macromolecules in confined geometries was proposed by Peters.[372] Recently, an atomic resolution BD method was developed by Comer and coworkers which was used to study the sequence dependence of ionic current in synthetic nanopores.[373,374] All atom MD simulations have been used with considerable success to investigate nanopore transport of

DNA and ionic current blockades,[375,376] nanopore unzipping of DNA hairpins,[380] the microscopic origin of the electrophoretic force on DNA in a nanopore,[378,381] and the effect of electrolyte on the DNA translocation rates.[391] For detailed description of the simulation protocols, interested readers are directed to recent reviews on this subject.[585,639,640]

6 Outlook

Advances in computational technologies and membrane protein structure determination methods are poised to make modeling and simulations of ion channels an integral part of future drug development efforts. The greatest obstacle so far is the lack of atomic-resolution structures of the majority of biomedically relevant ion channels. Several limitations pertain to the computational technology itself. Whereas all-atom molecular dynamics simulation of an ion channel can provide the most detailed information about the microscopic mechanism of its function, the method is currently limited by the accuracy of the classical force field and the microsecond time scale of the simulations on conventional computer clusters.

Tremendous advances in addressing both limitations have already been made. The first computational studies of ion channel systems using polarizable models have already been reported.[277,563] Thus, it is very likely that a full polarizable force field will become available within the next ten years. Another major advancement was the millisecond simulation of a membrane channel in its native environment that revealed the microscopic details of its voltage-dependent gating mechanism.[196] We hope that such a tremendous success of special purpose hardware will prompt the development of commodity special purpose hardware, which will make such long time scale simulations available to mainstream researchers. Finally, advances in computational methods will also aid the discovery of atomic-resolution structures, through either *de novo* structure prediction[641] or refinement of low resolution X-ray and cryo-EM structures.[443]

It would be, however, misleading to think that all questions pertaining to ion channels would be answered through all-atom MD. From a drug development perspective, high-throughput and accurate calculation of binding free energies of small chemical compounds is more important than a long time scale simulations of a single channel's action. Enabling such high-throughput docking is dependent on the availability of accurate generic force fields. Furthermore, as millisecond simulations become more available, describing possible chemical reactions between components of the system will become increasingly important. Finally, modeling a single channel in a membrane is only a first step toward the realistic modeling of *in vivo* processes. We anticipate continuum and implicit solvent approaches to play a pivotal role in the development of detailed, quantitative models of realistic biological membranes and small organelles that incorporate an ensemble of ion channels.

Acknowledgments

References

1. Doyle DA, Morais Cabral J, Pfuetzner RA, Kuo A, Gulbis JM, Cohen SL, Chait BT, MacKinnon R. Science. 1998; 280:69. [PubMed: 9525859]

2. Jiang Y, Lee A, Chen J, Ruta V, Cadene M, Chait BT, MacKinnon R. Nature. 2003; 423:33. [PubMed: 12721618]

3. Payandeh J, Scheuer T, Zheng N, Catterall W. Nature. 2011; 475:353. [PubMed: 21743477]

4. Cha A, Snyder GE, Selvin PR, Bezanilla F. Nature. 1999; 402:809. [PubMed: 10617201]

5. Glauner K, Mannuzzu L, Gandhi C, Isacoff E. Nature. 1999; 402:813. [PubMed: 10617202]

6. Posson D, Ge P, Miller C, Bezanilla F, Selvin P. Nature. 2005; 436:848. [PubMed: 16094368]

7. Posson DJ, Selvin PR. Neuron. 2008; 59:98. [PubMed: 18614032]

8. Kurnikova MG, Coalson RD, Graf P, Nitzan A. Biophys J. 1999; 76:642. [PubMed: 9929470]

9. Hess K, Ravaioli U, Gupta M, Aluru N, Eisenberg RS. VLSI Design. 2001; 13:179.

10. Edwards S, Corry B, Kuyucak S, Chung S-H. Biophys J. 2002; 83:1348. [PubMed: 12202360]

11. Nadler B, Hollerbach U, Eisenberg R. Phys Rev E. 2003; 68:021905.

12. Coalson RD, Kurnikova MG. IEEE Trans Nanobiosci. 2005; 4:81.

13. Cárdenas AE, Coalson RD, Kurnikova MG. Biophys J. 2000; 79:80. [PubMed: 10866939]

14. Zheng Q, Chen D, Wei G-W. J Comp Phys. 2011; 230:5239.

15. Zheng Q, Wei G-W. J Chem Phys. 2011; 134:194101. [PubMed: 21599038]

16. Bransburg-Zabary S, Kessel A, Gutman M, Ben-Tal N. Biochemistry. 2002; 41:6946. [PubMed: 12033927]

17. Krishnamurthy V, Chung S-H. IEEE Trans Nanobiosci. 2006; 5:126.

18. aÅqvist J, Warshel A. Biophys J. 1989; 56:171. [PubMed: 2473789]

19. Roux B, Prod'hom B, Karplus M. Biophys J. 1995; 68:876. [PubMed: 7538804]

20. Schumaker MF, Pomès R, Roux B. Biophys J. 2000; 79:2840. [PubMed: 11106593]

21. Roux B. Acc Chem Res. 2002; 35:366. [PubMed: 12069621]

22. Pomès R, Roux B. Biophys J. 2002; 82:2304. [PubMed: 11964221]

23. de Groot BL, Tieleman DP, Pohl P, Grubmüller H. Biophys J. 2002; 82:2934. [PubMed: 12023216]

24. Siva K, Elber R. Proteins: Struct, Func, Gen. 2003; 80:63.

25. Bingham NC, Smith NEC, Cross TA, Busath DD. Biopolymers. 2003; 71:593. [PubMed: 14635099]

26. Yu C-H, Pomès R. J Am Chem Soc. 2003; 125:13890. [PubMed: 14599229]

27. Yu C-H, Cukierman S, Pomès R. Biophys J. 2003; 84:816. [PubMed: 12547766]

28. Allen TW, Andersen OS, Roux B. J Am Chem Soc. 2003; 125:9868. [PubMed: 12904055]

29. Allen TW, Andersen OS, Roux B. J Gen Physiol. 2004; 124:679. [PubMed: 15572347]

30. Allen TW, Andersen OS, Roux B. Proc Natl Acad Sci USA. 2004; 101:117. [PubMed: 14691245]

31. Liu Z, Xu Y, Tang P. Biophys J. 2005; 88:3784. [PubMed: 15764669]

32. Corry B, Chung S-H. Eur Biophys J. 2005; 34:208. [PubMed: 15536565]

33. Baştuğ T, Kuyucak S. Eur Biophys J. 2005; 34:377. [PubMed: 15711809]

34. Baştuğ T, Gray-Weale A, Patra SM, Kuyucak S. Biophys J. 2006; 90:2285. [PubMed: 16415054]

35. Allen TW, Andersen OS, Roux B. Biophys Chem. 2006; 124:251. [PubMed: 16781050]

36. Allen TW, Andersen OS, Roux B. Biophys J. 2006; 90:3447. [PubMed: 16500984]

37. Mamonov AB, Kurnikova MG, Coalson RD. Biophys Chem. 2006; 124:268. [PubMed: 16797116]

38. Liu Z, Xu Y, Tang P. J Phys Chem B. 2006; 110:12789. [PubMed: 16800614]

39. Kelkar DA, Chattopadhyay A. Biochim Biophys Acta – Bioener. 2007; 1768:2011.

40. Baştuğ T, Kuyucak S. J Chem Phys. 2007; 126:105103. [PubMed: 17362089]

41. Baştuğ T, Chen P-C, Patra SM, Kuyucak S. J Chem Phys. 2008; 128:155104. [PubMed: 18433285]

42. De Fabritiis G, Coveney PV, Villà-Freixa J. Proteins: Struct, Func, Bioinf. 2008; 73:185.

43. Forney M, Janosi L, Kosztin I. Phys Rev E. 2008; 78:1.

44. Patel S, Davis JE, Bauer BA. J Am Chem Soc. 2009; 131:13890. [PubMed: 19788320]

45. Dryga A, Warshel A. J Phys Chem B. 2010; 114:12720. [PubMed: 20836533]

46. Li Y, Andersen OS, Roux B. J Phys Chem B. 2010; 114:13881. [PubMed: 20939567]

47. Balme S, Janot J-m, Berardo L, Bonhenry D, Kraszewski S, Picaud F, Ramseyer C, Gerhardt IC, Eug P. Nano Lett. 2011; 11:712. [PubMed: 21174453]

48. Giorgino T, De Fabritiis G. J Chem Theory Comput. 2011; 7:1943.

49. Kim T, Lee K, Morris P, Pastor R, Andersen O, Im W. Biophys J. 2012; 102:1551. [PubMed: 22500755]

50. Kato M, Warshel A. J Phys Chem B. 2005; 109:19516. [PubMed: 16853521]

51. Gordon D, Krishnamurthy V, Chung S-H. J Chem Phys. 2009; 131:134102. [PubMed: 19814538]

52. Mamonov AB, Coalson RD, Nitzan A, Kurnikova MG. Biophys J. 2003; 84:3646. [PubMed: 12770873]

53. Dorman VL, Jordan PC. Biophys J. 2004; 86:3529. [PubMed: 15189852]

54. Chen D, Wei G-W. J Chem Phys. 2012; 136:134109. [PubMed: 22482542]

55. Im W. J Mol Biol. 2002; 322:851. [PubMed: 12270719]

56. Miedema H, Meter-Arkema A, Wierenga J, Tang J, Eisenberg B, Nonner W, Hektor H, Gillespie D, Meijberg W. Biophys J. 2004; 87:3137. [PubMed: 15326033]

57. Miedema H, Vrouenraets M, Wierenga J, Gillespie D, Eisenberg B, Meijberg W, Nonner W. Biophys J. 2006; 91:4392. [PubMed: 16997866]

58. Aguilella-Arzo M, García-Celma JJ, Cervera J, Alcaraz A, Aguilella VM. Bioelectrochemistry. 2007; 70:320. [PubMed: 16769257]

59. Aguilella-Arzo M, Andrio A, Aguilella VM, Alcaraz A. Phys Chem Chem Phys. 2009; 11:358. [PubMed: 19088992]

60. García-Giménez E, López ML, Aguilella VM, Alcaraz A. Biochem Biophys Res Commun. 2011; 404:330. [PubMed: 21134352]

61. Aguilella VM, Queralt-Martín M, Aguilella-Arzo M, Alcaraz A. Integ Biol. 2011; 3:159.

62. Im W, Seefeld S, Roux B. Biophys J. 2000; 79:788. [PubMed: 10920012]

63. Im W, Roux B. J Chem Phys. 2001; 115:4850.

64. Marreiro D, Saraniti M, Aboud S. J Phys: Condens Matter. 2007; 19:215203.

65. Tieleman T, Berendsen B. Biophys J. 1998; 74:2786. [PubMed: 9635733]

66. Bond PJ, Faraldo-Gómez JD, Sansom MSP. Biophys J. 2002; 83:763. [PubMed: 12124263]

67. Im W, Roux B. J Mol Biol. 2002; 319:1177. [PubMed: 12079356]

68. Zachariae U, Helms V, Engelhardt H. Biophys J. 2003; 85:954. [PubMed: 12885642]

69. Danelon C, Suenaga A, Winterhalter M, Yamato I. Biophys Chem. 2003; 104:591. [PubMed: 12914905]

70. Varma S, Jakobsson E. Biophys J. 2004; 86:690. [PubMed: 14747308]

71. Varma S, Chiu S-WW, Jakobsson E. Biophys J. 2006; 90:112. [PubMed: 16183883]

72. Zachariae U, Klühspies T, De S, Engelhardt H, Zeth K. J Biol Chem. 2006; 281:7413. [PubMed: 16434398]

73. Khalid S, Bond PJ, Deol SS, Sansom MSP. Proteins: Struct, Func, Bioinf. 2006; 63:6.

74. Bond PJ, Sansom MSP. J Am Chem Soc. 2006; 128:2697. [PubMed: 16492056]

75. van Hijkoop VJ, Dammers AJ, Malek K, Coppens M-O. J Chem Phys. 2007; 127:085101. [PubMed: 17764300]

76. Bond PJ, Derrick JP, Sansom MSP. Biophys J. 2007; 92:L23. [PubMed: 17114231]

77. Chen M, Khalid S, Sansom MSP, Bayley H. Proc Natl Acad Sci USA. 2008; 105:6272. [PubMed: 18443290]

78. Chimerel C, Movileanu L, Pezeshki S, Winterhalter M, Kleinekathöfer U. Eur Biophys J. 2008; 38:121. [PubMed: 18726094]

79. Pezeshki S, Chimerel C, Bessonov AN, Winterhalter M, Kleinekathöfer U. Biophys J. 2009; 97:1898. [PubMed: 19804720]

80. Pongprayoon P, Beckstein O, Wee CL, Sansom MSP. Proc Natl Acad Sci USA. 2009; 106:21614. [PubMed: 19966228]

81. Biró I, Pezeshki S, Weingart H, Winterhalter M, Kleinekathöfer U. Biophys J. 2010; 98:1830. [PubMed: 20441746]

82. Kumar A, Hajjar E, Ruggerone P, Ceccarelli M. J Phys: Condens Matter. 2010; 22:454125. [PubMed: 21339612]

83. Faraudo J, Calero C, Aguilella-Arzo M. Biophys J. 2010; 99:2107. [PubMed: 20923644]

84. Vrouenraets M, Miedema H. Eur Biophys J. 2010; 39:1563. [PubMed: 20521145]

85. Calero C, Faraudo J, Aguilella-Arzo M. Phys Rev E. 2011; 83:1.

86. Modi N, Singh PR, Mahendran KR, Schulz R, Winterhalter M, Kleinekath U. J Phys Chem Lett. 2011; 2:2331.

87. Singh PR, Ceccarelli M, Lovelle M, Winterhalter M, Mahendran KR. J Phys Chem B. 2012; 116:4433. [PubMed: 22369436]

88. Noskov SY, Im W, Roux B. Biophys J. 2004; 87:2299. [PubMed: 15454431]

89. Misakian M, Kasianowicz JJ. J Membr Biol. 2003; 195:137. [PubMed: 14724760]

90. Aksimentiev A, Schulten K. Biophys J. 2005; 88:3745. [PubMed: 15764651]

91. Aguilella-Arzo M, Aguilella VM. Eur Phys J E. 2010; 31:429. [PubMed: 20419466]

92. Simakov NA, Kurnikova MG. J Phys Chem B. 2010; 114:15180. [PubMed: 21028776]

93. Bhattacharya S, Muzard J, Payet L, Bockelman U, Aksimentiev A, Viasnoff V. J Phys Chem C. 2011; 115:4255.

94. Egwolf B, Roux B. J Mol Biol. 2010; 401:831. [PubMed: 20624398]

95. Egwolf B, Luo Y, Walters DE, Roux B. J Phys Chem B. 2010; 114:2901. [PubMed: 20146515]

96. Shilov IY, Kurnikova MG. J Phys Chem B. 2003; 107:7189.

97. Mathé J, Aksimentiev A, Nelson DR, Schulten K, Meller A. Proc Natl Acad Sci USA. 2005; 102:12377. [PubMed: 16113083]

98. Wells DB, Abramkina V, Aksimentiev A. J Chem Phys. 2007; 127:125101. [PubMed: 17902937]

99. Bond PJ, Guy AT, Heron AJ, Bayley H, Khalid S. Biochemistry. 2011; 50:3777. [PubMed: 21428458]

100. O'Keeffe J, Cozmuta I, Bose D, Stolc V. Chem Phys. 2007; 342:25.

101. Luo Y, Egwolf B, Walters DE, Roux B. J Phys Chem B. 2010; 114:952. [PubMed: 20041673]

102. De Biase PM, Solano CJF, Markosyan S, Czapla L, Noskov SY. J Chem Theory Comput. 2012; 8:2540. [PubMed: 22798730]

103. Roux B, Bernèche S, Im W. Biochemistry. 2000; 39:13295. [PubMed: 11063565]

104. Grabe M, Lecar H, Jan YN, Jan LY. Proc Natl Acad Sci USA. 2004; 101:17640. [PubMed: 15591352]

105. Jogini V, Roux B. J Mol Biol. 2005; 354:272. [PubMed: 16242718]

106. Robertson JL, Palmer LG, Roux B. J Gen Physiol. 2008; 132:613. [PubMed: 19001143]

107. Jung Y-W, Lu B, Mascagni M. J Chem Phys. 2009; 131:215101. [PubMed: 19968368]

108. Nekouzadeh A, Rudy Y. PLoS ONE. 2011; 6:e20186. [PubMed: 21625456]

109. Gardner CL, Jones JR. J Theor Biol. 2011; 291:10. [PubMed: 21945149]

110. Allen TW, Chung SH. Biochim Biophys Acta. 2001; 1515:83. [PubMed: 11718664]

111. Chung S-H, Allen TW, Kuyucak S. Biophys J. 2002; 82:628. [PubMed: 11806907]

112. Burykin A, Kato M, Warshel A. Proteins: Struct, Func, Gen. 2003; 52:412.

113. Bernèche S, Roux B. Proc Natl Acad Sci USA. 2003; 100:8644. [PubMed: 12837936]

114. Chung S-H, Corry B. Biophys J. 2007; 93:44. [PubMed: 17434934]

115. Hoyles M, Krishnamurthy V, Siksik M, Chung S-H. Biophys J. 2008; 94:366. [PubMed: 17872961]

116. Gordon D, Chung S-H. Biophys J. 2011; 101:2671. [PubMed: 22261055]

117. Gordon D, Chen R, Ho J, Coote ML, Chung S-H. J Phys Chem B. 2012; 116:1933. [PubMed: 22257264]

118. Luzhkov VB, Åqvist J. Biochim Biophys Acta. 2000; 1481:360. [PubMed: 11018728]

119. Bernèche S, Roux B. Biophys J. 2000; 78:2900. [PubMed: 10827971]

120. Åqvist J, Luzhkov V. Nature. 2000; 404:881. [PubMed: 10786795]

121. Shrivastava IH, Sansom MS. Biophys J. 2000; 78:557. [PubMed: 10653771]

122. Luzhkov VB, Åqvist J. FEBS Lett. 2001; 495:191. [PubMed: 11334890]

123. Luzhkov VB, Åqvist J. Biochim Biophys Acta. 2001; 1548:194. [PubMed: 11513964]

124. Ranatunga KM, Shrivastava IH, Smith GR, Sansom MS. Biophys J. 2001; 80:1210. [PubMed: 11222285]

125. Isralewitz B, Baudry J, Gullingsrud J, Kosztin D, Schulten K. J Mol Graphics and Modeling. 2001; 19:13.

126. Bernèche S, Roux B. Nature. 2001; 414:73. [PubMed: 11689945]

127. Bernèche S, Roux B. Biophys J. 2002; 82:772. [PubMed: 11806919]

128. Biggin PC, Smith GR, Shrivastava I, Choe S, Sansom MS. Biochim Biophys Acta. 2001; 1510:1. [PubMed: 11342142]

129. Capener CE, Sansom MSP. J Phys Chem B. 2002:4543–4551.

130. Sansom MSP, Shrivastava IH. Curr Biol. 2002; 12:R65. [PubMed: 11818082]

131. Bright JN, Shrivastava IH, Cordes FS, Sansom MSP. Biopolymers. 2002; 64:303. [PubMed: 12124848]

132. Shrivastava IH, Peter Tieleman D, Biggin PC, Sansom MS. Biophys J. 2002; 83:633. [PubMed: 12124253]

133. Faraldo-Gómez JD, Smith GR, Sansom MSP. Eur Biophys J. 2002; 31:217. [PubMed: 12029334]

134. Shrivastava IH, Sansom MSP. Eur Biophys J. 2002; 31:207. [PubMed: 12029333]

135. Sansom MSP, Shrivastava IH, Bright JN, Tate J, Capener CE, Biggin PC. Biochim Biophys Acta. 2002; 1565:294. [PubMed: 12409202]

136. Eriksson MAL, Roux B. Biophys J. 2002; 83:2595. [PubMed: 12414693]

137. Domene C, Sansom MSP. Biophys J. 2003; 85:2787. [PubMed: 14581184]

138. Luzhkov VB, Österberg F, Åqvist J. FEBS Lett. 2003; 554:159. [PubMed: 14596932]

139. Luzhkov VB, Nilsson J, Århem P, Åqvist J. Biochim Biophys Acta. 2003; 1652:35. [PubMed: 14580995]

140. Beckstein O, Biggin PC, Bond P, Bright JN, Domene C, Grottesi A, Holyoake J, Sansom MS. FEBS Lett. 2003; 555:85. [PubMed: 14630324]

141. Noskov SY, Bernèche S, Roux B. Nature. 2004; 431:830. [PubMed: 15483608]

142. Miloshevsky GV, Jordan PC. Trends in Neurosciences. 2004; 27:308. [PubMed: 15165734]

143. Domene C, Grottesi A, Sansom MSP. Biophys J. 2004; 87:256. [PubMed: 15240462]

144. Tieleman DP, Robertson KM, Maccallum JL, Monticelli L. Int J Quantum Chem. 2004; 100:1071.

145. Monticelli L, Robertson KM, MacCallum JL, Tieleman DP. FEBS Lett. 2004; 564:325. [PubMed: 15111117]

146. Treptow W, Maigret B, Chipot C, Tarek M. Biophys J. 2004; 87:2365. [PubMed: 15454436]

147. Osterberg F, Åqvist J. FEBS Lett. 2005; 579:2939. [PubMed: 15893317]

148. Roux B. Annu Rev Biophys Biomol Struct. 2005; 34:153. [PubMed: 15869387]

149. Luzhkov VB, Åqvist J. Biochim Biophys Acta. 2005; 1747:109. [PubMed: 15680245]

150. Sansom MSP, Bond PJ, Deol SS, Grottesi A, Haider S, Sands ZA. Biochem Soc Trans. 2005; 33:916. [PubMed: 16246010]

151. Khalili-Araghi F, Tajkhorshid E, Schulten K. Biophys J. 2006; 91:L72. [PubMed: 16844753]

152. Sands ZA, Grottesi A, Sansom MSP. Biophys J. 2006; 90:1598. [PubMed: 16326912]

153. Hellgren M, Sandberg L, Edholm O. Biophys Chem. 2006; 120:1. [PubMed: 16253415]

154. Tieleman DP. Clin Exp Pharmacol Physiol. 2006; 33:893. [PubMed: 17002665]

155. Freites JA, Tobias DJ, White SH. Biophys J. 2006; 91:L90. [PubMed: 17012321]

156. Treptow W, Tarek M. Biophys J. 2006; 91:L81. [PubMed: 16980355]

157. Treptow W, Tarek M. Biophys J. 2006; 90:L64. [PubMed: 16533847]

158. Boiteux C, Kraszewski S, Ramseyer C, Girardet C. J Mol Mod. 2007; 13:699.

159. Faraldo-Gómez JD, Kutluay E, Jogini V, Zhao Y, Heginbotham L, Roux B. J Mol Biol. 2007; 365:649. [PubMed: 17070844]

160. Haider S, Khalid S, Tucker SJ, Ashcroft FM, Sansom MSP. Biochemistry. 2007; 46:3643. [PubMed: 17326663]

161. Kónǎ J, Minozzi M, Torre V, Carloni P. Theor Chem Acc. 2007; 117:1121.

162. Sands ZA, Sansom MSP. Structure. 2007; 15:235. [PubMed: 17292841]

163. Bostick DL, Brooks CL. Proc Natl Acad Sci USA. 2007; 104:9260. [PubMed: 17519335]

164. Gwan J-F, Baumgaertner A. J Chem Phys. 2007; 127:045103. [PubMed: 17672726]

165. Bond PJ, Sansom M. Proc Natl Acad Sci USA. 2007; 104:2631. [PubMed: 17301243]

166. Kutteh R, Vandenberg JI, Kuyucak S. J Phys Chem B. 2007; 111:1090. [PubMed: 17266262]

167. Pathak MM, Yarov-Yarovoy V, Agarwal G, Roux B, Barth P, Kohout S, Tombola F, Isacoff EY. Neuron. 2007; 56:124. [PubMed: 17920020]

168. Noskov SY, Roux B. Biophys Chem. 2006; 124:279. [PubMed: 16843584]

169. Domene C. Cent Eur J Chem. 2007; 5:635.

170. Tayefeh S, Kloss T, Thiel G, Hertel B, Moroni A, Kast SM. Biochemistry. 2007; 46:4826. [PubMed: 17397187]

171. Lindahl E, Sansom MSP. Curr Opin Struct Biol. 2008; 18:425. [PubMed: 18406600]

172. Han M, Zhang JZH. J Phys Chem B. 2008; 112:16966. [PubMed: 19093881]

173. Roux B. Biophys J. 2008; 95:4205. [PubMed: 18641071]

174. Fowler PW, Tai K, Sansom MSP. Biophys J. 2008; 95:5062. [PubMed: 18790851]

175. Recanatini M, Cavalli A, Masetti M. ChemMedChem. 2008; 3:523. [PubMed: 18224703]

176. Piccinini E, Ceccarelli M, Affinito F, Brunetti R, Bologna I, Fisica D, Monserrato C, Ca I-M, Fisica D. Meth. 2008:173–183.

177. Sompornpisut P, Roux B, Perozo E. Biophys J. 2008; 95:5349. [PubMed: 18676641]

178. Bjelkmar P, Niemelä PS, Vattulainen I, Lindahl E. PLoS Comput Biol. 2009; 5:e1000289. [PubMed: 19229308]

179. Treptow W, Tarek M, Klein ML. J Am Chem Soc. 2009; 131:2107. [PubMed: 19175309]

180. Domene C, Furini S. J Mol Biol. 2009; 389:637. [PubMed: 19393663]

181. Furini S, Beckstein O, Domene C. Proteins: Struct, Func, Bioinf. 2009; 74:437.

182. Furini S, Domene C. Proc Natl Acad Sci USA. 2009; 106:16074. [PubMed: 19805261]

183. Jensen MO, Borhani DW, Lindorff-Larsen K, Maragakis P, Jogini V, East-wood MP, Dror RO, Shaw DE. Proc Natl Acad Sci USA. 2010; 107:5833. [PubMed: 20231479]

184. Anishkin A, Milac AL, Guy HR. Proteins: Struct, Func, Bioinf. 2010; 78:932.

185. Khalili-Araghi F, Jogini V, Yarov-Yarovoy V, Tajkhorshid E, Roux B, Schulten K. Biophys J. 2010; 98:2189. [PubMed: 20483327]

186. Pan AC, Cuello LG, Perozo E, Roux B. J Gen Physiol. 2011; 138:571. [PubMed: 22124115]

187. Baþtud T, Kuyucak S. Biophys J. 2011; 100:629. [PubMed: 21281577]

188. Schiesaro, A.; Ecker, GF. Prediction of hERG Channel Inhibition Using In Silico Techniques. In: Gupta, SP., editor. Ion Channels and Their Inhibitors. Springer-Verlag; Berlin Heidelberg: 2011. p. 191-239.

189. Delemotte L, Tarek M, Klein ML, Amaral C, Treptow W. Proc Natl Acad Sci USA. 2011; 108:6109. [PubMed: 21444776]

190. Chakrapani S, Cordero-Morales JF, Jogini V, Pan AC, Cortes DM, Roux B, Perozo E. Nat Struct Mol Biol. 2011; 18:67. [PubMed: 21186363]

191. Furini S, Domene C. J Mol Biol. 2011; 409:867. [PubMed: 21540036]

192. Khalili-Araghi F, Tajkhorshid E, Roux B, Schulten K. Biophys J. 2012; 102:258. [PubMed: 22339862]

193. Knape K, Linder T, Wolschann P, Beyer A, Stary-Weinzinger A. PLoS ONE. 2011; 6:e28778. [PubMed: 22194911]

194. Domene C, Furini S. Biochemistry. 2012; 51:1559. [PubMed: 22316140]

195. Yang H, Gao Z, Li P, Yu K, Yu Y, Xu T-L, Li M, Jiang H. Biophys J. 2012; 102:1815. [PubMed: 22768937]

196. Jensen MO, Jogini V, Borhani DW, Leffler AE, Dror RO, Shaw DE. Science. 2012; 336:229. [PubMed: 22499946]

197. Treptow W, Klein ML. J Phys Chem Lett. 2012; 3:1017. [PubMed: 22523619]

198. Garofoli S, Jordan PC. Biophys J. 2003; 84:2814. [PubMed: 12719216]

199. Corry B, Vora T, Chung S-H. Biochim Biophys Acta. 2005; 1711:72. [PubMed: 15904665]

200. Huetz P, Boiteux C, Compoint M, Ramseyer C, Girardet C. J Chem Phys. 2006; 124:044703. [PubMed: 16460196]

201. Bisset D, Chung S-H. Biochim Biophys Acta. 2008; 1778:2273. [PubMed: 18582434]

202. Wee CL, Gavaghan D, Sansom MSP. Biophys J. 2010; 98:1558. [PubMed: 20409475]

203. Mafé S, Pellicer J, Cervera J. J Chem Phys. 2005; 122:204712. [PubMed: 15945769]

204. Treptow W, Marrink S-J, Tarek M. J Phys Chem B. 2008; 112:3277. [PubMed: 18293960]

205. Dryga A, Chakrabarty S, Vicatos S, Warshel A. Proc Natl Acad Sci USA. 2012; 109:3335. [PubMed: 22331900]

206. Dryga A, Chakrabarty S, Vicatos S, Warshel A. Biochim Biophys Acta. 2012; 1818:303. [PubMed: 21843502]

207. Guidoni L, Carloni P. Biochim Biophys Acta. 2002; 1563:1. [PubMed: 12007618]

208. Bucher D, Raugei S, Guidoni L, Dal Peraro M, Rothlisberger U, Carloni P, Klein ML. Biophys Chem. 2006; 124:292. [PubMed: 16737771]

209. Kariev AM, Znamenskiy VS, Green ME. Biochim Biophys Acta. 2007; 1768:1218. [PubMed: 17336921]

210. Bucher D, Guidoni L, Maurer P, Rothlisberger U. J Chem Theory Comput. 2009; 5:2173.

211. Bucher D, Rothlisberger U. J Gen Physiol. 2010; 135:549. [PubMed: 20513756]

212. Hung A, Tai K, Sansom MSP. Biophys J. 2005; 88:3321. [PubMed: 15722430]

213. Law RJ, Henchman RH, McCammon JA. Proc Natl Acad Sci USA. 2005; 102:6813. [PubMed: 15857954]

214. Gao M, Schulten K. Biophys J. 2006; 90:3267. [PubMed: 16473908]

215. Xu Y, Barrantes FJ, Luo X, Chen K, Shen J, Jiang H. J Am Chem Soc. 2005; 127:1291. [PubMed: 15669869]

216. Xu Y, Barrantes FJ, Shen J, Luo X, Zhu W, Chen K, Jiang H. J Phys Chem B. 2006; 110:20640. [PubMed: 17034254]

217. Cheng X, Wang H, Grant B, Sine SM, McCammon JA. PLoS Comput Biol. 2006; 2:e134. [PubMed: 17009865]

218. Law RJ, Lightstone FC. Biophys J. 2009; 97:1586. [PubMed: 19751663]

219. Brannigan G, Lebard DN, Hénin J, Eckenhoff RG, Klein ML. Proc Natl Acad Sci USA. 2010; 107:14122. [PubMed: 20660787]

220. Dimitropoulos N, Papakyriakou A, Dalkas GA, Chasapis CT, Poulas K, Spyroulias GA. Proteins: Struct, Func, Bioinf. 2011; 79:142.

221. Chen X, Cui Q, Tang Y, Yoo J, Yethiraj A. Biophys J. 2008; 95:563. [PubMed: 18390626]

222. Tang Y, Cao G, Chen X, Yoo J, Yethiraj A, Cui Q. Biophys J. 2006; 91:1248. [PubMed: 16731564]

223. Tang Y, Yoo J, Yethiraj A, Cui Q, Chen X. Biophys J. 2008; 95:581. [PubMed: 18390625]

224. Li S, Zhang X, Wang W. J Phys Chem B. 2009; 113:14431. [PubMed: 19845409]

225. Song C, Corry B. PLoS ONE. 2011; 6:e21204. [PubMed: 21731672]

226. Wiggins P, Phillips R. Proc Natl Acad Sci USA. 2004; 101:4071. [PubMed: 15024097]

227. Wiggins P, Phillips R. Biophys J. 2005; 88:880. [PubMed: 15542561]

228. Ursell T, Huang KC, Peterson E, Phillips R. PLoS Comput Biol. 2007; 3:e81. [PubMed: 17480116]

229. Vora T, Corry B, Chung S-H. Biochim Biophys Acta. 2006; 1758:730. [PubMed: 16781663]

230. Kong Y, Shen Y, Warth TE, Ma J. Proc Natl Acad Sci USA. 2002; 99:5999. [PubMed: 11972047]

231. Sukharev S, Durell SR, Guy HR. Biophys J. 2001; 81:917. [PubMed: 11463635]

232. Sukharev S, Betanzos M, Chiang C-SS, Guy HR. Nature. 2001; 409:720. [PubMed: 11217861]

233. Betanzos M, Chiang C-SS, Guy HR, Sukharev S. Nature Struct Biol. 2002; 9:704. [PubMed: 12172538]

234. Gullingsrud J, Kosztin D, Schulten K. Biophys J. 2001; 80:2074. [PubMed: 11325711]

235. Elmore DE, Dougherty DA. Biophys J. 2001; 81:1345. [PubMed: 11509350]

236. Bilston LE, Mylvaganam K. FEBS Lett. 2002; 512:185. [PubMed: 11852077]

237. Colombo G, Marrink SJ, Mark AE. Biophys J. 2003; 84:2331. [PubMed: 12668441]

238. Gullingsrud J, Schulten K. Biophys J. 2003; 85:2087. [PubMed: 14507677]

239. Gullingsrud J, Schulten K. Biophys J. 2004; 86:3496. [PubMed: 15189849]

240. Elmore DE, Dougherty DA. Biophys J. 2003; 85:1512. [PubMed: 12944269]

241. Sotomayor M, Schulten K. Biophys J. 2004; 87:3050. [PubMed: 15339798]

242. Anishkin A, Sukharev S. Biophys J. 2004; 86:2883. [PubMed: 15111405]

243. Spronk SA, Elmore DE, Dougherty DA. Biophys J. 2006; 90:3555. [PubMed: 16500980]

244. Sotomayor M, Vásquez V, Perozo E, Schulten K. Biophys J. 2007; 92:886. [PubMed: 17114233]

245. Corry B, Martinac B. Biochim Biophys Acta. 2008; 1778:1859. [PubMed: 17662237]

246. Corry B, Jayatilaka D. Biophys J. 2008; 95:2711. [PubMed: 18515397]

247. Anishkin A, Akitake B, Kamaraju K, Chiang C-S, Sukharev S. J Phys: Condens Matter. 2010; 22:454120. [PubMed: 21339607]

248. Gamini R, Sotomayor M, Chipot C, Schulten K. Biophys J. 2011; 101:80. [PubMed: 21723817]

249. Meyer GR, Gullingsrud J, Schulten K, Martinac B. Biophys J. 2006; 91:1630. [PubMed: 16751236]

250. Debret G, Valadié H, Stadler AM, Etchebest C. Proteins: Struct, Func, Gen. 2008; 71:1183.

251. Jeon J, Voth GA. Biophys J. 2008; 94:3497. [PubMed: 18212020]

252. Monticelli L, Kandasamy S, Periole X, Larson R, Tieleman DP, Marrink SJ. J Chem Theory Comput. 2008; 4:819.

253. Yefimov S, van der Giessen E, Onck P, Marrink SJ. Biophys J. 2008; 94:2994. [PubMed: 18192351]

254. Louhivuori M, Risselada HJ, van der Giessen E, Marrink SJ. Proc Natl Acad Sci USA. 2010; 107:19856. [PubMed: 21041677]

255. Corry B, Hurst AC, Pal P, Nomura T, Rigby P, Martinac B. J Gen Physiol. 2010; 136:483. [PubMed: 20876362]

256. Vásquez V, Sotomayor M, Cordero-Morales J, Schulten K, Perozo E. Science. 2008; 321:1210. [PubMed: 18755978]

257. Vásquez V, Sotomayor M, Cortes DM, Roux B, Schulten K, Perozo E. J Mol Biol. 2008; 378:55. [PubMed: 18343404]

258. Sotomayor M, van der Straaten TA, Ravaioli U, Schulten K. Biophys J. 2006; 90:3496. [PubMed: 16513774]

259. Choudhary OP, Ujwal R, Kowallis W, Coalson R, Abramson J, Grabe M. J Mol Biol. 2010; 396:580. [PubMed: 20005234]

260. Cohen J, Schulten K. Biophys J. 2004; 86:836. [PubMed: 14747319]

261. Suenaga A, Yeh JZ, Taiji M, Toyama A, Takeuchi H, Son M, Takayama K, Iwamoto M, Sato I, Narahashi T, Konagaya A, Goto K. Biophys Chem. 2006; 120:36. [PubMed: 16288955]

262. Rui H, Lee KI, Pastor RW, Im W. Biophys J. 2011; 100:602. [PubMed: 21281574]

263. Krammer E-M, Homblé F, Prévost M. PLoS ONE. 2011; 6:e27994. [PubMed: 22164223]

264. Cheng MH, Coalson RD. Biophys J. 2012; 102:1363. [PubMed: 22455919]

265. Corry B, O'Mara M, Chung S-H. Biophys J. 2004; 86:846. [PubMed: 14747320]

266. Bisset D, Corry B, Chung S-H. Biophys J. 2005; 89:179. [PubMed: 15863476]

267. Cheng MH, Mamonov AB, Dukes JW, Coalson RD. J Phys Chem B. 2007; 111:5956. [PubMed: 17487993]

268. Lee KI, Rui H, Pastor RW, Im W. Biophys J. 2011; 100:611. [PubMed: 21281575]

269. Burykin A, Warshel A. Biophys J. 2003; 85:3696. [PubMed: 14645061]

270. Stroud RM, Savage D, Miercke LJ, Lee JK, Khademi S, Harries W. FEBS Lett. 2003; 555:79. [PubMed: 14630323]

271. Jensen MO, Tajkhorshid E, Schulten K. Biophys J. 2003; 85:2884. [PubMed: 14581193]

272. de Groot BL, Frigato T, Helms V, Grubmüller H. J Mol Biol. 2003; 333:279. [PubMed: 14529616]

273. Chen H, Wu Y, Voth GA. Biophys J. 2006; 90:L73. [PubMed: 16581846]

274. Wang Y, Tajkhorshid E. J Nutrition. 2007; 137:1509S. [PubMed: 17513417]

275. Bostick DL, Brooks CL. PLoS Comput Biol. 2007; 3:e22. [PubMed: 17291160]

276. Bostick DL, Charles LLB. Biophys J. 2007; 92:L103. [PubMed: 17434945]

277. Wang S, Orabi EA, Baday S, Bernèche S, Lamoureux G. J Am Chem Soc. 201210.1021/ja300129x

278. Luzhkov VB, Almlöf M, Nervall M, Åqvist J. Biochemistry. 2006; 45:10807. [PubMed: 16953566]

279. Levitt DG. Biophys J. 1991; 59:271. [PubMed: 1706949]

280. Barcilon V, Chen D-P, Eisenberg R. SIAM J App Math. 1992; 52:1405.

281. Chen DP, Barcilon V, Eisenberg RS. Biophys J. 1992; 61:1372. [PubMed: 1376159]

282. Chen D, Eisenberg R. Biophys J. 1993; 64:1405. [PubMed: 7686784]

283. Chen DP, Eisenberg RS. Biophys J. 1993; 65:727. [PubMed: 7693003]

284. Chen D, Xu L, Tripathy a, Meissner G, Eisenberg B. Biophys J. 1997; 73:1337. [PubMed: 9284302]

285. Chen D, Lear J, Eisenberg B. Biophys J. 1997; 72:97. [PubMed: 8994596]

286. Syganow A, von Kitzing E. J Phys Chem. 1995; 99:12030.

287. Moy G, Corry B, Kuyucak S, Chung S-H. Biophys J. 2000; 78:2349. [PubMed: 10777732]

288. Corry B, Kuyucak S, Chung SH. Biophys J. 2000; 78:2364. [PubMed: 10777733]

289. Crozier P, Rowley R, Holladay N, Henderson D, Busath D. Phys Rev Lett. 2001; 86:2467. [PubMed: 11289956]

290. Gillespie D, Nonner W, Eisenberg RS. J Phys: Condens Matter. 2002; 14:12129.

291. Gillespie D, Nonner W, Eisenberg R. Phys Rev E. 2003; 68:1.

292. Koumanov A, Zachariae U, Engelhardt H, Karshikoff A. Eur Biophys J. 2003; 32:689. [PubMed: 12879311]

293. Kuyucak S, Baştuğ T. J Biophys. 2003; 29:429.

294. Corry B, Kuyucak S, Chung S-H. Biophys J. 2003; 84:3594. [PubMed: 12770869]

295. Beckstein O, Tai K, Sansom MSP. J Am Chem Soc. 2004; 126:14694. [PubMed: 15535674]

296. Graf P, Kurnikova MG, Coalson RD, Nitzan A. J Phys Chem B. 2004; 108:2006.

297. Kessel A, Tieleman DP, Ben-Tal N. Eur Biophys J. 2004; 33:16. [PubMed: 13680212]

298. Baumgartner W. Comput Biol Chem. 2004; 28:67. [PubMed: 14871642]

299. Roux B, Allen T, Bernche S, Im W. Quart Rev Biophys. 2004; 37:15.

300. Gillespie D, Xu L, Wang Y, Meissner G. J Phys Chem B. 2005; 109:15598. [PubMed: 16852978]

301. Aguilella-Arzo M, Aguilella VM, Eisenberg RS. Eur Biophys J. 2005; 34:314. [PubMed: 15756588]

302. Cheng MH, Coalson RD. J Phys Chem B. 2005; 109:488. [PubMed: 16851040]

303. Hwang H, Schatz GC, Ratner MA. J Phys Chem B. 2006; 110:6999. [PubMed: 16571014]

304. Kandt C, Ash WL, Tieleman DP. Meth. 2007; 41:475.

305. Singer A, Norbury J. SIAM J App Math. 2009; 70:949.

306. Bolintineanu DS, Sayyed-Ahmad A, Davis HT, Kaznessis YN. PLoS Comput Biol. 2009; 5:e1000277. [PubMed: 19180178]

307. Eisenberg B. J Phys Chem C. 2010; 114:20719.

308. Eisenberg B. Chem Phys Lett. 2011; 511:1. [PubMed: 21799541]

309. Lu B, Zhou Y. Biophys J. 2011; 100:2475. [PubMed: 21575582]

310. Eisenberg B. Adv Chem Phys. 2012:77–223.

311. Krishnamurthy V, Chung S-H. IEEE Trans Nanobiosci. 2005; 4:102.

312. Vora T, Bisset D, Chung S-H. Biophys J. 2008; 95:1600. [PubMed: 18456826]

313. Gordon D, Krishnamurthy V, Chung S-H. Mol Phys. 2008; 106:1353.

314. Vora T, Corry B, Chung S-H. Eur Biophys J. 2008; 38:45. [PubMed: 18594804]

315. Song C, Corry B. Biophys J. 2010; 98:404. [PubMed: 20141753]

316. Krishnamurthy V, Luk KY. IEEE/ACM Trans Comp Biol Bioinfo. 2011; 8:273.

317. Lee KI, Jo S, Rui H, Egwolf B, Roux B, Pastor RW, Im W. J Comput Chem. 2012; 33:331. [PubMed: 22102176]

318. Csányi E, Boda D, Gillespie D, Kristóf T. Biochim Biophys Acta. 2012; 1818:592. [PubMed: 22080102]

319. Smondyrev AM, Voth GA. Biophys J. 2002; 83:1987. [PubMed: 12324417]

320. Domene C, Bond PJ, Sansom MSP. Adv Prot Chem. 2003; 66:159.

321. Tarek M, Maigret B, Chipot C. Biophys J. 2003; 85:2287. [PubMed: 14507693]

322. Biggin, PC.; Grottesi, A.; Sansom, MSP. From Prokaryotes to Eukaryotes: Molecular Modeling and Simulation Studies of Ion Channels. In: Kubalski, A.; Martinac, B., editors. Bacterial Ion Channels And Their Eukaryotic Homologs. ASM Press; Washington, DC: 2005. p. 133-152.

323. Tajkhorshid, E.; Cohen, J.; Aksimentiev, A.; Sotomayor, M.; Schulten, K. Towards an Understanding of Membrane Channels. In: Kubalski, A.; Martinac, B., editors. Bacterial Ion Channels: And Their Eukaryotic Homologs. ASM Press; Washington, DC: 2005. p. 133-152.

324. Gumbart J, Wang Y, Aksimentiev A, Tajkhorshid E, Schulten K. Curr Opin Struct Biol. 2005; 15:423. [PubMed: 16043343]

325. Hwang H, Schatz GC, Ratner MA. J Phys Chem B. 2006; 110:26448. [PubMed: 17181305]

326. Carpenter T, Bond PJ, Khalid S, Sansom MSP. Biophys J. 2008; 95:3790. [PubMed: 18621807]

327. Shaikh SA, Tajkhorshid E. Biophys J. 2008; 95:5153. [PubMed: 18790845]

328. Pietra F. J Phys Org Chem. 2008; 21:997.

329. Delemotte L, Dehez F, Treptow W, Tarek M. J Phys Chem B. 2008; 112:5547. [PubMed: 18412411]

330. Maffeo C, Aksimentiev A. Biophys J. 2009; 96:4853. [PubMed: 19527644]

331. Patargias G, Martay H, Fischer WB. J Biomol Struct Dyn. 2009; 27:1. [PubMed: 19492858]

332. Mustafa M, Henderson DJ, Busath DD. Proteins: Struct, Func, Bioinf. 2009; 76:794.

333. Khalili-Araghi F, Gumbart J, Wen P-C, Sotomayor M, Tajkhorshid E, Schulten K. Curr Opin Struct Biol. 2009; 19:128. [PubMed: 19345092]

334. Khurana E, Dal Peraro M, DeVane R, Vemparala S, DeGrado WF, Klein ML. Proc Natl Acad Sci USA. 2009; 106:1069. [PubMed: 19144924]

335. Pan J, Tieleman DP, Nagle JF, Kucerka N, Tristram-Nagle S. Biochim Biophys Acta. 2009; 1788:1387. [PubMed: 19248763]

336. Nury H, Poitevin F, Van Renterghem C, Changeux J-P, Corringer P-J, Delarue M, Baaden M. Proc Natl Acad Sci USA. 2010; 107:6275. [PubMed: 20308576]

337. Cheng MH, Coalson RD, Tang P. J Am Chem Soc. 2010; 132:16442. [PubMed: 20979415]

338. Zhu F, Hummer G. Proc Natl Acad Sci USA. 2010; 107:19814. [PubMed: 21041674]

339. Kutzner C, Grubmüller H, de Groot BL, Zachariae U. Biophys J. 2011; 101:809. [PubMed: 21843471]

340. Wilson MA, Wei C, Bjelkmar P, Wallace BA, Pohorille A. Biophys J. 2011; 100:2394. [PubMed: 21575573]

341. Stansfeld PJ, Sansom MSP. Structure. 2011; 19:1562. [PubMed: 22078556]

342. Chen C-C, Krüger J, Sramala I, Hsu H-J, Henklein P, Chen Y-MA, Fischer WB. Biochim Biophys Acta. 2011; 1808:572. [PubMed: 20708597]

343. Raunest M, Kandt C. Biochemistry. 2012; 51:1719. [PubMed: 22313049]

344. Furini S, Domene C. PLoS Comput Biol. 2012; 8:e1002476. [PubMed: 22496637]

345. Becucci L, Cembran A, Karim CB, Thomas DD, Guidelli R, Gao J, Veglia G. Biophys J. 2009; 96:L60. [PubMed: 19450461]

346. Gumbart J, Khalili-Araghi F, Sotomayor M, Roux B. Biochim Biophys Acta. 2011; 1818:294. [PubMed: 22001851]

347. Carnevale V, Treptow W, Klein ML. J Phys Chem Lett. 2011; 2:2504.

348. Bhattacharya S, Derrington IM, Pavlenok M, Niederweis M, Gundlach JH, Aksimentiev A. ACS Nano. 2012; 6:6960. In Press. [PubMed: 22747101]

349. Graf P, Nitzan A, Kurnikova MG, Coalson RD. J Phys Chem B. 2000; 104:12324.

350. Peter C, Hummer G. Biophys J. 2005; 89:2222. [PubMed: 16006629]

351. Boda D, Valiskó M, Eisenberg B, Nonner W, Henderson D, Gillespie D. Phys Rev Lett. 2007; 98:1.

352. Thøgersen L, Schiøtt B, Vosegaard T, Nielsen NC, Tajkhorshid E. Biophys J. 2008; 95:4337. [PubMed: 18676652]

353. Plank G, Zhou L, Greenstein JL, Cortassa S, Winslow RL, O'Rourke B, Trayanova NA. Phil Trans R Soc Lond A. 2008; 366:3381.

354. Eisenberg B, Hyon Y, Liu C. J Chem Phys. 2010; 133:104104. [PubMed: 20849161]

355. Hannongbua, S.; Treesuwan, W.; Boonyarat, W. Advanced Molecular Modeling Techniques Applied to Ion Channels Blockers. In: Gupta, SP., editor. Ion Channels and Their Inhibitors. Springer-Verlag; Berlin Heidelberg: 2011. p. 53-78.

356. Zheng W, Auerbach A. PLoS Comput Biol. 2011; 7:e1001046. [PubMed: 21253563]

357. Boda D, Busath DD, Eisenberg B, Henderson D, Nonner W. Phys Chem Chem Phys. 2002; 4:5154.

358. Boda D, Henderson D, Busath DD. Mol Phys. 2002; 100:2361.

359. Cervera J, Schiedt B, Ramirez P. Europhys Lett. 2005; 71:35.

360. Vidal J, Gracheva ME, Leburton J-P. Nanoscale Res Lett. 2006; 2:61.

361. Gracheva M, Leburton J-P. Nanotechnology. 2007; 18:145704.

362. Vidal J, Gracheva M, Leburton J-P. Nanoscale Res Lett. 2007; 2:61.

363. Cervera J, Alcaraz A, Schiedt B, Neumann R, Ramirez P. J Phys Chem C. 2007; 111:12265.

364. Vlassiouk I, Smirnov S, Siwy Z. Nano Lett. 2008; 8:1978. [PubMed: 18558784]

365. Gillespie D, Boda D, He Y, Apel P, Siwy ZS. Biophys J. 2008; 95:609. [PubMed: 18390596]

366. Kosińska ID, Hänggi P. Phys Rev E. 2008; 77:1.

367. Reiner JE, Kasianowicz JJ, Nablo BJ, Robertson JWF. Proc Natl Acad Sci USA. 2010; 107:12080. [PubMed: 20566890]

368. Zhang Y, Voth GA. J Chem Theory Comput. 2011; 7:2277.

369. Zhang M, Yeh L, Qian S, Hsu J. J Phys Chem C. 2012; 116:4793.

370. Yeh, L-h; Zhang, M.; Qian, S.; Hsu, J-p; Tseng, S. J Phys Chem C. 2012; 116:8672.

371. Carr R, Comer J, Ginsberg M, Aksimentiev A. Lab Chip. 2011; 11:3766. [PubMed: 21986816]

372. Peters MH. J Chem Phys. 2011; 134:025105. [PubMed: 21241153]

373. Comer J, Aksimentiev A. J Phys Chem C. 2012; 116:3376.

374. Timp W, Comer J, Aksimentiev A. Biophys J. 2012; 102:L37. [PubMed: 22677395]

375. Aksimentiev A, Heng JB, Timp G, Schulten K. Biophys J. 2004; 87:2086. [PubMed: 15345583]

376. Heng JB, Aksimentiev A, Ho C, Marks P, Grinkova YV, Sligar S, Schulten K, Timp G. Biophys J. 2006; 90:1098. [PubMed: 16284270]

377. Lu D, Aksimentiev A, Shih AY, Cruz-Chu E, Freddolino PL, Arkhipov A, Schulten K. Phys Bio. 2006; 3:S40. [PubMed: 16582464]

378. Luan B, Aksimentiev A. Phys Rev E. 2008; 78:021912.

379. Carr R, Weinstock IA, Sivaprasadarao A, Müller A, Aksimentiev A. Nano Lett. 2008; 8:3916. [PubMed: 18844424]

380. Comer J, Dimitrov V, Zhao Q, Timp G, Aksimentiev A. Biophys J. 2009; 96:593. [PubMed: 19167307]

381. Luan B, Aksimentiev A. J Phys: Condens Matter. 2010; 22:454123. [PubMed: 21339610]

382. Gracheva M, Xiong A, Aksimentiev A, Schulten K, Timp G, Leburton J-P. Nanotechnology. 2006; 17:622.

383. Gracheva M, Aksimentiev A, Leburton J-P. Nanotechnology. 2006; 17:3160.

384. Sigalov G, Comer J, Timp G, Aksimentiev A. Nano Lett. 2008; 8:56. [PubMed: 18069865]

385. Cruz-Chu ER, Aksimentiev A, Schulten K. J Phys Chem C. 2009; 113:1850.

386. Dorvel B, Sigalov G, Zhao Q, Comer J, Dimitrov V, Mirsaidov U, Aksimentiev A, Timp G. Nucl Acids Res. 2009; 37:4170. [PubMed: 19433506]

387. Wang D, Timp W, Shim J, Mirsaidov U, Comer J, Aksimentiev A, Timp G. Biophys J. 2010; 98:599a.

388. Comer, J.; Aksimentiev, A. Nanopore Force Spectroscopy: Insights from Molecular Dynamics Simulations. In: Bashir, R.; Iqbal, S., editors. Nanopores: Sensing and Fundamental Biological Interactions. Vol. Chapter 14. Springer Science and Business Media, LLC; New York: 2011. p. 335-356.

389. Sathe C, Zou X, Leburton J-P, Schulten K. ACS Nano. 2011; 5:8842. [PubMed: 21981556]

390. Wanunu M, Bhattacharya S, Xie Y, Tor Y, Aksimentiev A, Drndic M. ACS Nano. 2011; 5:9345. [PubMed: 22067050]

391. Kowalczyk SW, Wells DB, Aksimentiev A, Dekker C. Nano Lett. 2012; 12:1038. [PubMed: 22229707]

392. Wells DB, Belkin M, Comer J, Aksimentiev A. Nano Lett. 2012; 8:4117. [PubMed: 22780094]

393. Edmonds CM, Hudiono YC, Ahmadi AG, Hesketh PJ, Nair S. J Chem Phys. 2012; 136:065105. [PubMed: 22360225]

394. Saha KK, Drndić M, Nikolić BK. Nano Lett. 2012; 12:50. [PubMed: 22141739]

395. Hille, B. Ionic channels of excitable membranes. 3. Sinauer Associates; Sunderland, MA: 2001.

396. Hodgkin AL, Huxley AF. J Physiol. 1952; 117:500. [PubMed: 12991237]

397. Hodgkin AL, Huxley AF. J Physiol. 1952; 117:500. [PubMed: 12991237]

398. Alberts, B.; Johnson, A.; Lewis, J.; Raff, M.; Roberts, K.; Walter, P. Molecular Biology of The Cell. 5. Garland Science; New York & London: 2007.

399. Watanabe H, Sugiura S, Kafuku H, Hisada T. Biophys J. 2004; 87:2074. [PubMed: 15345582]

400. Wong J, Goktepe S, Kuhl E. Comput Method Appl M. 2011; 200:3139.

401. Rowat P. Neur Comp. 2007; 19:1215.

402. Tuckwell HC, Jost J. Physica A. 2009; 388:4115.

403. Linaro D, Storace M, Giugliano M. PLoS Comput Biol. 2011; 7:e1001102. [PubMed: 21423712]

404. Che Y-Q, Wang J, Zhou S-S, Deng B. Chaos Soliton Fract. 2009; 40:1588.

405. Beard DA. PLoS Comput Biol. 2005; 1:e36. [PubMed: 16163394]

406. Townsley LE, Tucker WA, Sham S, Hinton JF. Biochemistry. 2001; 40:11676. [PubMed: 11570868]

407. Chang G, Spencer RH, Lee AT, Barclay MT, Rees DC. Science. 1998; 282:2220. [PubMed: 9856938]

408. Bass RB, Strop P, Barclay M, Rees DC. Science. 2002; 298:1582. [PubMed: 12446901]

409. Conroy MJ, Durand A, Lupo D, Li X-DD, Bullough PA, Winkler FK, Merrick M. Proc Natl Acad Sci USA. 2007; 104:1213. [PubMed: 17220269]

410. Uysal S, Vásquez V, Tereshko V, Esaki K, Fellouse F, Sidhu S, Koide S, Perozo E, Kossiakoff A. Proc Natl Acad Sci USA. 2009; 106:6644. [PubMed: 19346472]

411. Long SB, Tao X, Campbell EB, MacKinnon R. Nature. 2007; 450:376. [PubMed: 18004376]

412. Gonen T, Cheng Y, Sliz P, Hiroaki Y, Fujiyoshi Y, Harrison SC, Walz T. Nature. 2005; 438:633. [PubMed: 16319884]

413. Miyazawa A, Fujiyoshi Y, Unwin N. Nature. 2003; 423:949. [PubMed: 12827192]

414. Unwin N. J Mol Biol. 2005; 346:967. [PubMed: 15701510]

415. Cowan S, Schirmer T, Rummel G, Steiert M, Ghosh R, Pauptit R, Jansonius J, Rosenbusch J. Nature. 1992; 358:727. [PubMed: 1380671]

416. Dutzler R, Campbell EB, MacKinnon R. Science. 2003; 300:108. [PubMed: 12649487]

417. Song L, Hobaugh MR, Shustak C, Cheley S, Bayley H, Gouaux JE. Science. 1996; 274:1859. [PubMed: 8943190]

418. Malasics A, Gillespie D, Nonner W, Henderson D, Eisenberg B, Boda D. Biochim Biophys Acta Biomembr. 2009; 1788:2471.

419. Giri J, Fonseca J, Boda D, Henderson D, Eisenberg B. Phys Bio. 2011; 8:026004. [PubMed: 21263167]

420. Mackay DH, Berens PH, Wilson KR, Hagler AT. Biophys J. 1984; 46:229. [PubMed: 6206901]

421. Morais-Cabral JH, Zhou Y, MacKinnon R. Nature. 2001; 414:37. [PubMed: 11689935]

422. Wulff H, Calabresi PA, Allie R, Yun S, Pennington M, Beeton C, Chandy KG. J Clin Invest. 2003; 111:1703. [PubMed: 12782673]

423. Judge SIV, Bever CT. Pharmacol Ther. 2006; 111:224. [PubMed: 16472864]

424. Parsegian A. Nature. 1969; 221:844. [PubMed: 5765058]

425. Rashid MH, Kuyucak S. J Phys Chem B. 2012; 116:4812. [PubMed: 22480371]

426. Kung C. Nature. 2005; 436:647. [PubMed: 16079835]

427. Kung C, Martinac B, Sukharev S. Annu Rev Microbiol. 2010; 64:313. [PubMed: 20825352]

428. Sukharev SI, Blount P, Martinac B, Blattner FR, Kung C. Nature. 1994; 368:265. [PubMed: 7511799]

429. Levina N, Totemeyer S, Stokes NR, Louis P, Jones MA, Booth IR. EMBO J. 1999; 18:1730. [PubMed: 10202137]

430. Wang W, Black SS, Edwards MD, Miller S, Morrison EL, Bartlett W, Dong C, Naismith JH, Booth IR. Science. 2008; 321:1179. [PubMed: 18755969]

431. Liu Z, Gandhi CS, Rees DC. Nature. 2009; 461:120. [PubMed: 19701184]

432. Martinac B, Buechner M, Delcour AH, Adler J, Kung C. Proc Natl Acad Sci USA. 1987; 84:2297. [PubMed: 2436228]

433. Weiss MS, Schulz GE. J Mol Biol. 1992; 227:493. [PubMed: 1328651]

434. Kreusch A, Schulz G. J Mol Biol. 1994; 243:891. [PubMed: 7525973]

435. Cowan SW, Garavito RM, Jansonius JN, Jenkins JA, Karlsson R, König N, Pai EF, Pauptit RA, Rizkallah PJ, Rosenbusch JP. Structure. 1995; 3:1041. [PubMed: 8589999]

436. Schirmer T, Keller TA, Wang YF, Rosenbusch JP. Science. 1995; 267:512. [PubMed: 7824948]

437. Dutzler R, Rummel G, Albertí S, Hernández-Allés S, Phale P, Rosenbusch J, Benedí V, Schirmer T. Structure. 1999; 7:425. [PubMed: 10196126]

438. Moraes TF, Bains M, Hancock REW, Strynadka NCJ. Nat Struct Mol Biol. 2007; 14:85. [PubMed: 17187075]

439. Biswas S, Mohammad MM, Movileanu L, van der Berg B. Structure. 2008; 16:1027. [PubMed: 18611376]

440. Tamber S, Hancock REW. FEMS Microbiol Lett. 2006; 260:23. [PubMed: 16790014]

441. Liu J, Eren E, Vijayaraghavan J, Cheneke BR, Indic M, van den Berg B, Movileanu L. Biochemistry. 2012; 51:2319. [PubMed: 22369314]

442. Cheneke BR, van der Berg B, Movileanu L. Biochemistry. 2011; 50:4987. [PubMed: 21548584]

443. Cheneke BR, Indic M, van den Berg B, Movileanu L. Biochemistry. 2012; 010.1021/bi300332z

444. Vila J, Martí S, Sánchez-Céspedes J. J Antimicrob Chemo. 2007; 59:1210.

445. Song L, Hobaugh MR, Shustak C, Cheley S, Bayley H, Gouaux JE. Science. 1996; 274:1859. [PubMed: 8943190]

446. Kasianowicz J, Robertson JWF, Chan ER, Reiner JE, Stanford VM. Ann Rev Anal Chem. 2008; 1:737.

447. Kasianowicz JJ, Brandin E, Branton D, Deamer DW. Proc Natl Acad Sci USA. 1996; 93:13770. [PubMed: 8943010]

448. Faller M, Niederweis M, Schulz GE. Science. 2004; 303:1189. [PubMed: 14976314]

449. Butler T, Pavlenok M, Derrington I, Niederweis M, Gundlach J. Proc Natl Acad Sci USA. 2008; 105:20647. [PubMed: 19098105]

450. Derrington IM, Collins MD, Pavlenok M, Niederweis M, Gundlach JH. Biophys J. 2010; 98:422a.

451. Manrao E, Derrington I, Pavlenok M, Niederweis M, Gundlach J. PLoS ONE. 2011; 6:e25723. [PubMed: 21991340]

452. Roos N, Benz R, Brdiczka D. Biochim Biophys Acta. 1982; 686:204. [PubMed: 7082663]

453. Hiller S, Garces RG, Malia TJ, Orekhov VY, Colombini M, Wagner G. Science. 2008; 321:1206. [PubMed: 18755977]

454. Ujwal R, Cascio D, Colletier J-P, Faham S, Zhang J, Toro L, Ping P. Proc Natl Acad Sci USA. 2008; 105:2.

455. Bayrhuber M, Meins T, Habeck M, Becker S, Giller K, Villinger S, Vonrhein C, Griesinger C, Zweckstetter M, Zeth K. Proc Natl Acad Sci USA. 2008; 105:15370. [PubMed: 18832158]

456. Colombini M. Trends Biochem Sci. 2009; 34:382. [PubMed: 19647437]

457. Hiller S, Abramson J, Mannella C, Wagner G, Zeth K. Trends Biochem Sci. 2010; 35:514. [PubMed: 20708406]

458. Hiller S, Raschle T, Yu T-Y, Rice AJ, Walz T, Wagner G. Biochim Biophys Acta –Bioener. 2010; 1797:66.

459. Chen T-Y. Annu Rev Physiol. 2005; 67:809. [PubMed: 15709979]

460. Dutzler R, Campbell EB, Cadene M, Chait BT, MacKinnon R. Nature. 2002; 415:287. [PubMed: 11796999]

461. Accardi A, Miller C. Nature. 2004; 427:803. [PubMed: 14985752]

462. Steinlein OK, Bertrand D. Biochem Pharm. 2008; 76:1175. [PubMed: 18691557]

463. Rose JE. Biochem Pharm. 2007; 74:1263. [PubMed: 17826746]

464. Marini AM, Soussi-Boudekou S, Vissers S, Andre B. Mol Cell Biol. 1997; 17:4282. [PubMed: 9234685]

465. Ninnemann O, Jauniaux JC, Frommer WB. EMBO J. 1994; 13:3464. [PubMed: 8062823]

466. Marini AM, Vissers S, Urrestarazu A, André B. EMBO J. 1994; 13:3456. [PubMed: 8062822]

467. Khademi S, O'Connell J, Remis J, Robles-Colmenares Y, Miercke LJW, Stroud RM. Science. 2004; 305:1587. [PubMed: 15361618]

468. Javelle A, Lupo D, Ripoche P, Fulford T, Merrick M, Winkler FK. Proc Natl Acad Sci USA. 2008; 105:5040. [PubMed: 18362341]

469. Gruswitz F, O'Connell J, Stroud RM. Proc Natl Acad Sci USA. 2007; 104:42. [PubMed: 17190799]

470. Javelle A, Lupo D, Zheng L, Li X-DD, Winkler FK, Merrick M. J Biol Chem. 2006; 281:39492. [PubMed: 17040913]

471. Gao J, Truhlar DG. Annu Rev Phys Chem. 2002; 53:467. [PubMed: 11972016]

472. Kamerlin SCL, Vicatos S, Dryga A, Warshel A. Annu Rev Phys Chem. 2011; 62:41. [PubMed: 21034218]

473. Modi N, Winterhalter M, Kleinekathöfer U. Nanoscale. 2012; 4:6166. [PubMed: 23198289]

474. Maffeo C, Schöpflin R, Brutzer H, Stehr R, Aksimentiev A, Wedemann G, Seidel R. Phys Rev Lett. 2010; 105:158101. [PubMed: 21230940]

475. Simonson T, Carlsson J, Case DA. J Am Chem Soc. 2004; 126:4167. [PubMed: 15053606]

476. Rocchia W, Alxov E, Honig B. J Phys Chem B. 2001; 105:6507.

477. Baker N, Sept D, Joseph S, Hoist M, McCammon J. Proc Natl Acad Sci USA. 2001; 98:10037. [PubMed: 11517324]

478. Ramírez P, Aguilella-Arzo M, Alcaraz A, Cervera J, Aguilella VM. Cell Biochem Biophys. 2006; 44:287. [PubMed: 16456229]

479. Woolley G, Biggin P, Schultz A, Lien L, Jaikaran D, Breed J, Crowhurst K, Sansom M. Biophys J. 1997; 73:770. [PubMed: 9251793]

480. Nonner W, Chen D, Eisenberg B. Biophys J. 1998; 74:2327. [PubMed: 9591660]

481. Roth R. J Phys: Condens Matter. 2010; 22:063102. [PubMed: 21389360]

482. Woolf T, Roux B. Proc Natl Acad Sci USA. 1994; 91:11631. [PubMed: 7526400]

483. Hummer G. New J Phys. 2005; 7:34.

484. Paine PL, Scherr P. Biophys J. 1975; 15:1087. [PubMed: 1203442]

485. Roux B. Biophys J. 1999; 77:139. [PubMed: 10388746]

486. Corry B, Allen T, Kuyucak S, Chung S. Biophys J. 2001; 80:195. [PubMed: 11159395]

487. Cooper K, Jakobsson E, Wolynes P. Prog Biophys Mol Biol. 1985; 46:51. [PubMed: 2410952]

488. Mackerell AD. J Comput Chem. 2004; 25:1584. [PubMed: 15264253]

489. MacKerell; D, Bashford AD, Bellott, Dunbrack L, Evanseck RJD, Field MJ, Fischer S, Gao J, Guo H, Ha S, Joseph-McCarthy D, Kuchnir L, Kuczera K, Lau FTK, Mattos C, Michnick S, Ngo T, Nguyen DT, Prodhom B, Reiher WE, Roux B, Schlenkrich M, Smith JC, Stote R, Straub J, Watanabe M, Wiórkiewicz-Kuczera J, Yin D, Karplus M. J Phys Chem B. 1998; 102:3586.

490. Weiner PK, Kollman PA. J Comput Chem. 1981; 2:287.

491. Cornell WD, Cieplak P, Bayly CI, Gould IR, Merz KM, Ferguson DM, Spellmeyer DC, Fox T, Caldwell JW, Kollman PA. J Am Chem Soc. 1995; 117:5179.

492. Jorgensen WL, Maxwell DS, Tirado-Rives J. J Am Chem Soc. 1996; 118:11225.

493. Kaminski GA, Friesner RA, Tirado-Rives J, Jorgensen WL. J Phys Chem B. 2001; 105:6474.

494. Hermans J, Berendsen HJC, Van Gunsteren WF, Postma JPM. Biopolymers. 1984; 23:1513.

495. Schmid N, Eichenberger AP, Choutko A, Riniker S, Winger M, Mark AE, van Gunsteren WF. Eur Biophys J. 2011; 40:843. [PubMed: 21533652]

496. Klauda JB, Venable RM, Freites JA, O'Connor JW, Tobias DJ, Mondragon-Ramirez C, Vorobyov I, MacKerell AD, Pastor RW. J Phys Chem B. 2010; 114:7830. [PubMed: 20496934]

497. Wang J, Wolf RM, Caldwell JW, Kollman PA, Case DA. J Comput Chem. 2004; 25:1157. [PubMed: 15116359]

498. Liu Y, Chipot C, Shao X, Cai W. Phys Bio. 2011; 8:056005. [PubMed: 21865621]

499. Daura X, Mark AE, van Gunsteren WF. J Comput Chem. 1998; 19:535.

500. Berger O, Edholm O, Jähnig F. Biophys J. 1997; 72:2002. [PubMed: 9129804]

501. Cordomí A, Caltabiano G, Pardo L. J Chem Theory Comput. 2012; 8:948.

502. Aksimentiev, A.; Wells, D.; Sotomayor, M. Membrane Protein Tutorial. http://www.ks.uiuc.edu/Training/Tutorials/science/membrane/mem-tutorial.pdf%relax

503. Humphrey W, Dalke A, Schulten K. J Mol Graphics. 1996; 14:33.

504. Brooks BR, Bruccoleri RE, Olafson BD, States DJ, Swaminathan S, Karplus M. J Comput Chem. 1983:187–217.

505. Jo S, Lim JB, Klauda JB, Im W. Biophys J. 2009; 97:50. [PubMed: 19580743]

506. Ayton GS, Voth GA. Curr Opin Struct Biol. 2009; 19:138. [PubMed: 19362465]

507. Marrink SJ, de Vries AH, Tieleman DP. Biochim Biophys Acta. 2009; 1788:149. [PubMed: 19013128]

508. Nielsen SO, Lopez CF, Srinivas G, Klein ML. J Phys: Condens Matter. 2004; 16:R481.

509. Yesylevskyy SO, Schäfer LV, Sengupta D, Marrink SJ. PLoS Comput Biol. 2010; 6:e1000810. [PubMed: 20548957]

510. Wu Z, Cui Q, Yethiraj A. J Phys Chem B. 2010; 114:10524. [PubMed: 20701383]

511. Sali A, Blundell TL. J Mol Biol. 1993; 234:779. [PubMed: 8254673]

512. Capener CE, Shrivastava IH, Ranatunga KM, Forrest LR, Smith GR, Sansom MS. Biophys J. 2000; 78:2929. [PubMed: 10827973]

513. Roux B. Comput Phys Commun. 1995; 91:275.

514. Kollman P. Chem Rev. 1993; 93:2395.

515. Pohorille A, Jarzynski C, Chipot C. J Phys Chem B. 2010; 114:10235. [PubMed: 20701361]

516. Torrie G, Valleau J. J Comp Phys. 1977; 23:187.

517. Kumar S, Bouzida D, Swendsen RH, Kollman PA, Rosenberg JM. J Comput Chem. 1992; 13:1011.

518. Woo H-J, Roux B. Proc Natl Acad Sci USA. 2005; 102:6825. [PubMed: 15867154]

519. Singh UC, Brown FK, Bash PA, Kollman PA. J Am Chem Soc. 1987; 109:1607.

520. Grubmüller H, Heymann B, Tavan P. Science. 1996; 271:997. [PubMed: 8584939]

521. Isralewitz B, Izrailev S, Schulten K. Biophys J. 1997; 73:2972. [PubMed: 9414212]

522. Izrailev S, Stepaniants S, Balsera M, Oono Y, Schulten K. Biophys J. 1997; 72:1568. [PubMed: 9083662]

523. Stepaniants S, Izrailev S, Schulten K. J Mol Mod. 1997; 3:473.

524. Marrink S-J, Berger O, Tieleman P, Jähnig F. Biophys J. 1998; 74:931. [PubMed: 9533704]

525. Kosztin D, Izrailev S, Schulten K. Biophys J. 1999; 76:188. [PubMed: 9876133]

526. Hummer G, Szabo A. Acc Chem Res. 2005; 38:504. [PubMed: 16028884]

527. Jarzynski C. Phys Rev Lett. 1997; 78:2690.

528. Bucher D, Guidoni L, Rothlisberger U. Biophys J. 2007; 93:2315. [PubMed: 17526559]

529. Arkin IT, Xu HF, Jensen MO, Arbely E, Bennett ER, Bowers KJ, Chow E, Dror RO, Eastwood MP, Flitman-Tene R, Gregersen BA, Klepeis JL, Kolossvary I, Shan YB, Shaw DE. Science. 2007; 317:799. [PubMed: 17690293]

530. Warshel A, Sussman F, King G. Biochemistry. 1986; 25:8368. [PubMed: 2435316]

531. Li L, Vorobyov I, Mackerell AD, Allen TW. Biophys J. 2007; 94:L11. [PubMed: 17981901]

532. Li L, Vorobyov I, Allen TW. J Phys Chem B. 2008; 112:9574. [PubMed: 18636765]

533. Yoo J, Cui Q. Biophys J. 2008; 94:L61. [PubMed: 18199662]

534. MacCallum JL, Bennett WFD, Tieleman DP. Biophys J. 2008; 94:3393. [PubMed: 18212019]

535. Yoo J, Cui Q. Biophys J. 2010; 99:1529. [PubMed: 20816065]

536. Johansson ACV, Lindahl E. J Phys Chem B. 2009; 113:245. [PubMed: 19118487]

537. Honig B, Sharp K, Yang AS. J Phys Chem. 1993; 97:1101.

538. Lim C, Bashford D, Karplus M. J Phys Chem. 1991; 95:5610.

539. Warshel A, Papazyan A. Curr Opin Struct Biol. 1998; 8:211. [PubMed: 9631295]

540. Ullmann GM, Knapp E-W. Eur Biophys J. 1999; 28:533. [PubMed: 10541792]

541. Srinivasan J, Trevathan MW, Beroza P, Case DA. Theor Chem Acc. 1999; 101:426.

542. Koumanov A, Rüterjans H, Karshikoff A. Proteins: Struct, Func, Gen. 2002; 46:85.

543. Mongan J, Case DA, McCammon JA. J Comput Chem. 2004; 25:2038. [PubMed: 15481090]

544. Mongan J, Case DA. Curr Opin Struct Biol. 2005; 15:157. [PubMed: 15837173]

545. Khandogin J, Brooks CL. Biochemistry. 2006; 45:9363. [PubMed: 16878971]

546. Gunner G, Mao J, Song Y, Kim J. Biochim Biophys Acta – Bioener. 2006; 1757:942.

547. Spassov VZ, Yan L. Prot Sci. 2008; 17:1955.

548. Karshikoff A, Spassov V, Cowan SW, Ladenstein R, Schirmer T. J Mol Biol. 1994; 240:372. [PubMed: 8035460]

549. Tanizaki S, Feig M. J Chem Phys. 2005; 122:124706. [PubMed: 15836408]

550. Gordon JC, Myers JB, Folta T, Shoja V, Heath LS, Onufriev A. Nucl Acids Res. 2005; 33:W368. [PubMed: 15980491]

551. Olsson MHM, Søndergaard CR, Rostkowski M, Jensen JH. J Chem Theory Comput. 2011; 7:525.

552. Jo S, Vargyas M, Vasko-Szedlar J, Roux B, Im W. Nucl Acids Res. 2008; 36:W270. [PubMed: 18508808]

553. Shaw DE, Chao JC, Eastwood MP, Gagliardo J, Grossman JPP, Ho CR, Lerardi DJ, Kolossváry I, Klepeis JL, Layman T, McLeavey C, Deneroff MM, Moraes MA, Mueller R, Priest EC, Shan Y, Spengler J, Theobald M, Towles B, Wang SC, Dror RO, Kuskin JS, Larson RH, Salmon JK, Young C, Batson B, Bowers KJ. Comm ACM. 2008; 51:91.

554. Shaw DE. J Comput Chem. 2005; 26:1318. [PubMed: 16013057]

555. Dror RO, Jensen MO, Borhani DW, Shaw DE. J Gen Physiol. 2010; 135:555. [PubMed: 20513757]

556. Dror RO, Dirks RM, Grossman JP, Xu H, Shaw DE. Annu Rev Biochem. 2012; 41:429.

557. Dror RO, Pan AC, Arlow DH, Borhani DW, Maragakis P, Shan Y, Xu H, Shaw DE. Proc Natl Acad Sci USA. 2011; 108:13118. [PubMed: 21778406]

558. Rosenbaum DM, Zhang C, Lyons JA, Holl R, Aragao D, Arlow DH, Rasmussen SGF, Choi H-JJ, Devree BT, Sunahara RK, Chae PS, Gellman SH, Dror RO, Shaw DE, Weis WI, Caffrey M, Gmeiner P, Kobilka BK. Nature. 2011; 469:236. [PubMed: 21228876]

559. Kruse AC, Hu J, Pan AC, Arlow DH, Rosenbaum DM, Rosemond E, Green HF, Liu T, Chae PS, Dror RO, Shaw DE, Weis WI, Wess J, Kobilka BK. Nature. 2012; 482:552. [PubMed: 22358844]

560. Jensen MO, Dror RO, Xu HF, Borhani DW, Arkin IT, Eastwood MP, Shaw DE. Proc Natl Acad Sci USA. 2008; 105:14430. [PubMed: 18787121]

561. Vorobyov IV, Anisimov VM, MacKerell AD. J Phys Chem B. 2005; 109:18988. [PubMed: 16853445]

562. Jiao D, King C, Grossfield A, Darden TA, Ren P. J Phys Chem B. 2006; 110:18553. [PubMed: 16970483]

563. Yu H, Whitfield TW, Harder E, Lamoureux G, Vorobyov I, Anisimov VM, Mackerell AD, Roux B. J Chem Theory Comput. 2010; 6:774. [PubMed: 20300554]

564. Siu SWI, Vácha R, Jungwirth P, Böckmann RA. J Chem Phys. 2008; 128:125103. [PubMed: 18376978]

565. Harder E, MacKerell AD, Roux B. J Am Chem Soc. 2009; 131:2760. [PubMed: 19199514]

566. Lopes PEM, Roux B, MacKerell AD. Theor Chem Acc. 2009; 124:11. [PubMed: 20577578]

567. Ren P, Ponder JW. J Comput Chem. 2002; 23:1497. [PubMed: 12395419]

568. Grossfield A, Ren P, Ponder JW. J Am Chem Soc. 2003; 125:15671. [PubMed: 14664617]

569. Ponder JW, Wu C, Ren P, Pande VS, Chodera JD, Schnieders MJ, Haque I, Mobley DL, Lambrecht DS, DiStasio RA, Head-Gordon M, Clark GNI, Johnson ME, Head-Gordon T. J Phys Chem B. 2010; 114:2549. [PubMed: 20136072]

570. Lamoureux G, Alexander D, MacKerell J, Roux B. J Chem Phys. 2003; 119:5185.

571. Baker CM, Lopes PEM, Zhu X, Roux B, MacKerell AD. J Chem Theory Comput. 2010; 6:1181. [PubMed: 20401166]

572. Vorobyov I, Li L, Allen TW. J Phys Chem B. 2008; 112:9588. [PubMed: 18636764]

573. Luan B, Carr R, Caffrey M, Aksimentiev A. Proteins: Struct, Func, Bioinf. 2010; 78:21153.

574. Cherezov V, Wei L, Jeremy D, Luan B, Aksimentiev A, Katritch V, Caffrey M. Proteins: Struct, Func, Bioinf. 2008; 71:24.

575. Luan B, Caffrey M, Aksimentiev A. Biophys J. 2007; 93:3058. [PubMed: 17938421]

576. Hodgkin A, Keynes R. J Physiol. 1955; 128:61. [PubMed: 14368575]

577. Iannuzzi M, Laio A, Parrinello M. Phys Rev Lett. 2003; 90:238302. [PubMed: 12857293]

578. Bussi G, Laio A, Parrinello M. Phys Rev Lett. 2006; 96:090601. [PubMed: 16606249]

579. Ensing B, De Vivo M, Liu Z, Moore P, Klein M. Acc Chem Res. 2006; 39:73. [PubMed: 16489726]

580. Decrouy A, Juteau M, Proteau S, Teijiera J, Rousseau E. J Mol Cell Cardiol. 1996; 28:767. [PubMed: 8732504]

581. Kovacs RJ, Nelson MT, Simmerman HK, Jones LR. J Biol Chem. 1988; 263:18364. [PubMed: 2848034]

582. Becucci L, Papini M, Verardi R, Veglia G, Guidelli R. Soft Matter. 2012; 8:3881.

583. Feng L, Campbell EB, Hsiung Y, MacKinnon R. Science. 2010; 330:635. [PubMed: 20929736]

584. Sachs JN, Crozier PS, Woolf TB. J Chem Phys. 2004; 121:10847. [PubMed: 15634036]

585. Aksimentiev A. Nanoscale. 2010; 2:468. [PubMed: 20644747]

586. Yang Z, van der Straaten TA, Ravaioli U, Liu Y. J Comp Electron. 2005; 4:167.

587. Paine PL, Scherr P. Biophys J. 1975; 15:1087. [PubMed: 1203442]

588. Menestrina G. J Membr Biol. 1986; 90:177. [PubMed: 2425095]

589. Gu LQ, Bayley H. Biophys J. 2000; 79:1967. [PubMed: 11023901]

590. Mohammad MM, Movileanu L. J Phys Chem B. 2010; 114:8750. [PubMed: 20540583]

591. Frankenhaeuser BYB. J Physiol. 1960; 152:159. [PubMed: 13824559]

592. Bezanilla F, Armstrong CM. J Gen Physiol. 1972; 60:588. [PubMed: 4644327]

593. Neyton J, Miller C. J Gen Physiol. 1988; 92:569. [PubMed: 3235974]

594. Allen TW, Hoyles M. Chem Phys Lett. 1999; 313:358.

595. Thompson AN, Kim I, Panosian TD, Iverson TM, Allen TW, Nimigean CM. Nat Struct Mol Biol. 2009; 16:1317. [PubMed: 19946269]

596. Kim I, Allen TW. Proc Natl Acad Sci USA. 2011; 108:17963. [PubMed: 22011574]

597. Benz R, Egli C, Hancock R. Biochim Biophys Acta. 1993; 1149:224. [PubMed: 8323941]

598. Perozo E, Cortes DM, Sompornpisut P, Kloda A, Martinac B. Nature. 2002; 418:942. [PubMed: 12198539]

599. Perozo E, Kloda A, Cortes DM, Martinac B. Nature Struct Biol. 2002; 9:696. [PubMed: 12172537]

600. Lee S-Y, Lee A, Chen J, MacKinnon R. Proc Natl Acad Sci USA. 2005; 102:15441. [PubMed: 16223877]

601. Long SB, Campbell EB, MacKinnon R. Science. 2005; 309:897. [PubMed: 16002581]

602. Zúñiga L, Márquez V, González-Nilo FD, Chipot C, Cid LP, Sepúlveda FV, Niemeyer MI. PLoS ONE. 2011; 6:e16141. [PubMed: 21283586]

603. Chen P-C, Kuyucak S. Biophys J. 2009; 96:2577. [PubMed: 19348743]

604. Chen P-C, Kuyucak S. Biophys J. 2011; 100:2466. [PubMed: 21575581]

605. Bezrukov SM, Vodyanoy I, Parsegian VA. Nature. 1994; 370:279. [PubMed: 7518571]

606. Akeson M, Branton D, Kasianowicz JJ, Brandin E, Deamer DW. Biophys J. 1999; 77:3227. [PubMed: 10585944]

607. Meller A, Nivon L, Brandin E, Golovchenko J, Branton D. Proc Natl Acad Sci USA. 2000; 97:1079. [PubMed: 10655487]

608. Vercoutere W, Winters-Hilt S, Olsen H, Deamer D, Haussler D, Akeson M. Nature Biotech. 2001; 19:248.

609. Kasianowicz JJ, Bezrukov SM. Biophys J. 1995; 69:94. [PubMed: 7545444]

610. Li J, Stein D, McMullan C, Branton D, Aziz MJ, Golovchenko JA. Nature. 2001; 412:166. [PubMed: 11449268]

611. Heng JB, Ho C, Kim T, Timp R, Aksimentiev A, Grinkova YV, Sligar S, Schulten K, Timp G. Biophys J. 2004; 87:2905. [PubMed: 15326034]

612. Storm AJ, Chen JH, Ling XS, Zandergen HW, Dekker C. Nature Mater. 2003; 2:537. [PubMed: 12858166]

613. Garaj S, Hubbard W, Reina A, Kong J, Branton D, Golovchenko JA. Nature. 2010; 467:190. [PubMed: 20720538]

614. Merchant CA, Healy K, Wanunu M, Ray V, Peterman N, Bartel J, Fischbein MD, Venta K, Luo Z, Johnson ATC, Drndic M. Nano Lett. 2010; 10:2915. [PubMed: 20698604]

615. Schneider GF, Kowalczyk SW, Calado VE, Pandraud G, Zandbergen HW, Vandersypen LMK, Dekker C. Nano Lett. 2010; 10:3163. [PubMed: 20608744]

616. Gu Q, Braha O, Conlan S, Cheley S, Bayley H. Nature. 1999; 398:686. [PubMed: 10227291]

617. Gu LQ, Serra MD, Vincent B, Vigh G, Cheley S, Braha O, Bayley H. Proc Natl Acad Sci USA. 2000; 97:3959. [PubMed: 10760267]

618. Kang, X-f; Cheley, S.; Rice-Ficht, A.; Bayley, H. J Am Chem Soc. 2007; 129:4701. [PubMed: 17375923]

619. Liu A, Zhao Q, Guan X. Anal Chim Acta. 2010; 675:106. [PubMed: 20800721]

620. Nakane J, Wiggin M, Marziali A. Biophys J. 2004; 87:615. [PubMed: 15240494]

621. Zhao Q, Sigalov G, Dimitrov V, Dorvel B, Mirsaidov U, Sligar S, Aksimentiev A, Timp G. Nano Lett. 2007; 7:1680. [PubMed: 17500578]

622. Hornblower B, Coombs A, Whitaker RD, Kolomeisky A, Picone SJ, Meller A, Akeson M. Nature Mater. 2007; 4:315.

623. Dekker C. Nature Nanotech. 2007; 2:209.

624. Howorka S, Siwy Z. Chem Soc Rev. 2009; 38:2360. [PubMed: 19623355]

625. Venkatesan BM, Polans J, Comer J, Sridhar S, Wendell D, Aksimentiev A, Bashir R. Biomed Microdevices. 2011; 13:671. [PubMed: 21487665]

626. Timp W, Mirsaidov U, Wang D, Comer J, Aksimentiev A, Timp G. IEEE Tran Nanotechnol. 2010; 9:281.

627. Wanunu M. Phys Life Rev. 2012; 1:1.

628. Muthukumar M. J Chem Phys. 1999; 111:10371.

629. Slonkina E, Kolomeisky AB. J Chem Phys. 2003; 118:7112.

630. Muthukumar M. J Chem Phys. 2003; 118:5174.

631. Howorka S, Movileanu L, Lu X, Magnon M, Cheley S, Braha O, Bayley H. J Am Chem Soc. 2000; 122:2411.

632. Howorka S, Bayley H. Biophys J. 2002; 83:3202. [PubMed: 12496089]

633. Bezrukov SM, Kasianowicz JJ. Phys Rev Lett. 1993; 70:2352. [PubMed: 10053539]

634. Muthukumar M, Kong CY. Proc Natl Acad Sci USA. 2006; 103:5273. [PubMed: 16567657]

635. Robertson JWF, Rodrigues CG, Stanford VM, Rubinson KA, Krasilnikov OV, Kasianowicz JJ. Proc Natl Acad Sci USA. 2007; 104:8207. [PubMed: 17494764]

636. Derrington I, Butler T, Collins M, Manrao E, Pavlenok M, Niederweis M, Gundlach J. Proc Natl Acad Sci USA. 2010; 107:16060. [PubMed: 20798343]

637. Manrao EA, Derrington IM, Laszlo AH, Langford KW, Hopper MK, Gillgren N, Pavlenok M, Niederweis M, Gundlach JH. Nature Biotech. 2012; 30:349.

638. Rincon-Restrepo M, Mikhailova E, Bayley H, Maglia G. Nano Lett. 2011; 11:746. [PubMed: 21222450]

639. Comer, J.; Wells, DB.; Aksimentiev, A. Modeling nanopores for sequencing DNA. In: Zuccheri, G.; Samori, B., editors. DNA Nanotechnology, Methods and Protocols. Vol. 749. Humana Press; New York: 2011. p. 317-358.Chapter 22

640. Wells, DB.; Bhattacharya, S.; Carr, R.; Maffeo, C.; Ho, A.; Comer, J.; Aksimentiev, A. Optimization of the molecular dynamics method for simulations of DNA and ion transport through biological nanopores. In: Gracheva, ME., editor. Nanopore-based technology: single molecule characterization and DNA sequencing. Vol. 870. Humana Press; New York: 2012. p. 165-186.Chapter 10

641. Yarov-Yarovoy V, DeCaen PG, Westenbroek RE, Pana CY, Scheuer T, Baker D, Catterall WA. Proc Natl Acad Sci USA. 2012; 109:E93. [PubMed: 22160714]

Biographies
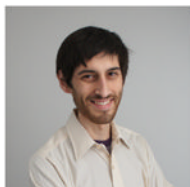
Christopher Maffeo

Christopher Maffeo received his B.Sc. in physics from the University of California Santa Barbara in 2006. He joined the Aksimentiev group in December 2006. After studying the structural and conductance properties of the phospholamban pentamer, he has focused his efforts on understanding the kinetics, energetics and electrostatics of various DNA–DNA and DNA–protein interactions.

Swati Bhattacharya

Swati Bhattacharya is a postdoctoral fellow in the group of Aleksei Aksimentiev at the University of Illinois at Urbana-Champaign. She received her Ph.D. in physics for work on the adsorption of polymers at surfaces under the supervision of Thomas Vilgis in 2009 from the Max Planck Institute for Polymer Research in Mainz. Her current research activities include computational modeling aimed at developing applications of nanopores particularly for DNA sequencing.

Jejoong Yoo

Jejoong Yoo received his B.Sc. in Physics and Molecular Biology from Seoul National University (SNU) in 2001 and a Ph.D. in Biophysics from University of Wisconsin-Madison under the guidance of Prof. Qiang Cui for his study of membranes and membrane proteins using molecular dynamics simulations in 2005–2010. In 2010, he joined the Aksimentiev group in the Department of Physics at University of Illinois at Urbana-Champaign as a postdoctoral fellow in Center for the Physics of Living Cells. He is currently interested in understanding how the structural and dynamical properties of nucleic acid systems are effectively modulated by various types of cations.
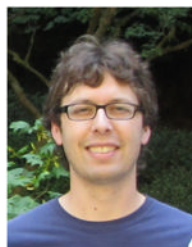
David Wells

David Wells received his B.Sc. in Physics at the University of Washington in 2005. He joined Professor Aksimentiev's group in 2006, and has since performed MD simulation studies of proteins, DNA and synthetic nanopores. He earned his Ph.D. in physics from the University of Illinois at Urbana-Champaign during the Summer of 2012.

Aleksei Aksimentiev

Aleksei Aksimentiev received his Master's degree in physics from the Ivan Franko Lviv State University, Lviv, Ukraine, and his Ph.D. in chemistry from the Institute of Physical Chemistry, Warsaw, Poland. After a brief postdoctoral training at Mitsui Chemicals, Japan, he joined the Theoretical and Computational Biophysics Group, Urbana, IL, as a Postdoctoral Research Associate. In 2005, he became a Faculty Member of the Physics Department at the University of Illinois, where he is currently a Professor of physics. His research interests include systems that combine biological macromolecules and man-made nanostructures, membrane proteins, and molecular machinery of DNA replication.
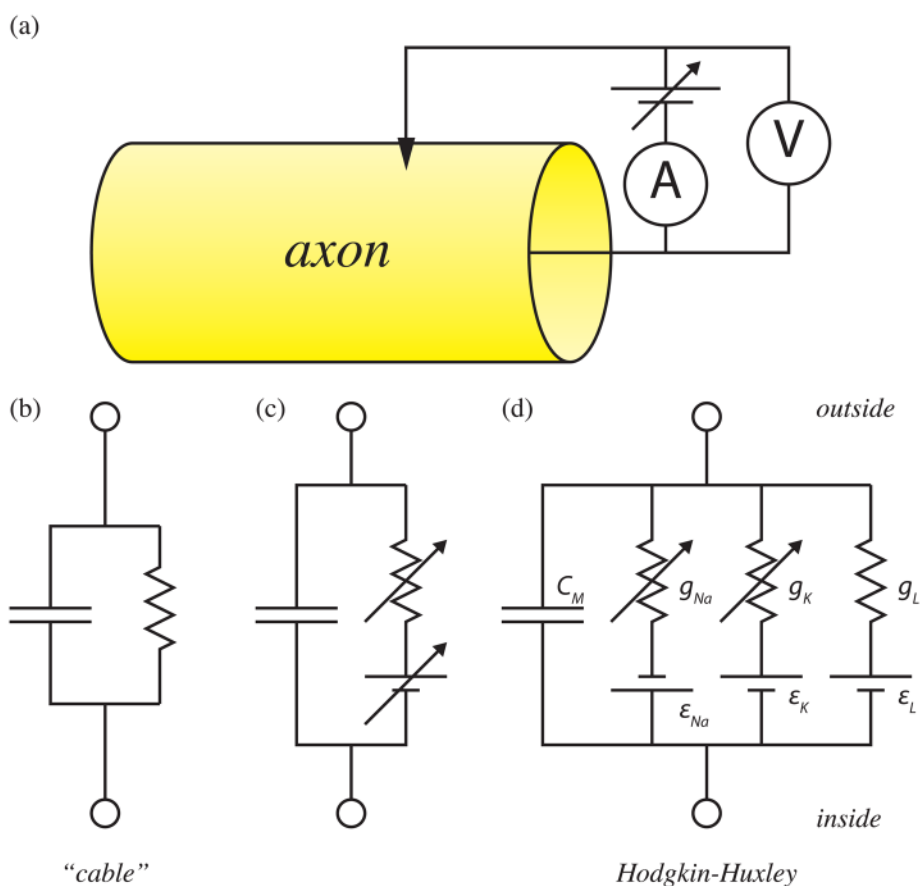
Figure 1.
Evolution of the equivalent circuit diagrams of nerve axon models. (*a*) Schematic representation of an axon. Conductance experiments are performed by maintaining a given transmembrane voltage and measuring the resulting ionic current. (*b*) Cable model of the axon. (*c*) Refined model including a (variable) membrane emf and variable membrane resistance. (*d*) Hodgkin- Huxley model, which describes the emfs and conductivities of potassium and sodium separately, and also includes a small leakage current.
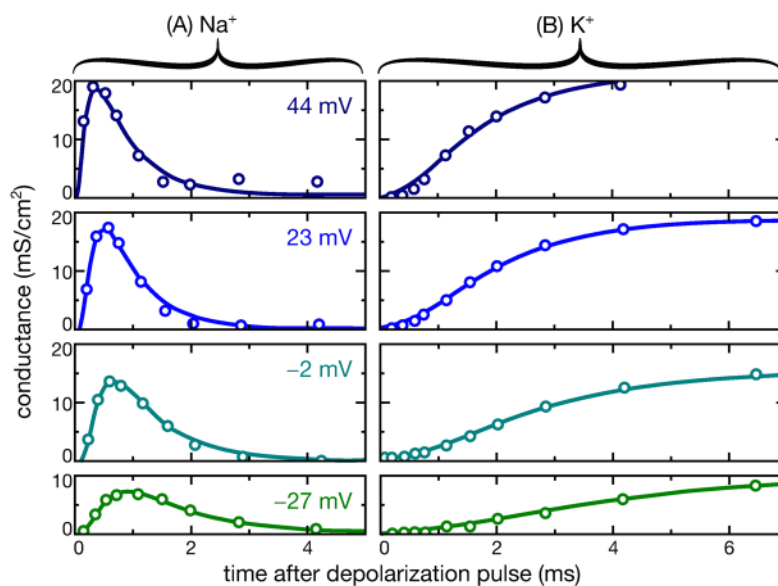
Figure 2.
Conductance of squid axon membrane to sodium (a) and potassium (b) at various applied voltages. Voltage was held at the rest value of −65 mV, then increased to the displayed value at $t = 0$. While potassium conductance rises and saturates under an applied potential, sodium conductance initially rises but subsequently returns to zero. Adapted with permission from Reference 397. Copyright 1952 Wiley.
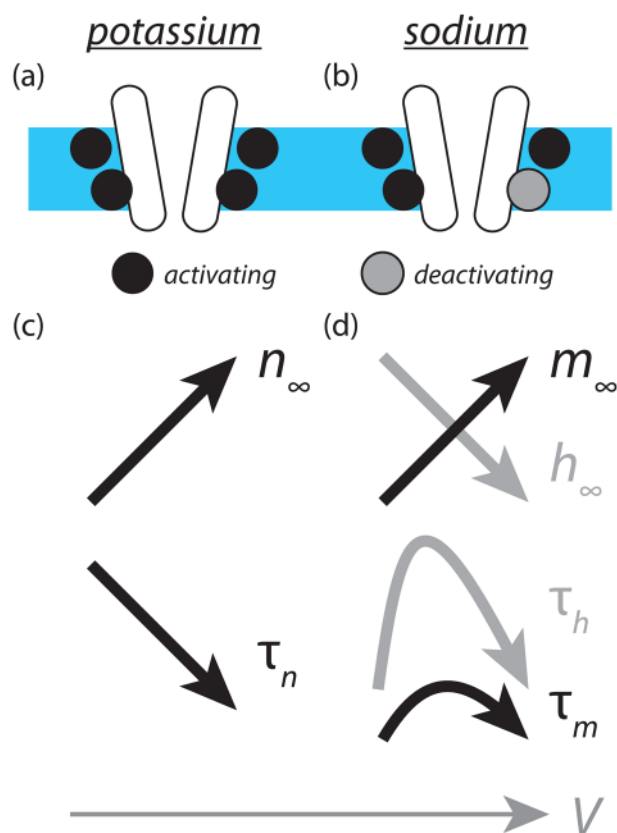
122222444444433344444444444444444444
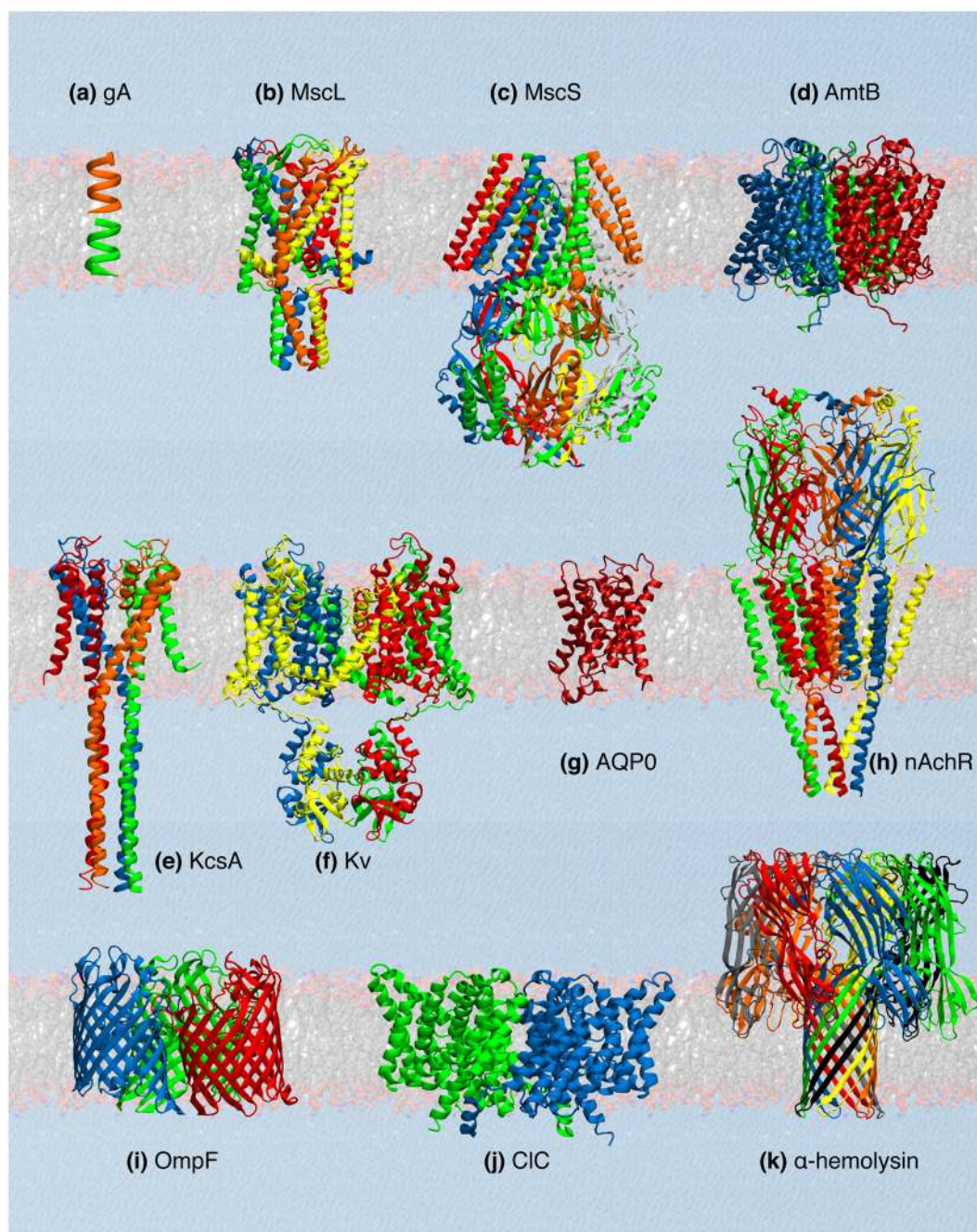
Figure 4.
Molecular graphics images of membrane channels listed in Table 1. The channels shown are: (a) gramicidin A (gA), 1JNO;[406] (b) mechanosensitive channel of large conductance (MscL), 2OAR;[407] (c) mechanosensitive channel of small conductance (MscS), 2OAU;[408] (d) ammonium transporter (AmtB), 2NUU;[409] (e) K^+ channel (KcsA), 3EFF;[410] (f) voltage-gated K^+ channel (Kv), 2R9R;[411] (g) aquaporin 0 (AQP0), 2B6O;[412] (h) nicotinic acetylcholine receptors (nAchR), 2BG9;[413,414] (i) bacterial outer-membrane porin (OmpF), 2OMF;[415] (j) bacterial chloride channel (ClC), 1OTS;[416] (k) bacterial toxin (α-hemolysin), 7AHL.[417]
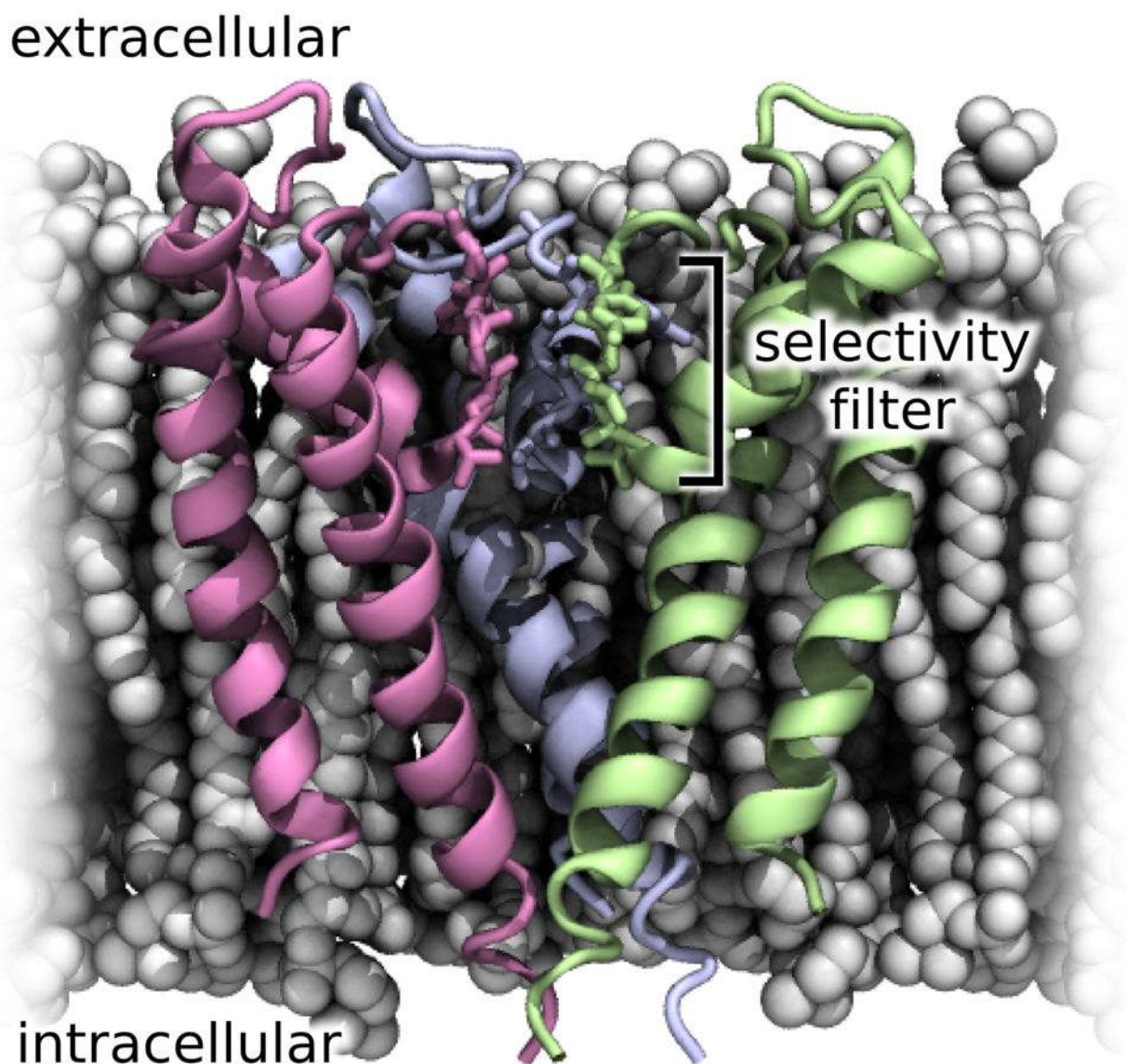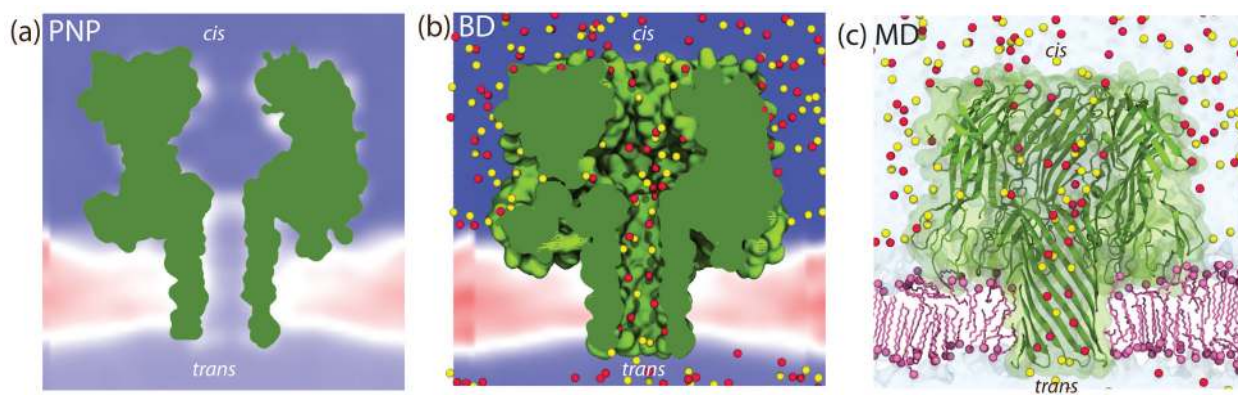
Figure 5.
Pore region of the KcsA K$^+$ ion channel embedded in a lipid bilayer membrane. The image shows the first crystallographically determined structure of a K$^+$ channel,[1] which did not include the long cytoplasmic helices depicted in Figure 4e. One of the four subunits of the KcsA tetramer is not shown to provide a clear view of the selectivity filter. The lipid bilayer is depicted as grey van der Waals spheres.
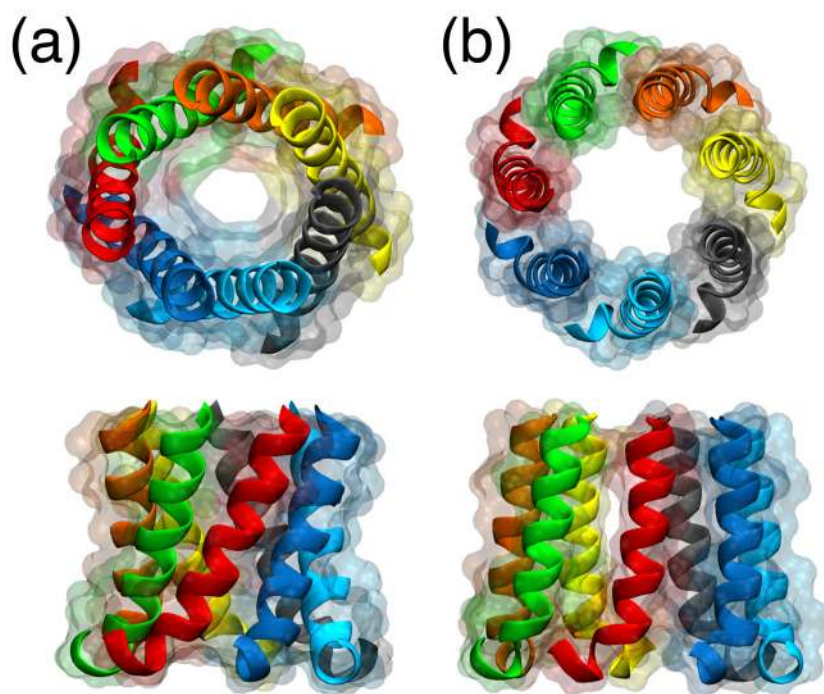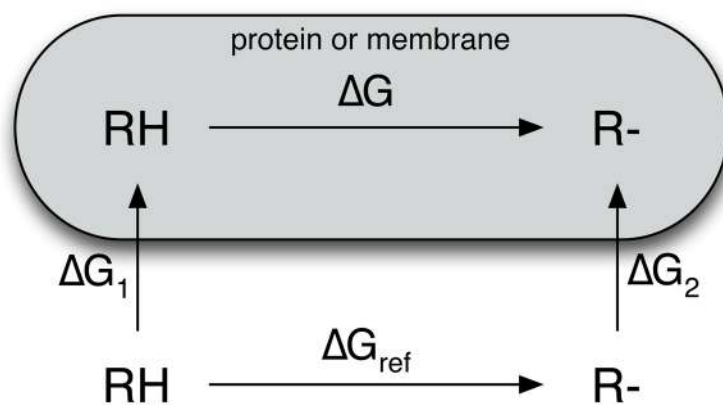
Figure 6.
Comparison of the pores formed by seven TM3 helices of MscS in nonconducting[408] (a) and open[430] (b) conformations, viewed from the periplasm (top) and from within the membrane (bottom).
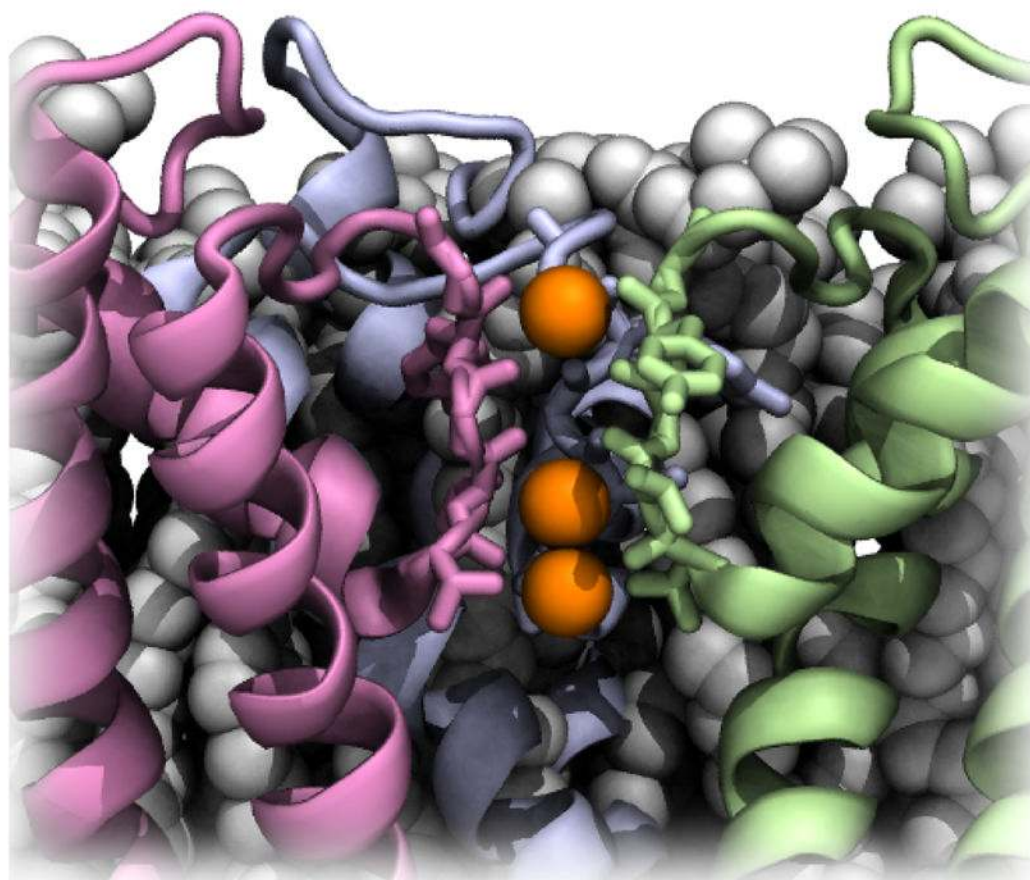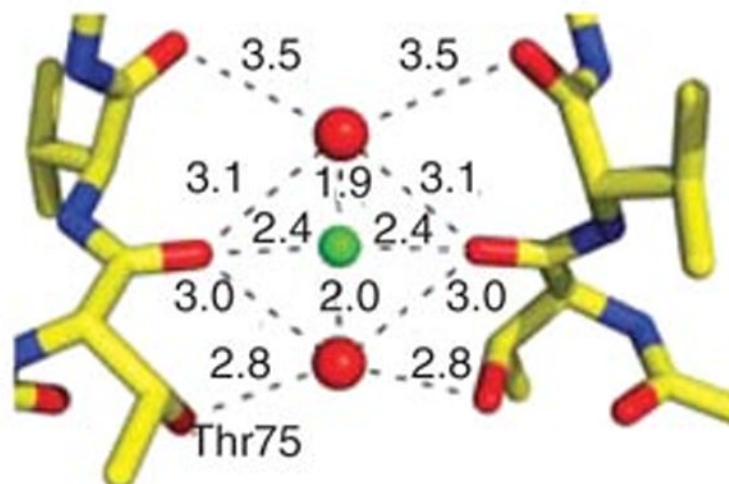
Figure 7.
A schematic illustrations of the PNP (a) BD (b) and all-atom MD (c) modeling methods applied to the same system—an α-hemolysin channel embedded in a lipid bilayer membrane and surrounded by an electrolyte solution. In panel (a), the ions are described as continuous density, whereas the water, protein and membrane are treated as continuum dielectric media. In the BD model (panel b), only ions are represented explicitly, whereas all other components are either implicitly modeled or approximated by continuum media. All atoms are treated explicitly in the all-atom MD method (panel c).

Figure 8.
Thermodynamic cycle for calculations of a pK_a shift. RH and R^- denote protonated and deprotonated states, respectively, of a titratable group. The gray box indicates a region near a protein or a membrane. ΔG_{ref} and ΔG denote free energies of deprotonation in water and in protein or membrane environment, respectively. ΔG_1 and ΔG_2 are transfer free energies of RH and R^- from water to protein or membrane environment, respectively.
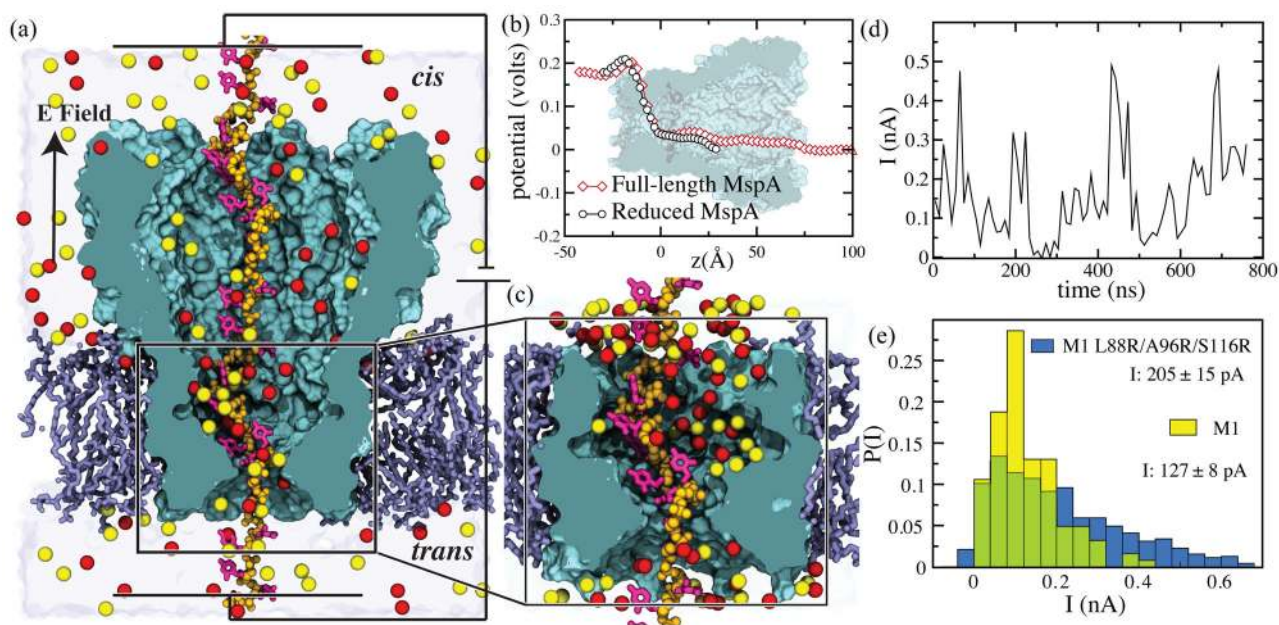
Figure 9.
The selectivity filter of KcsA. The system is depicted as in Figure 5, but additionally with K^+ ions resolved in the X-ray structure (orange spheres). In the active state, the selectivity filter will always contain at least two K^+ ions separated by a single water molecule.

Figure 10.
Na$^+$ (green sphere) and K$^+$ (red spheres) ions occupy different binding sites in the selectivity filter of a potassium channel. Early FEP simulations indicated a large free energy cost $\Delta\Delta G$ for exchanging K$^+$ with Na$^+$ at the K$^+$binding sites. $\Delta\Delta G$ may actually be smaller if the ion is free to move to its preferred binding site. Adapted with permission from Macmillan Publishers Ltd: Nature Structural & Molecular Biology (Reference 595), copyright 2009.

Figure 11.
(a) Cut-away view of the full-length MspA nanopore embedded in a lipid membrane with a DNA strand threaded through. The MspA is represented by a teal molecular surface, the lipid membrane by purple lines and the DNA bases are shown in magenta colored licorice representation. (b) Average electrostatic potentials along the symmetry axis of the full and truncated MspA nanopores at a transmembrane bias of 180 mV. The electrostatic potentials are computed from MD simulations of open pore MspA nanopores. (c) Cut-away view of the reduced MspA system. The DNA is covalently joined to itself across the periodic boundary. (d) The ionic current trace of a sample trajectory in of a poly(dC) strand threaded through the MspA nanopore. (e) Ionic current histograms obtained from ensemble simulations of the M1 MspA (yellow) and its arginine variant, M1 L88R/A96R/S116R (blue). The overlap of the two histograms is shown in green. The histograms were constructed using 100 ns averages of the instantaneous ionic current. Adapted with permission from Reference 348. Copyright 2012. American Chemical Society.

Table 1

Modeling and simulation studies in the general area of ion channels organized according to the system type and computational models employed.

System		Methods				
	Continuum	Implicit solvent MD	All-atom MD	Hybrid	CG	Others (QM)
gramicidins	8–15	16,17	18–51	52,53		54
outer-membrane porins	55–61	55,62–64	55,65–87	55		
α-Hemolysin	88–93	88,90,94,95	90,93,96–99	90,93,100–102		
K$^+$ channels	103–109	110–117	29,88,111–113,116–197, 425, 595, 596, 602–604	107,198–202	203–206	207–211
nAChR			212–220			
MscL/MscS	221–228	225,229	230–248,248–257	225,258	222,258	
Anion channels (VDAC, ClC)	259		260–264	265–268		
aquaporins			269–274			
NH$_4^+$ transporters			275–278			
Other channels	279–310	311–318	299,312,319–348	302,330,337,349–356	357,358	
Synthetic nanopores	359–370	371–374	375–391	350,382,383,392	393	394